JAERI-M
91-227

EVALUATION REPORT ON CCTF CORE-II

REFLOOD TEST C2-15 (RUN 75)

— INVESTIGATION OF FLECHT-SET COUPLING TEST RESULTS —

January 1992

Tsutomu OKUBO, Tadashi IGUCHI
Hajime AKIMOTO and Yoshio MURAO

日 本 原 子 力 研 究 所
Japan Atomic Energy Research Institute

JAERI-Mレポートは，日本原子力研究所が不定期に公刊している研究報告書です。
入手の問合わせは，日本原子力研究所技術情報部情報資料課（〒319-11茨城県那珂郡東海村）あて，お申しこしください。なお，このほかに財団法人原子力弘済会資料センター（〒319-11 茨城県那珂郡東海村日本原子力研究所内）で複写による実費頒布をおこなっております。

JAERI-M reports are issued irregularly.
Inquiries about availability of the reports should be addressed to Information Division, Department of Technical Information, Japan Atomic Energy Research Institute, Tokai-mura, Naka-gun, Ibaraki-ken 319-11, Japan.

編集兼発行　日本原子力研究所
印　　刷　㈱原子力資料サービス

JAERI-M 91-227

Evaluation Report on CCTF Core-II Reflood Test C2-15 (Run 75) — Investigation of FLECHT-SET coupling test results —

Tsutomu OKUBO, Tadashi IGUCHI
Hajime AKIMOTO and Yoshio MURAO

Department of Reactor Engineering
Tokai Research Establishment
Japan Atomic Energy Research Institute
Tokai-mura, Naka-gun, Ibaraki-ken

(Received December 18, 1991)

This report presents an evaluation on the CCTF Core-II Test C2-15 (Run 75). The purpose of the test is to investigate whether the thermo-hydrodynamic behavior is different between the CCTF and the FLECHT-SET reflooding tests. For this purpose, test conditions of the present test were set as close as possible to those of concerned FLECHT-SET 2714B experiment, taking account of differences in facility design.

Investigating results of both the tests, the following conclusions are obtained:

(1) Some discrepancies were observed in the measured test conditions between the two tests. Out of them, difference in the Acc injection duration was large and affected test results, such as the water accumulation in the downcomer and the core and the core cooling, during the initial period. However, this effect was found to become small with time.

(2) Taking account of this difference and the difference in the broken cold leg pressure loss coefficient between the two facilities, the overall reflooding behavior is judged to be similar in the two facilities.

(3) The CCTF test results showed the core heat transfer enhancement in the higher power region due to its steep radial power distribution, where-

as the FLECHT-SET did not due to its rather flat radial power distribution. This enhancement was observed significantly at 1.83 m but was smaller at the higher elevation.

(4) The heat transfer was nearly identical between the two tests and an existing correlation could well predict the heat transfer coefficients of both the tests at the location where the heat transfer enhancement mentioned above (3) were small, during the time period when the effect of the difference in the Acc injection mentioned above (1) were small.

(5) Therefore, the core cooling is expected to be almost the same in the CCTF and the FLECHT-SET under the same core boundary conditions and core radial power distribution.

Keywords: Reactor Safety, PWR, LOCA, ECCS, Reflooding, Quenching, Two-phase Flow, Heat Transfer, Core Radial Power Distribution, CCTF Core-II, FLECHT-SET

JAERI－M 91－227

大型再冠水円筒第2次炉心試験C2－15（Run 75）評価報告書
―― FLECHT－SET結合試験結果の検討 ――

日本原子力研究所東海研究所原子炉工学部
大久保 努・井口 正・秋本 肇・村尾 良夫

（1991年12月18日受理）

本報告書は，円筒第2次炉心試験C2－15（Run 75）の評価報告書である。本試験は，CCTFおよびFLECHT－SETによる再冠水実験の間に熱水力学的挙動の差が有るか否かを検討する為に実施された。このため，本試験の条件は，装置の設計上の相違を考慮した上で，FLECHT－SET 2714B実験と可能な限り同一に設定された。

両試験の結果を検討して，以下の結論が得られた。

(1) 両試験で達成された条件にはいくつかの点に相違が見られた。この中では，Acc注水期間の相違が大きく，初期のダウンカマーや炉心の蓄水や炉心冷却等の試験結果に大きな影響を与えたと考えられる。しかしながら，その影響は時間とともに小さくなった。

(2) この相違や破断コールドレグでの圧力損失係数の相違を考慮すれば，全体的な再冠水挙動は，両装置に於いて同じであると判断される。

(3) CCTF試験では，急峻な炉心半径方向出力分布により高出力領域で熱伝達の増加が観測されたが，FLECHT－SETでは半径方向分布がほぼ平坦のため観測されなかった。この熱伝達の増加は，1.83m位置で顕著であったが，それより上方では小さくなった。

(4) 上記(3)で述べた熱伝達の増加が小さい位置では，上記(1)で述べたAcc注水の差による効果が小さい期間において両試験に於ける熱伝達がほぼ同一であり，既存の熱伝達率相関式により両試験の熱伝達率が良く予測できた。

(5) 以上のことから，CCTFとFLECHT－SETにおける炉心冷却は，同一の炉心境界条件と炉心半径方向出力分布の下では，ほぼ同一になると予想される。

東海研究所：〒319－11 茨城県那珂郡東海村白方字白根2－4

Contents

目　　次

List of Tables

List of Figures

1. Introduction

A reflood test program[1] using large scale test facilities has been conducted at the Japan Atomic Energy Research Institute (JAERI). The facilities are the Cylindrical Core Test Facility (CCTF) and the Slab Core Test Facility (SCTF). This report presents an evaluation for the CCTF Core-II FLECHT-SET coupling test, Test C2-15 (Run 75).

The CCTF is an experimental facility designed to simulate a full-height core section, four primary loops and their components of a 1,000 MWe class pressurized water reactor (PWR). This facility is used to provide information on thermo-hydrodynamic behaviors in the core, downcomer and upper plenum including integral system effects during the refill and reflood phases of a large-break loss-of-coolant accident (LOCA) in a PWR.

The objectives of the test program using the CCTF are:

a. Demonstration of capability of emergency core cooling system (ECCS) during refill and reflood period.
b. Verification of reflood analysis codes.
c. Collection of information to improve the thermo-hydrodynamic models in the analysis codes.

As the first series of the CCTF tests, twenty-seven CCTF Core-I tests were conducted. This series of tests presented a lot of information[2] on the system thermo-hydrodynamic behavior as well as the core behavior during the refill and reflood phases of a LOCA in a PWR. The CCTF Core-I test series was initiated in March 1979 and terminated in April 1981. Subsequently, as the second series of the CCTF tests, the CCTF Core-II test series was initiated in March 1982. The special purposes of the CCTF Core-II test program are to investigate the effects of alternative ECCS such as the upper plenum, the downcomer and the combined injections as well as to extend the experimental range of the Core-I tests.

Test C2-15 (Run 75) was conducted in order to investigate the differences in reflooding behavior between in the CCTF and the FLECHT-SET Phase B facility[3],[4]. In the CCTF Core-I test series, three FLECHT-SET coupling tests were performed[5] for the same purpose as for the present test. However, as presented in reference 5, the coupling was not very good, because the test conditions such as the system pressure and the LPCI injection rate were different a lot from those of the concerned FLECHT-SET tests, and hence, the test results were different significantly. There-

fore, the test conditions of the present test were set to be as close as possible to those for the FLECHT-SET 2714B experiment[3],[4]. In this report, the test results are presented and discussed. Selected data of the present test are presented in Appendix B for better understanding of the test results.

Major characteristics of the present test are summarized in the following:

1. Test name

   FLECHT-SET 2714B coupling test

2. Test number

   C2-15 (Run 75)

3. Objective of test

   To investigate differences in reflooding behavior between in the CCTF and the FLECHT-SET Phase B facility

4. Features of test

   (1) Lower plenum injection

   (2) High ECC water subcooling (40 K)

   (3) Low system pressure (0.13 MPa)

2. Test Description

2.1 Test Facility

The CCTF Core-II was designed in consideration of the following objectives and criteria:

a. Design objectives

(1) The facility should provide the capability to reasonably simulate flow conditions in the primary system of a PWR during the refill and reflood phases of a LOCA.

(2) The downcomer design should provide ECC water flow behavior throughout the test which is reasonably representative of that of the PWR downcomer.

b. Design criteria

(1) Reference reactors are the Trojan reactor in the USA and in certain aspects the Ohi reactor in Japan.

(2) Vertical dimensions and locations of system components are kept as close as possible to those of the reference reactors.

(3) Flow areas of system components are scaled down in proportion to the scaling factor of core flow area.

(4) The facility is equipped with four primary coolant loops which are composed of three intact loops and one broken loop.

(5) A 200% cold leg large-break is simulated in the broken loop.

(6) The ECCS consists of two accumulator systems (Acc) and a low pressure coolant injection system (LPCI), and injection locations are the upper plenum, the downcomer, the hot legs as well as the lower plenum and the cold legs.

(7) Maximum allowable pressure of the facility is 588 kPa (6 kg/cm^2 absolute).

(8) Maximum allowable temperature of simulated fuel rods is 1173 K (900 ^{o}C).

(9) Maximum allowable temperature of components in the primary system except simulated fuel rod assemblies is 623 K (350 ^{o}C).

(10) The reactor pressure vessel contains approximately 2,000 electrically heated rods simulating the fuel rods.

(11) Design of upper plenum internals is based on that of a new 17 x 17 type Westinghouse fuel assembly.

(12) Flow resistance of each loop is adjusted by an orifice in the pump simulator.

(13) The containment system consists of two tanks.

A bird's-eye view of the CCTF is shown in Fig. 2.1. The scaled dimensions of the components are given in Table 2.1.

The differences in the design of the Core-II facility from the Core-I are:

(1) Axial and local peaking factors of heater rods

(2) Edge shape of grid spacers

(3) Upper plenum structures (upper plenum internals, plugging devices in end box region and a upper ring)

(4) Vent valves

(5) Alternative ECCS (downcomer, upper plenum and hot leg injection)

(6) Instruments

2.1.1 Pressure Vessel and Internals

The pressure vessel is of a cylindrical type as shown in Figs. 2.2 and 2.3. Height is the same as the reference reactor pressure vessel. Radial direction is scaled down in proportion to the core flow area scaling, that is, 1/21.44. The upper ring was newly installed in the Core-II facility for installation of the upper plenum ECC water injection lines and instruments. The upper plenum injection lines are shown in Figs. 2.4 and 2.5. The upper plenum injection is adopted in some 2-loop PWRs in Japan and the USA. Four vent valves and two downcomer ECC water injection nozzles, which are sometimes called Core Flooding Nozzles (CFN), are also newly equipped in the Core-II facility as shown in Figs. 2.2 and 2.3. Vent valves and CFNs are for the simulation of a Babcock & Wilcox (B&W) type PWR. Downcomer injection nozzles also exist in a couple of recent Japanese 2-loop PWRs. Location of Core Flooding Nozzles is shown in Fig. 2.6 in detail.

Cross section of the pressure vessel is shown in Fig. 2.3 and the dimensions are given in Fig. 2.7. The core consists of thirty-two 8 x 8 electrically heated rod bundles arranged in a cylindrical configuration and simulates a Westinghouse 15 x 15 type fuel assemblies.

The downcomer is an annulus of 61.5 mm gap. In determining the gap size, the flow area of the core baffle region was added to that of the downcomer region. Thus, the core baffle flow area is included in the

downcomer simulation and is not simulated separately in the vessel inserting stainless steel fillers to prevent fluid flow.

The vessel wall is constructed of carbon steel which is cladded with the 5 mm thick stainless steel plate. The wall is 90 mm thick to simulate the stored energy as reasonably as possible during ECC water injection.

Design of upper plenum internals is based on that of the new Westinghouse 17 x 17 type fuel assemblies instead of the old type one simulated in the Core-I facility. The internals consists of ten control rod guide tubes, ten support columns and twelve open boles as shown in Fig. 2.8. Radius of each internals is scaled down by a factor of 8/15 from that of an actual reactor. They are illustrated in Fig. 2.9. Flow resistance baffles are inserted into the control rod guide tubes. The baffles consist of two kinds of baffle plates and a shaft. The baffle plates are shown in Fig. 2.10.

End boxes are attached beneath the upper Core support plate (UCSP). Structure for one heater rod bundle is shown in Fig. 2.11. Plugging devices are installed newly in the Core-II facility as shown in Figs. 2.11 and 2.12 to simulate the flow resistance more correctly.

2.1.2 Heater Rod Assembly

Heater rod assemblies simulating the fuel assembly consist of thirty-two 8 x 8 array rod bundles. Each bundle consists of fifty-seven electrically heated rods and seven non-heated rods as shown in Fig. 2.13. The core is usually subdivided into three regions to achieve a desired radial power distribution. This is shown in Fig. 2.3. The high, medium and low power regions are named A, B and C regions, respectively. Local peaking factor of heater rods in a bundle is unity, that is, all heater rods in a bundle have the same power density in the Core-II facility.

A heater rod consists of a nichrome heating element, magnesium oxide (MgO) and boron nitride (BN) insulators, and Inconel-600 sheath. BN is used for only central part of the heated region and MgO for the other part as shown in Fig. 2.14. Heated length and outer diameter of the heater rods are 3.66 m and 10.7 mm, respectively, which are identical to the corresponding dimensions of actual PWR fuel rods. Sheath wall thickness is 1.0 mm and is thicker than the actual fuel cladding, because of the requirements for thermocouple installation. Heating element is a helical

coil with a varying pitch to generate a 17-step chopped cosine axial power profile as shown in Fig. 2.15. Peaking factor is 1.40, instead of 1.492 for a Core-I rod.

Non-heated rods are either stainless steel pipes or solid bars of 13.8 mm O.D.. The pipes are utilized for installation of instruments such as superheated steam probes and thermocouples. The bars are used for supporting the assembly loads.

Heater rods and non-heated rods are held in radial position by gird spacers which are located at six elevations along the axial length as shown in Fig. 2.15. A grid spacer is a lattice structure composed of stainless steel plates of 0.4 mm and 0.8 mm thick and 40 mm high, whose edges are sharpened in the Core-II. Rod pitch is 14.3 mm which is the same as that of the reference PWR.

Heater rods penetrate through the bottom plate of the vessel to facilitate lead out of the power cables from the bottom of the vessel. The outer diameter of the rods in the lower plenum is reduced to 8.6 mm. Three-Phase electric current is used for heater rods and the electrical neutral point is at the top of the rods where they are interconnected to each other.

2.1.3 Primary Loops and ECCS

Primary loops consist of three intact loops and a broken loop. Each loop consists of hot leg and cold leg pipings, a steam generator simulator and a pump simulator. The 200 percent cold leg large break is simulated for the broken loop. The broken cold leg is connected to two containment tanks through blowdown valves. The primary loop arrangement is shown in Figs. 2.16 and 2.17.

Inner diameter of the piping is scaled down in proportion to the core flow area scaling. Length of each piping section is almost the same as the corresponding section of the reference PWR.

The steam generator simulators are of the U-tube and shell type as shown in Fig. 2.18. Tube length is about 5 m shorter than in the reference PWR. Vertical height of the steam generator simulators is also about 5 m lower than in the reference PWR. The primary coolant passes through the tube side and the secondary coolant is stagnant in the shell side. The steam generator simulators of two loops are housed in a single shell as-

sembly which has two compartments, one simulator for each loop in one compartment. Wall thickness of the U-tube is 2.9 mm compared to 1.27 mm of the reference PWR, because of a higher pressure difference between the primary and secondary sides in the simulator.

The pump simulator consists of casing and duct simulators and an orifice plate as shown in Fig. 2.19. Loop flow resistance is simulated with the orifice plate. Each orifice plate has a hole with diameter and thickness of 95 mm and 10 mm, respectively.

The ECCS consists of two Accs and a LPCI. The injection points are at each cold leg, lower plenum, upper plenum, downcomer and each hot leg. The upper plenum, downcomer and hot leg injection system was newly installed after Test C2-2 (Run 56) for the alternative ECCS tests. In the new injection system, two accumulator tanks are used for ECC water injection.

2.1.4 Instrumentation

Instrumentation is divided into two groups. One of them is JAERI-supplied instruments measuring temperatures, absolute pressures, differential pressures, water levels and flow rates. Thermocouples measure temperatures of rod surface, fluid and structure. Absolute pressures are measured in the upper and lower plena, steam generator plena and containment tanks. Differential pressure measurements are carried out at many locations covering the whole system almost completely. In the ECC water supply tanks and the containment tank 1, liquid levels are measured. Flow meters measure ECC water flow rates. Furthermore, flow rates in the downcomer, the cross-over leg pipings and the vent line from the containment tank 2 to the atmosphere are measured with drag disk flow meters, pitot tubes and a venturi tube, respectively. Total number of the JAERI-supplied instruments is 1,338 channels as summarized in Table 2.2 and signals from these instruments are recorded on a magnetic tape.

The other group of the instrumentation is the USNRC-supplied instruments. They are advanced instrumentation for two-phase flow measurement. Kinds and quantities of those are tabulated in Table 2.3. Total number is 540 channels.

2.2 Test Conditions and Procedures

2.2.1 Test Conditions

Summary of the test conditions are presented in Table 2.4. Distinctive features of the present test are lower plenum injection, high ECC water subcooling and low system pressure. Major characteristics of the test conditions are described in the following:

(1) Containment pressure

Containment pressure was planned to be kept at 134 kPa taking account of the larger broken cold leg pressure drop in the CCTF[5]. Due to this, upper plenum pressure was expected to be 175 kPa as in the FLECHT- SET 2714B experiment.

(2) ECC water injection rate

Acc injection rate and duration were set to 109 x 10^{-3} m^3/s and 19 s, respectively, to correctly simulate those of the FLECHT-SET 2714B experiment. LPCI injection rate was set to 3.83 x 10^{-3} m^3/s to keep downcomer water level at 4.27 m preventing downcomer water from overflowing. However, when needed, LPCI injection rate was varied manually to keep downcomer water level at a specified one. This is the same method as in the FLECHT-SET 2714B experiment.

(3) Core power

Total core power and peak linear power density were set to the same values as in the FLECHT-SET 2714B experiment. This resulted in the radial power distribution of 1.423 : 1.164 : 0.771 due to the limitation of maximum power in the low power region, whereas in the FLECHT-SET 2714B experiment it was flat although local power distribution was 1.2 : 0.97 : 0.92.

(4) Initial clad temperature

Initial peak clad temperature was planned to be 823 K at reflood initiation. This value is lower by 43 K than the nominal value in the FLECHT-SET 2714B experiment but very close to its measured values.

(5) Other major conditions

The ECC water of 340 K was injected only into the lower plenum as in the FLECHT-SET 2714B experiment.

2.2.2 Test Procedures

In preparation for the test, the accumulator tanks, the LPCI tank, the saturated water tank and the secondary sides of the steam generator simulators were filled with water which was purified with ion exchange regin. After all components and instruments were inspected for mechanical and electrical leakages, instruments were checked for zero points and sensitivity.

After these preparatory operation, the primary system was heated with preheaters to its specified temperature (381 K) and pressurized to a specified pressure (134 kPa) by steam. Water in the accumulator tanks was electrically heated to its specified temperature (340 K) and pressurized with nitrogen gas to provide sufficient head to achieve injection flow required. Water in the LPCI tank was also heated to its specified temperature (340 K) and was circulated through the circulation line including the LPCI line so as to preheat the line to the same temperature as the water. Water in the saturated water tank was heated up to the same temperature (340 K) as the ECC water. Water in the secondary side of each steam generator simulator was also heated and pressurized to a specified temperature (539 K) and pressure (5.2 MPa).

After establishing initial conditions of the test, electric power for preheating was turned off and the lower plenum was filled to a specified level (0.9 m) with water from the saturated water tank. When the water level in the lower plenum reached a specified level and other initial condition of the test stabilized in the allowable tolerance, electric power was applied to heater rods in the core and data recording was started. This is the initiation of the test, *i.e.* 0 s. The temperature rise of rods were monitored by using a computer. When a specified clad surface temperature (755 K) was reached by four rods, Acc injection (0.109 m^3/s) into the lower plenum was initiated. This specified clad temperature (755 K) of heater rods for initiation of coolant injection was predetermined by interpolation between the clad temperature (381 K) after preheating and the clad temperature (823 K) assumed for the time of bottom of core recovery (BOCREC). The system pressure was maintained at the specified initial pressure (134 kPa) throughout the test by controlling outlet valve of the containment tank 2. Decay of power input to rods was programmed to begin when water level reached bottom of heated region of the core, *i.e.* at the

BOCREC time. Specified power decay was obtained by normalizing decay curve of the ANS standard x 1.2 + ^{238}U capture decay x 1.1 at 30 seconds after shutdown.

At a specified time (19 s) after the initiation of Acc injection, the Acc injection mode was transferred to the LPCI injection mode. The LPCI injection rate of 3.83×10^{-3} m^3/s was varied manually when needed to maintain downcomer water level at 4.27 m.

Generated steam and entrained water flowed via broken and intact loops to the containment tanks. The steam was then vented to the atmosphere to maintain pressure in the containment tanks constant.

When all thermocouples on surface of heater rods indicated quenching of rods, power supply to heater rods and ECC water injection were turned off. After this, data recording was ended terminating the test.

The chronology of events is presented in Table 2.5.

Table 2.1 CCTF component scaled dimensions

Component		PWR	JAERI	Ratio
Pressure vessel				
Vessel inside diameter	(mm)	4394 (173")	1084	
Vessel thickness	(mm)	216 (8 1/2")	90	
Core barrel outside diameter	(mm)	3874	961	
Core barrel inside diameter	(mm)	3760	929	
Thermal shield outside diameter	(mm)	4170		
Thermal shield inside diameter	(mm)	4030		
Downcomer length	(mm)	4849	4849	1/1
Downcomer gap	(mm)	114.3	61.5	
Downcomer (+ buffle) flow area	(m^2)	4.23	0.197	1/21.44
Lower plenum volume	(m^3)	29.6	1.38	1/21.44
Upper plenum volume	(m^3)	43.6	2.04	1/21.44
Fuel (heater rod) assembly				
Number of bundles	(－)	193	32	
Rod array	(－)	15 × 15	8 × 8	
Rod heated length	(mm)	3660	3660	1/1
Rod pitch	(mm)	14.3	14.3	1/1
Fuel rod outside diameter	(mm)	10.72	10.7	1/1
Thimble tube diameter	(mm)	13.87	13.8	1/1
Instrument tube diameter	(mm)	13.87	13.8	1/1
Number of heater rods	(－)	39372	1824	1/21.58
Number of non-heated rods	(－)	4053	224	1/18.09
Core flow area	(m^2)	5.29	0.25	1/21.2
Core fluid volume	(m^3)	17.95	0.915	1/19.6
Primary loop				
Hot leg inside diameter	(mm)	736.6 (29")	155.2	1/4.75
Hot leg flow area	(m^2)	0.426	0.019	1/22.54
Hot leg length	(mm)	3940	3940	1/1
Pump suction inside diameter	(mm)	787.4 (31")	155.2	1/5.07
Pump suction flow area	(m^2)	0.487	0.019	1/25.77
Pump suction length	(mm)	7950	7950	1/1

Table 2.1 (Continued)

Component		PWR	JAERI	Ratio
Cold leg inside diameter	(mm)	698.5 (27.5")	155.2	1/4.50
Cold leg flow Area	(m^2)	0.383	0.019	1/20.26
Cold leg length	(mm)	5600	5600	1/1
Steam generator simulator				
Number of tubes	(－)	3388	158	1/21.44
Tube length (average)	(m)	20.5	15.2	1/1.35
Tube outside diameter	(mm)	22.225 (0.875")	25.4	
Tube inside diameter	(mm)	19.7 (0.05")	19.6	1/1
Tube wall thickness	(mm)	1.27	2.9	
Heat transfer area	(m^2)	4784 (51500 ft^2)	192	1/24.92
Tube flow area	(m^2)	1.03	0.048	1/21.44
Inlet plenum volume	(m^3)	4.25	0.198	1/21.44
Outlet plenum volume	(m^3)	4.25	0.198	1/21.44
Primary side volume	(m^3)	30.50 (1077 ft^3)	1.2	1/25.41
Secondary side volume	(m^3)	157.33 (5556 ft^3)	2.5	1/62.93
Containment tank - I	(m^3)		30	
Containment tank - II	(m^3)		50	
Storage tank	(m^3)		25	
Acc. tank	(m^3)		5	
Saturated water tank	(m^3)		3.5	
Elevation				
Bottom of heated region in core	(mm)	0	0	
Top of heated region in core	(mm)	3660	3660	0
Top of downcomer	(mm)	4849	4849	0
Bottom of downcomer	(mm)	0	0	0
Centerline of cold leg	(mm)	5198	4927	- 271
Bottom of cold leg (inside)	(mm)	4849	4849	0
Centerline of loop seal lower end	(mm)	2056	2047	- 9
Bottom of Loop seal lower end	(mm)	1662	1959	+ 297

Table 2.1 (Continued)

Component		PWR	JAERI	Ratio
Center of hot leg	(mm)	5198	4927	- 271
Bottom of hot leg (inside)	(mm)	4830	4849	+ 19
Bottom of upper core plate	(mm)	3957	3957	0
Top of lower core plate	(mm)	- 108	- 50	+ 58
Bottom of tube sheet of steam generator simulator	(mm)	7308	7307	- 1
Lower end of steam generator simulator plenum	(mm)	5713	5712	- 1
Top of tubes of steam generator simulator (avg)	(mm)	17952.7	14820	

Table 2.2 List of items measured with JAERI-supplied instruments

Item	Number of channels
Rod surface temperature	673
Core fluid temperature	40
Core barrel wall temperature	10
UP fluid temperature	120
UP wall temperature	36
DC fluid temperature	20
DC wall temperature	40
LP fluid temperature	8
LP wall temperature	4
SG primary side fluid temperature	24
SG secondary side fluid temperature	66
Primary loop piping fluid temperature	94
Primary loop piping wall temperature	4
Water supply tank fluid temperature	12
Core differential pressure	28
DC differential pressure	20
UP differential pressure	8
LP differential pressure	1
SG primary side differential pressure	8
Primary loop differential pressure	52
Pressure	15
Water level	7
Flow rate	39
Electric power	9
Total	1338

Note

UP : Upper plenum, DC : Downcomer

LP : Lower plenum, SG : Steam generator

Table 2.3 List of USNRC-provided instruments

Instrument	Number of sets	Number of sensors
DC FDG	18	162
DC VOP	1	1
DC drag disk	4	8
Core velocimeter	4	4
Core flag probe	12	24
Core LLD	6	96
LP LLD	3	15
End box turbine meter	8	8
UP turbine meter	4	4
UP FDG	11	110
UP film probe	2	4
UP prong probe	2	4
UP VOP	1	1
VV turbine meter	2	2
VV string probe	2	2
HL film probe	2	4
HL VOP	1	1
Reference probe	1	1
Spool piece	8	89
Total	92	540

Note

DC : Downcomer, FDG : Fluid distribution grid,
VOP : Video optical probe, LLD : Liquid level detector,
LP : Lower plenum, UP : Upper plenum,
VV : Vent valve

Table 2.4 Summary of test conditions

1. Test type : FLECHT-SET 2714B coupling
2. Tset No. : C2-15 (Run 75)
3. Test Date : October 12, 1984
4. Initial Power : Total; 9.23 MW; Average linear; 1.38 kW/m
5. Relative radial power shape to average linear power

Zone :	A	B	C
Ratio :	1.42	1.17	0.77

6. Pressure (MPa)

   Upper plenum; 0.18 (varied)
   Containment; 0.15 (varied)
   Steam generator secondary; 5.2

7. Temperature (K)

   Downcomer wall; 380
   Vessel internals; 380
   Primary piping wall; 380
   Lower plenum liquid; 344
   ECC liquid; 340
   Steam generator secondary; 538
   Peak clad temperature at ECC initiation; 763

8. ECC injection type; Lower plenum
9. Pump K-factor : 15
10. ECC flow rates and duration :

    Acc : 107×10^{-3} m^3/s from 47.5 to 79.0 s
    LPCI : 3.83×10^{-3} (varied) m^3/s from 79.0 to 967.0 s

11. Initial water level in lower plenum : 0.87 m
12. Power control : ANS × 1.2 + Actinide × 1.1 (30 sec after scram)
13. Peak temperature at BOCREC : 827 K

Table 2.5 Chronology of events for test

Event	Time (s)
Test initiated (Heater rods power on) (Data recording initiated)	0.0
Accumulator injection initiated	47.5
Bottom of core recovery (BOCREC)	56.0
Power decay initiated	58.0
LPCI injection initiated	67.5
Accumulator injection ended	79.0
All heater rods quenched	719.0
Power off	967.0
LPCI injection ended	967.0
Test ended (Data recording ended)	997.0

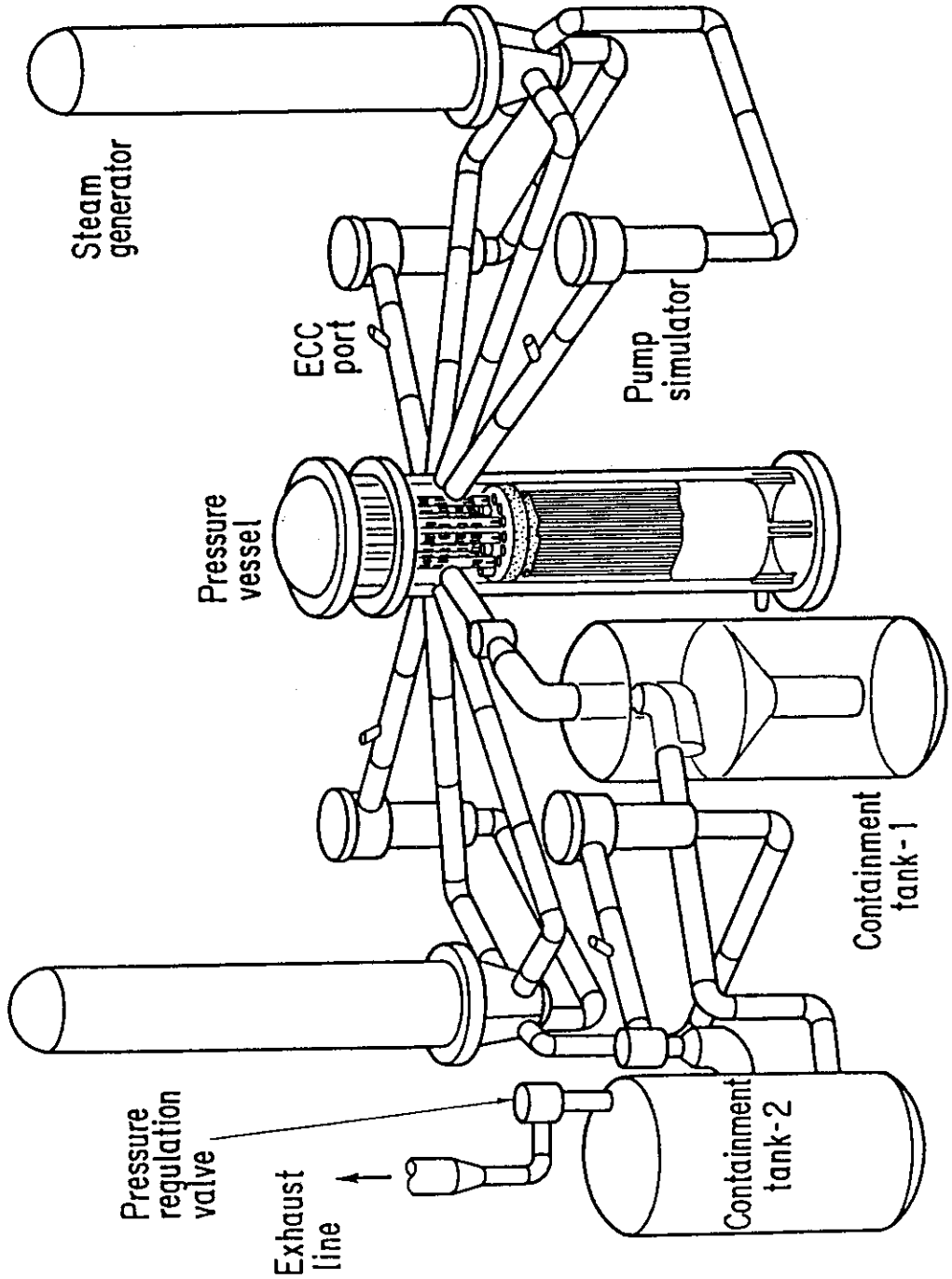

Fig. 2.1 Bird's-eye view of CCTF

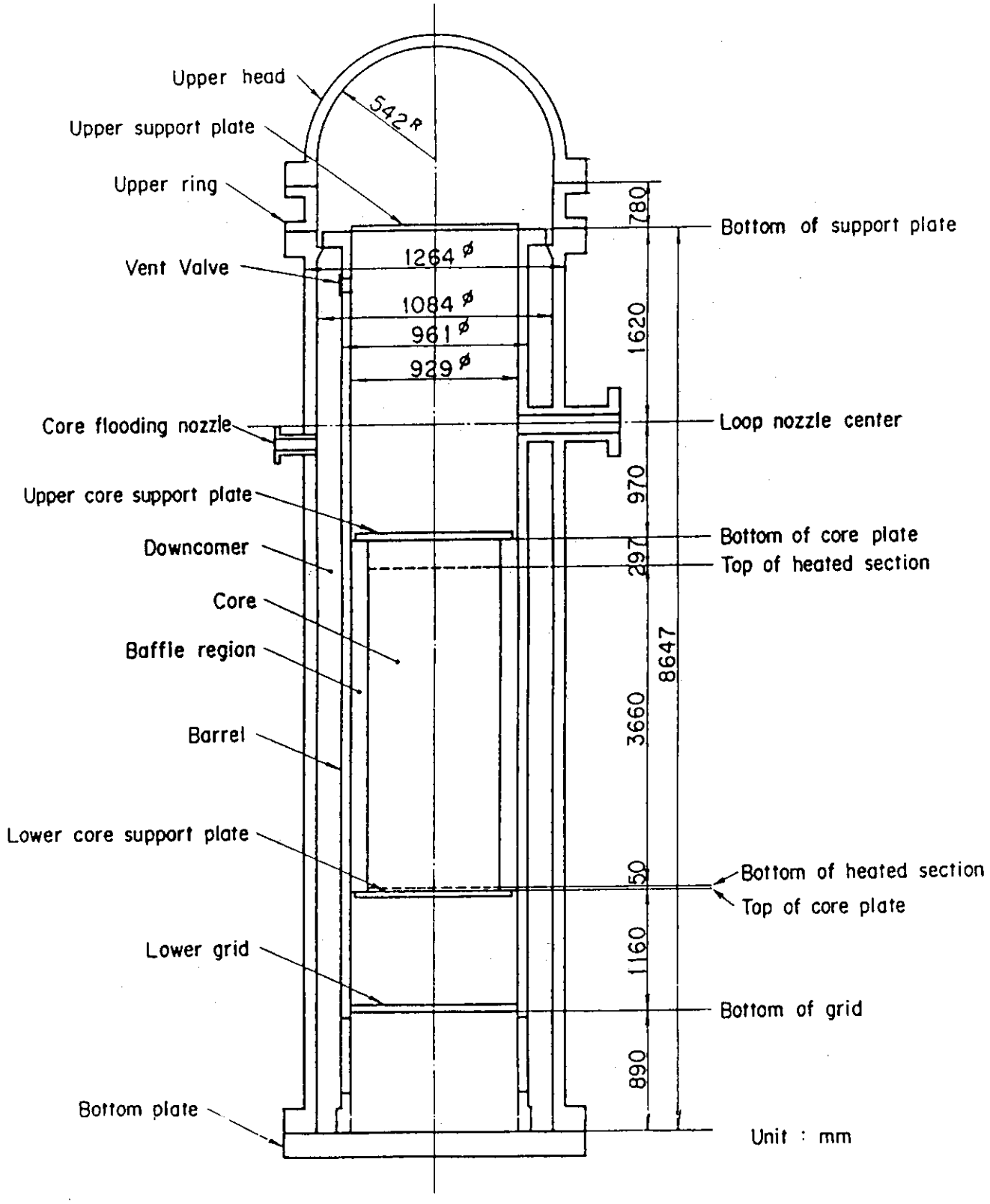

Fig. 2.2 CCTF Core-II pressure vessel

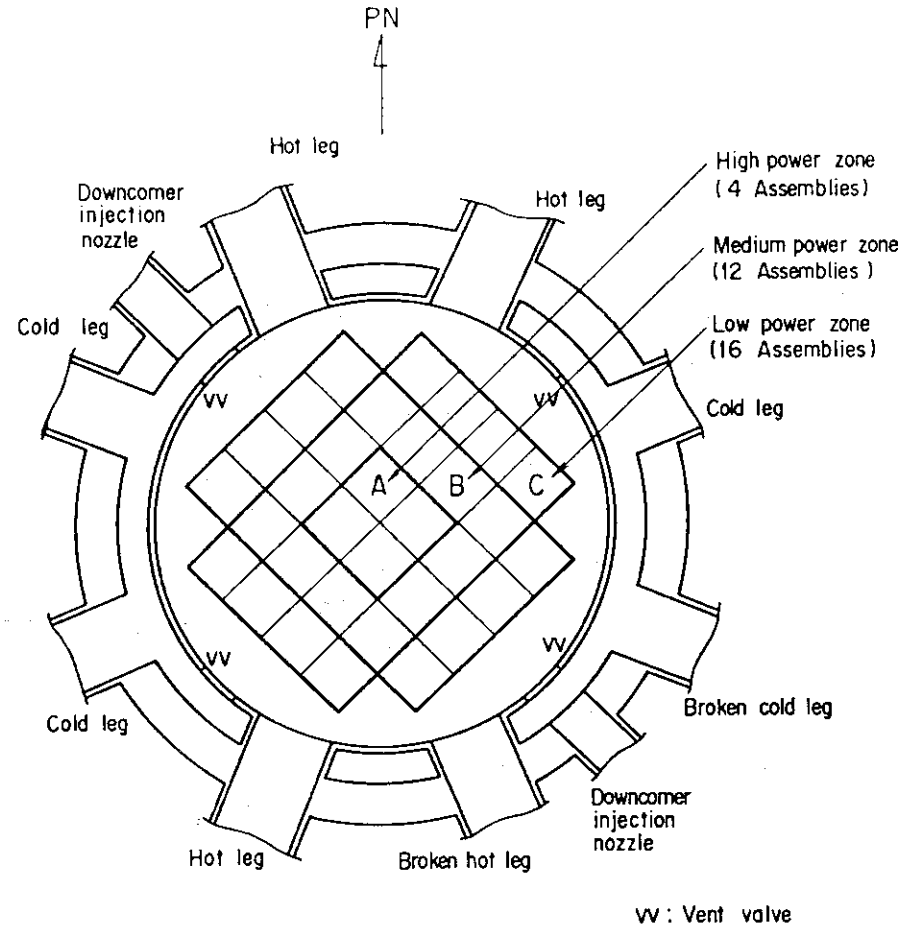

Fig. 2.3 Cross section of CCTF Core-II pressure vessel

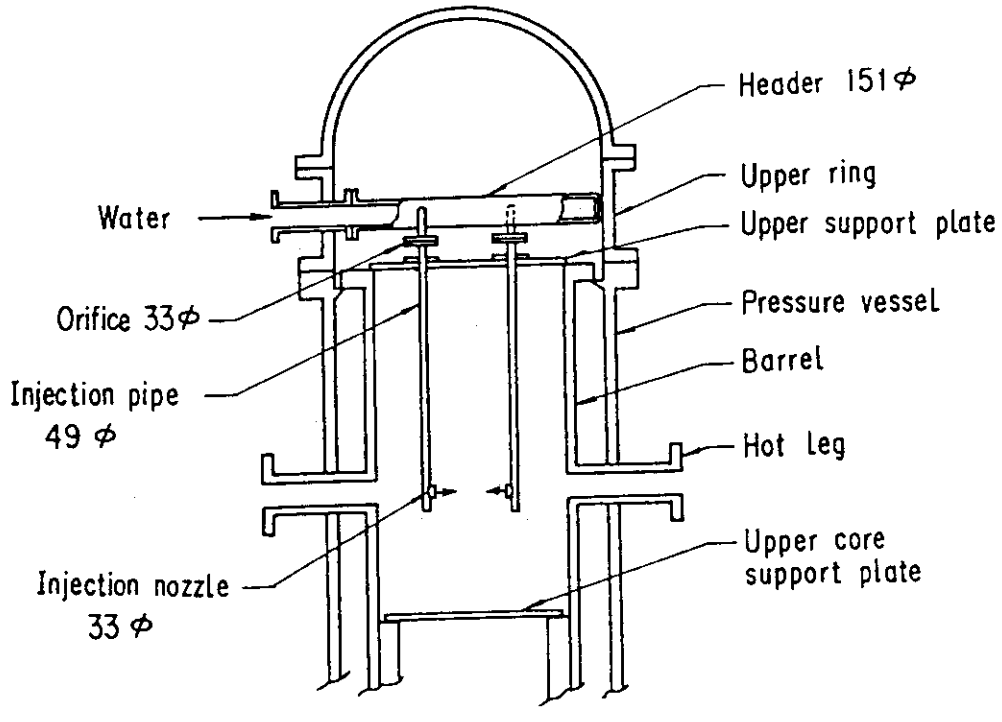

Fig. 2.4 Configuration of upper plenum injection line

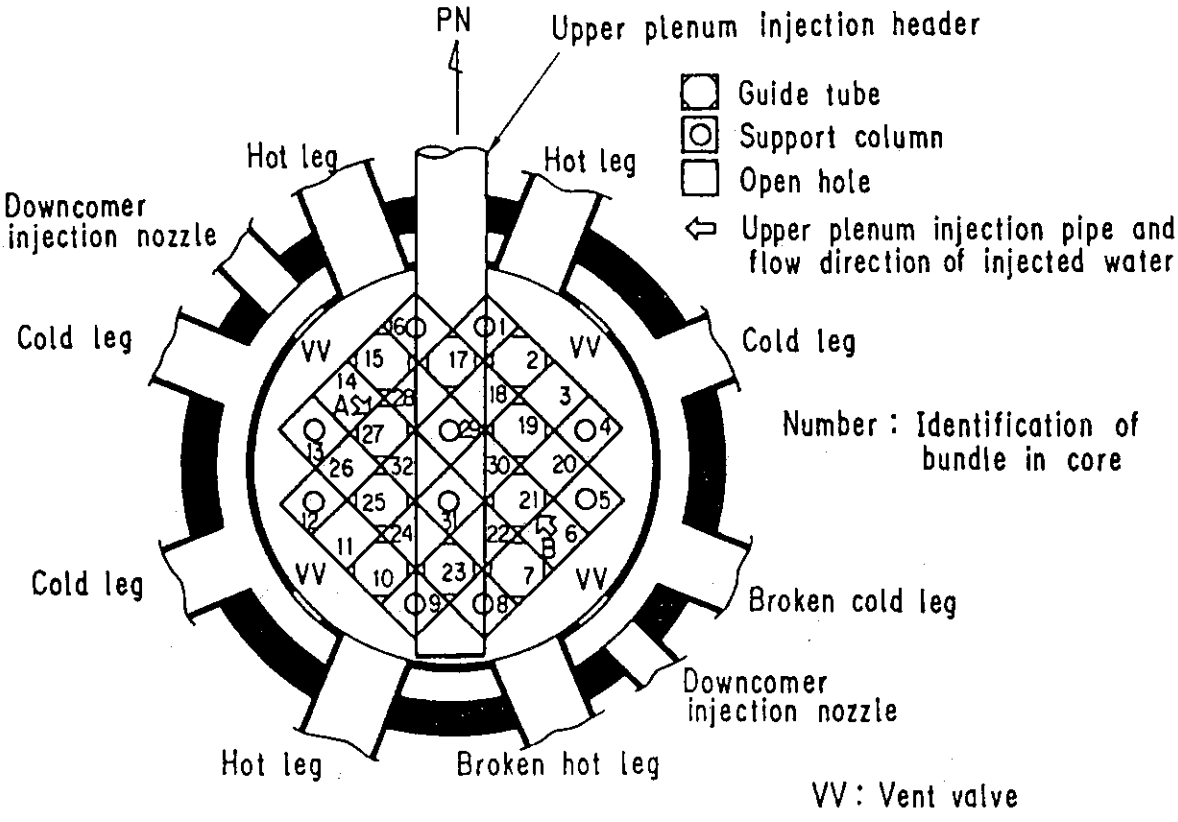

Fig. 2.5 Arrangement and location of upper plenum injection line

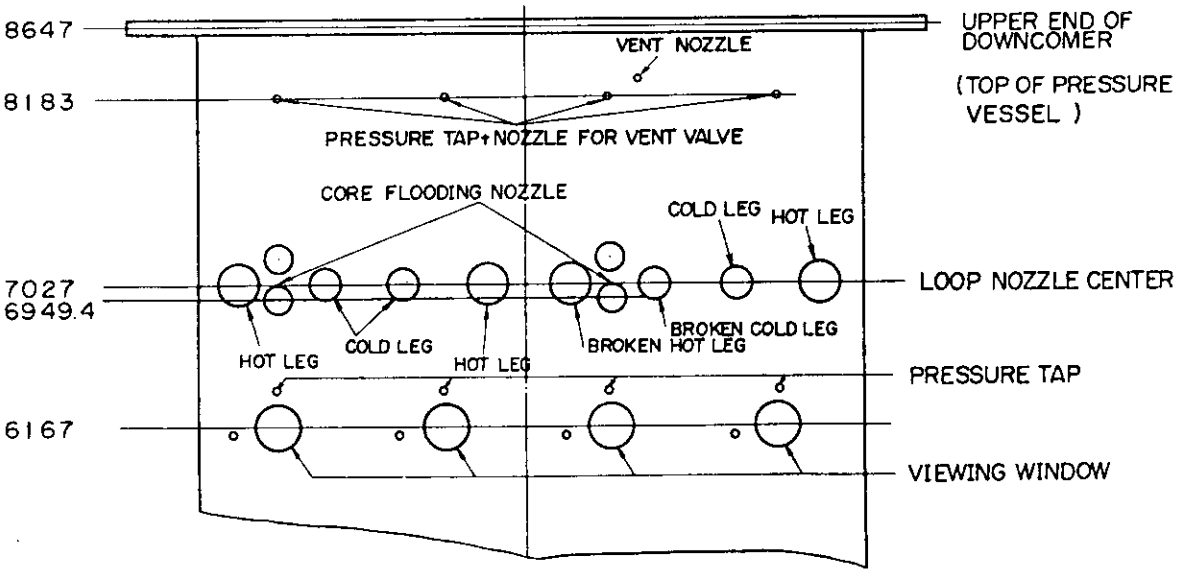

Fig. 2.6 Location of Core Flooding Nozzles

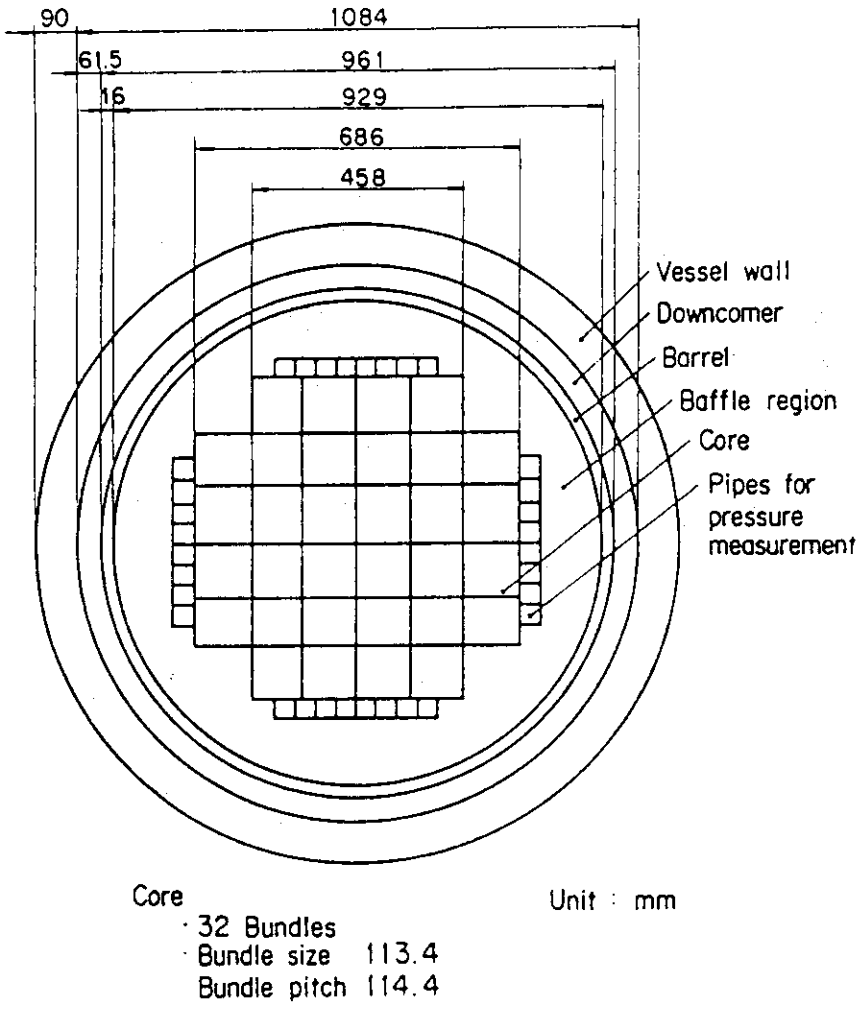

Fig. 2.7 Dimension of CCTF Core-II pressure vessel cross section

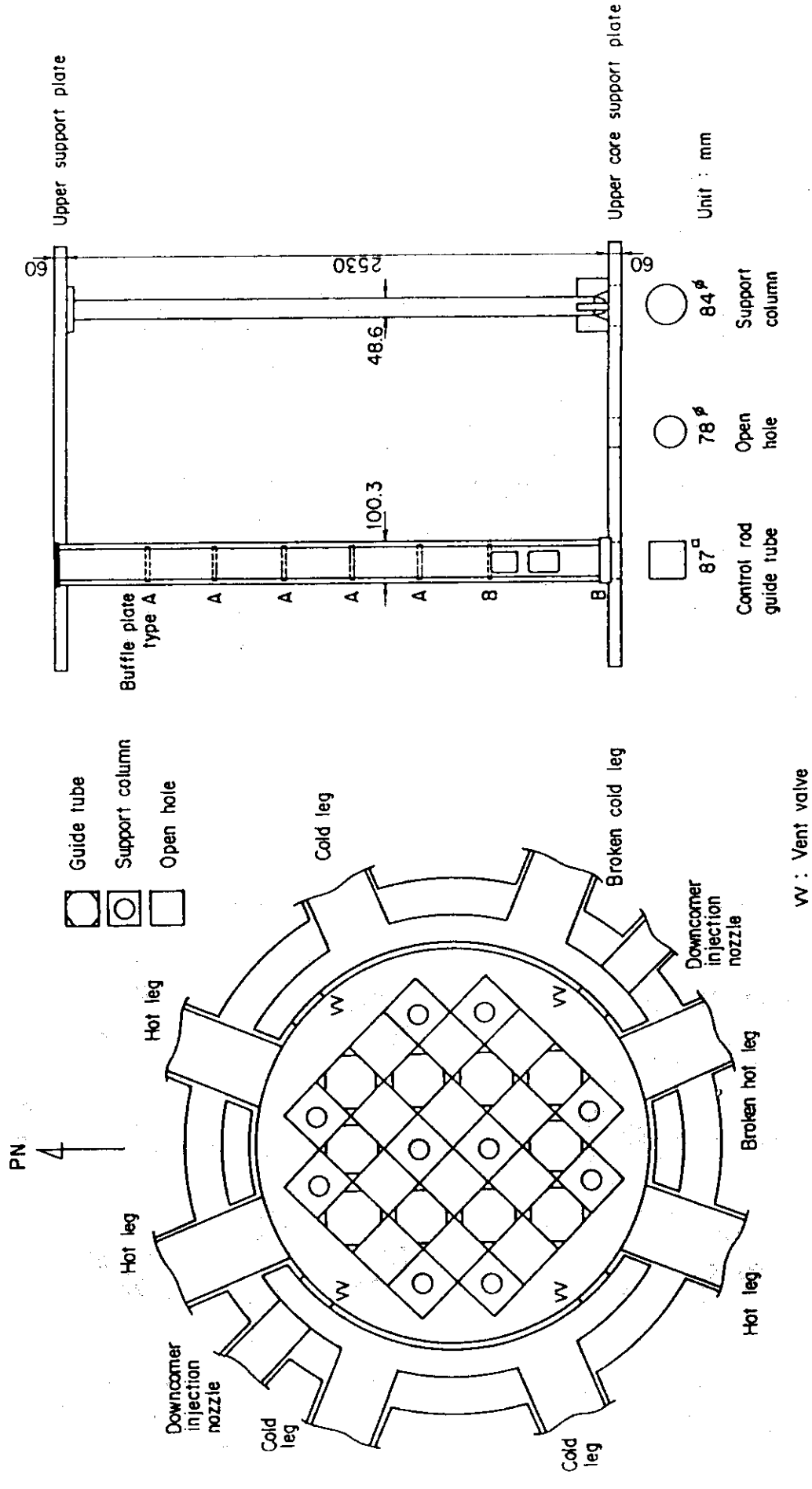

Fig. 2.8 Arrangement of upper plenum internals

Fig. 2.9 Upper plenum internals

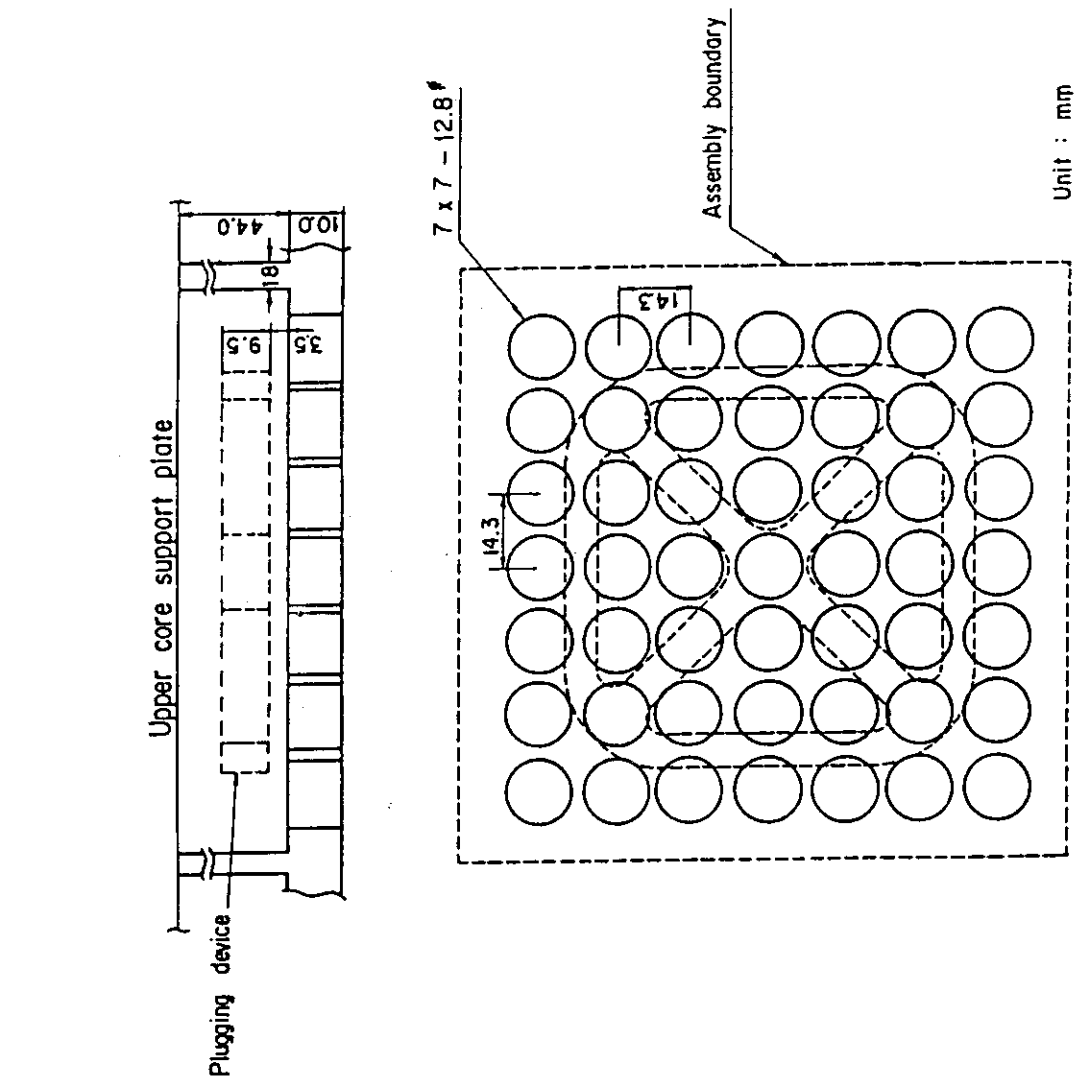

Fig. 2.11 End box

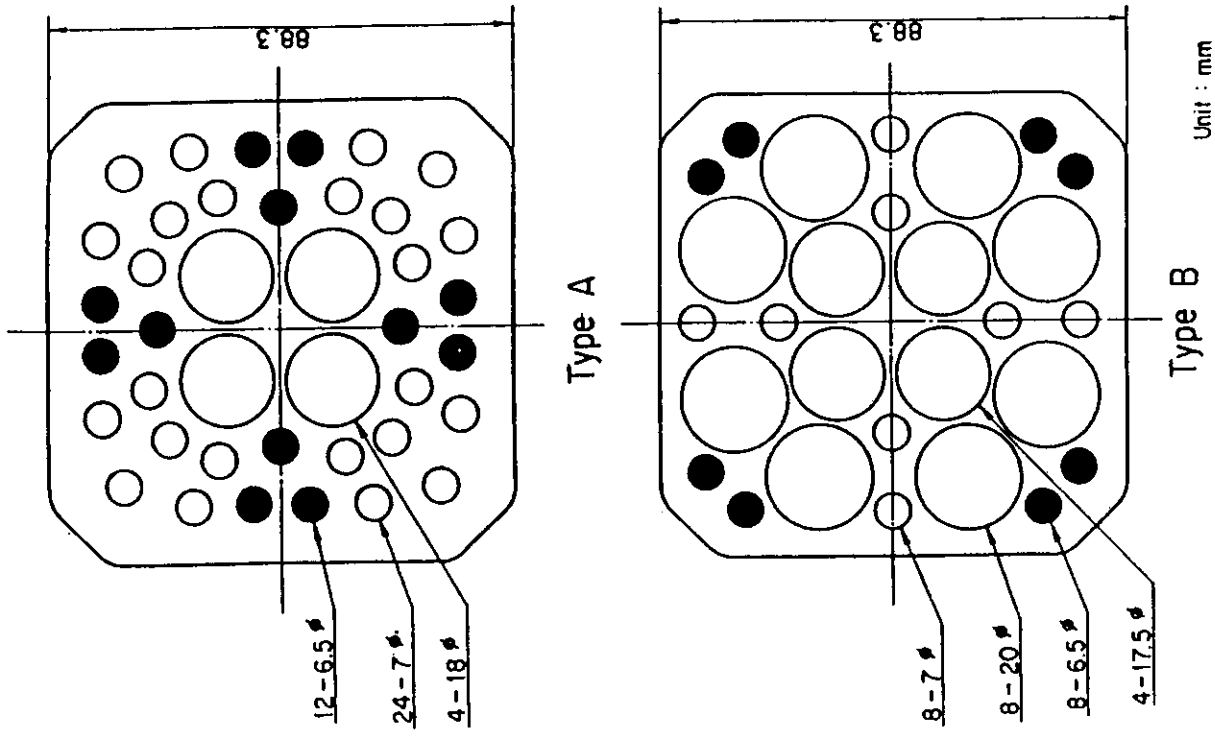

Fig. 2.10 Buffle plates in control rod guide tube

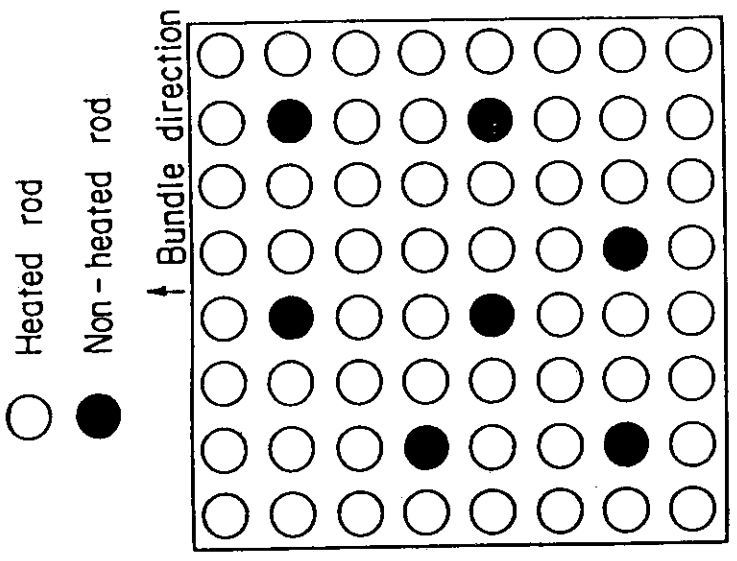

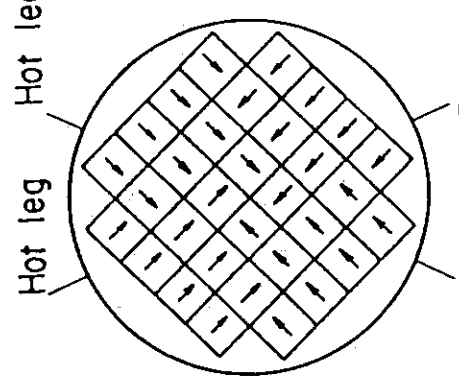

Fig. 2.13 Arrangement of non-heated rods and bundle direction

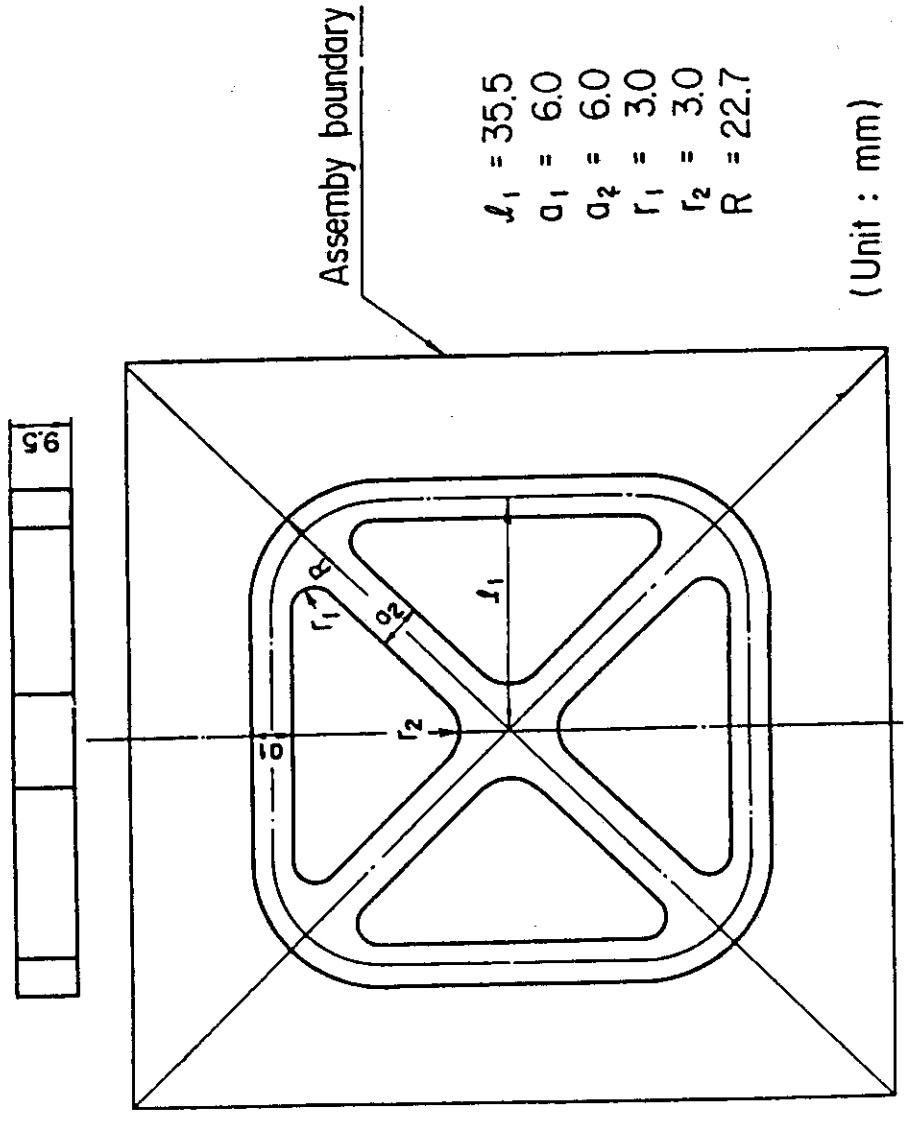

Fig. 2.12 Dimensions of plugging device

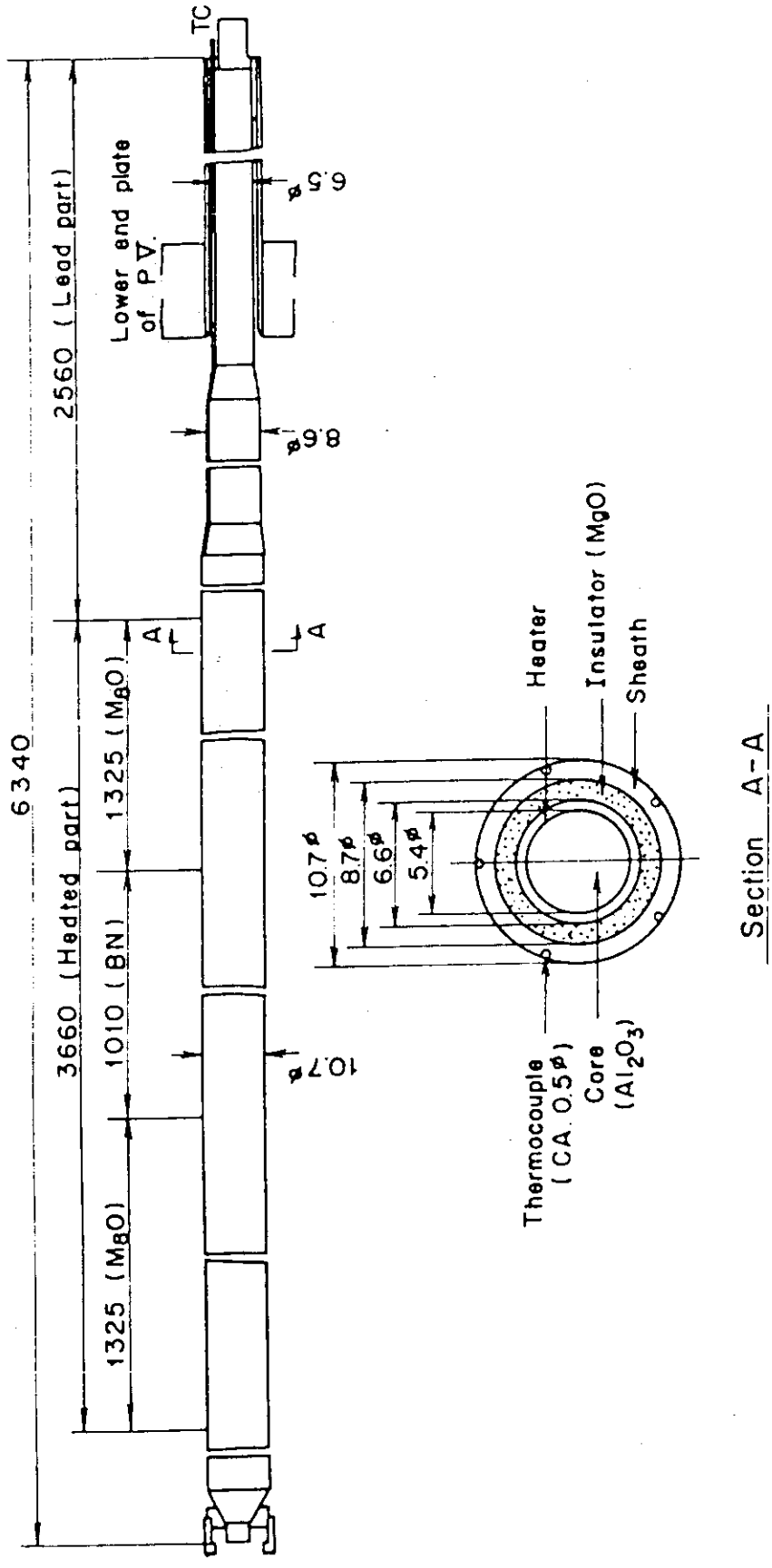

Fig. 2.14 Heater rod

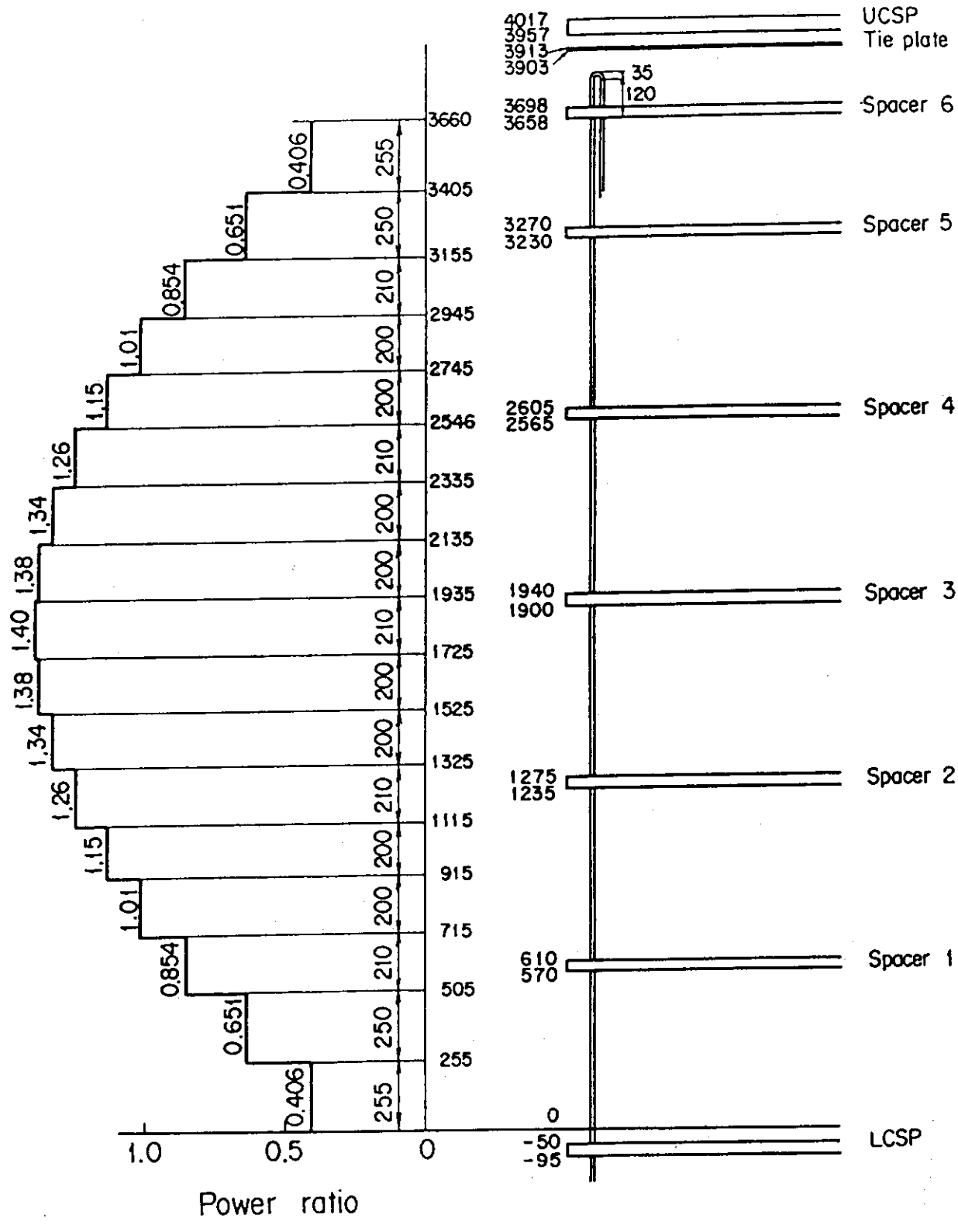

Fig. 2.15 Axial power profile of CCTF Core-II heater rod

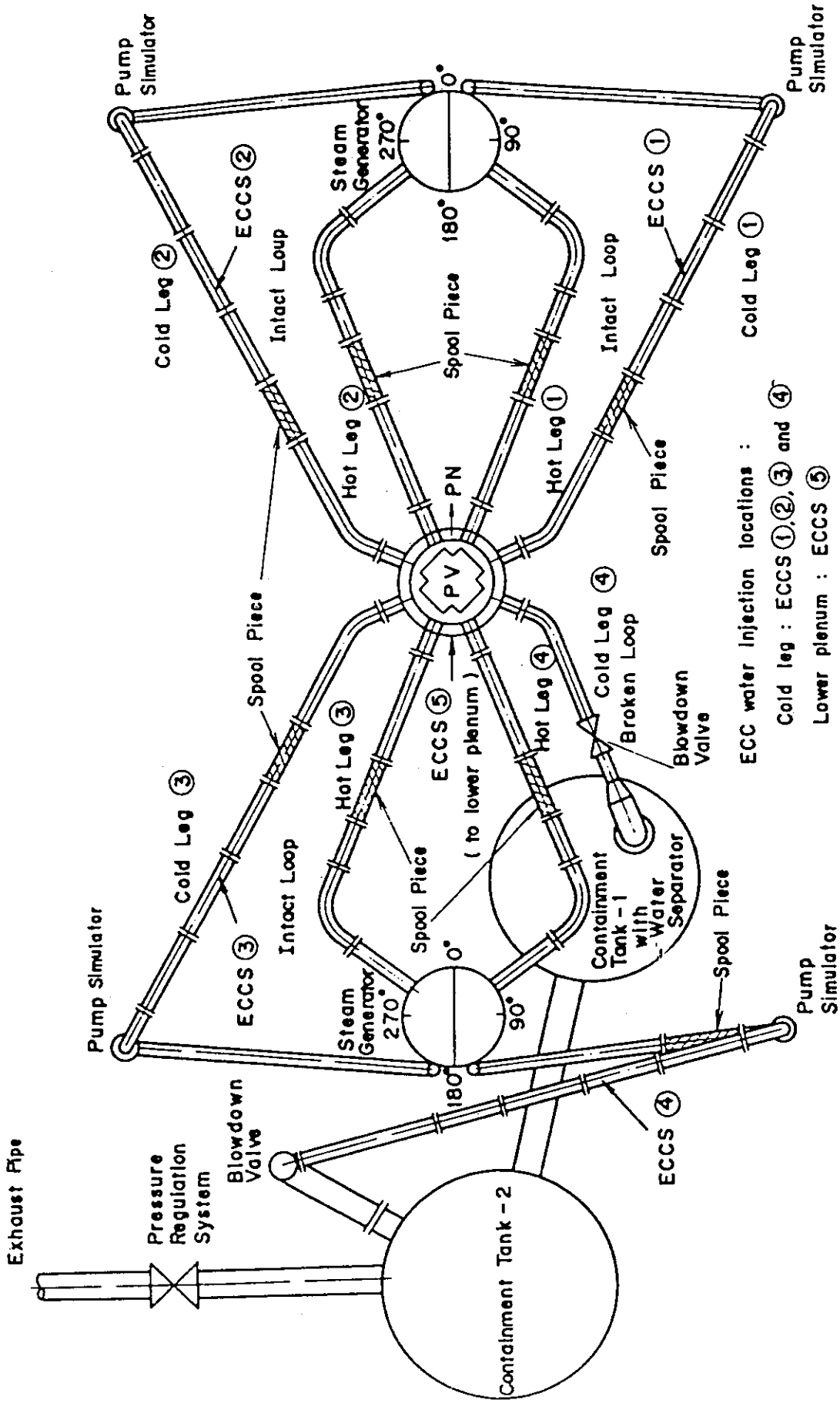

Fig. 2.16 Top view of primary loop pipings

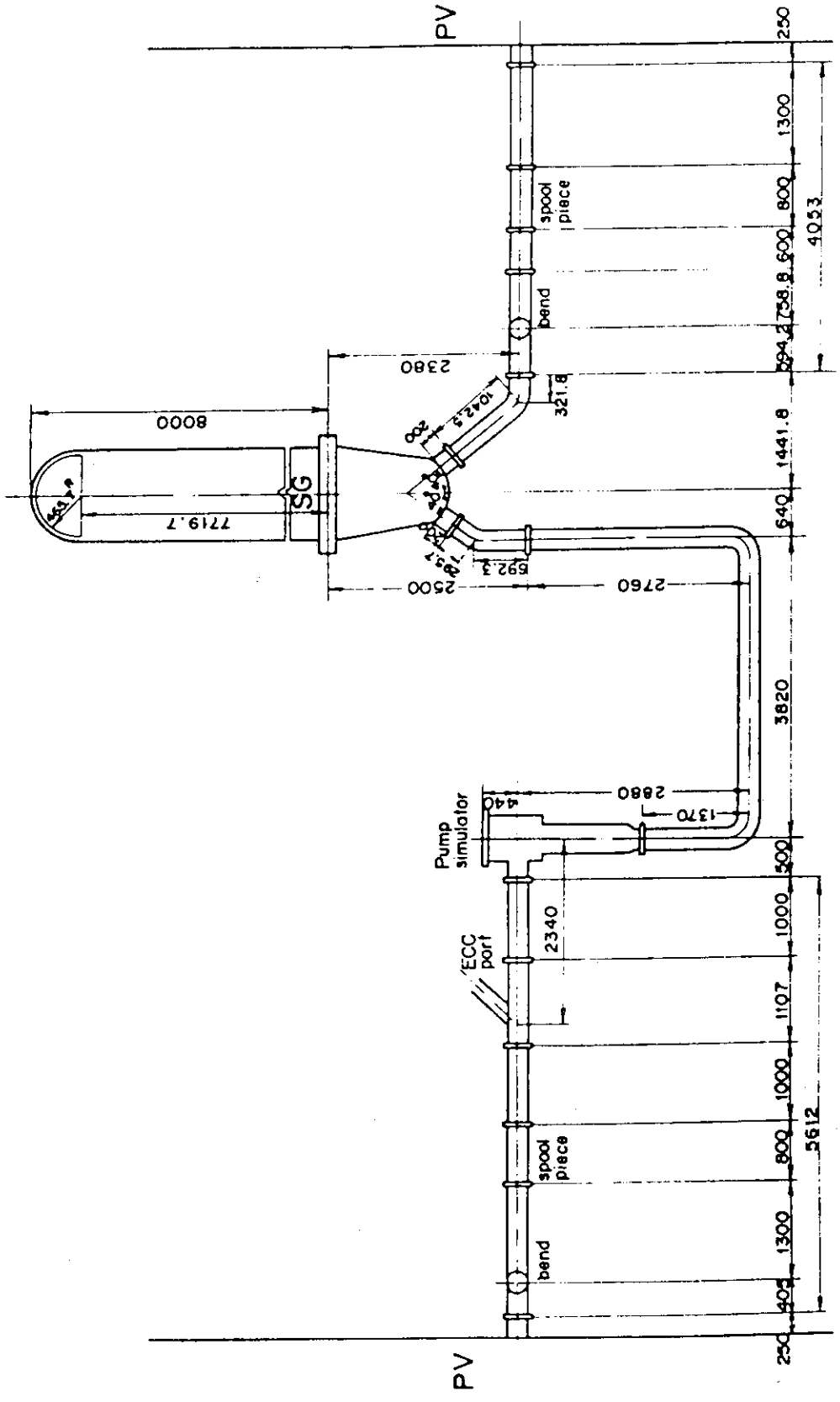

Fig. 2.17 Dimensions of primary loop

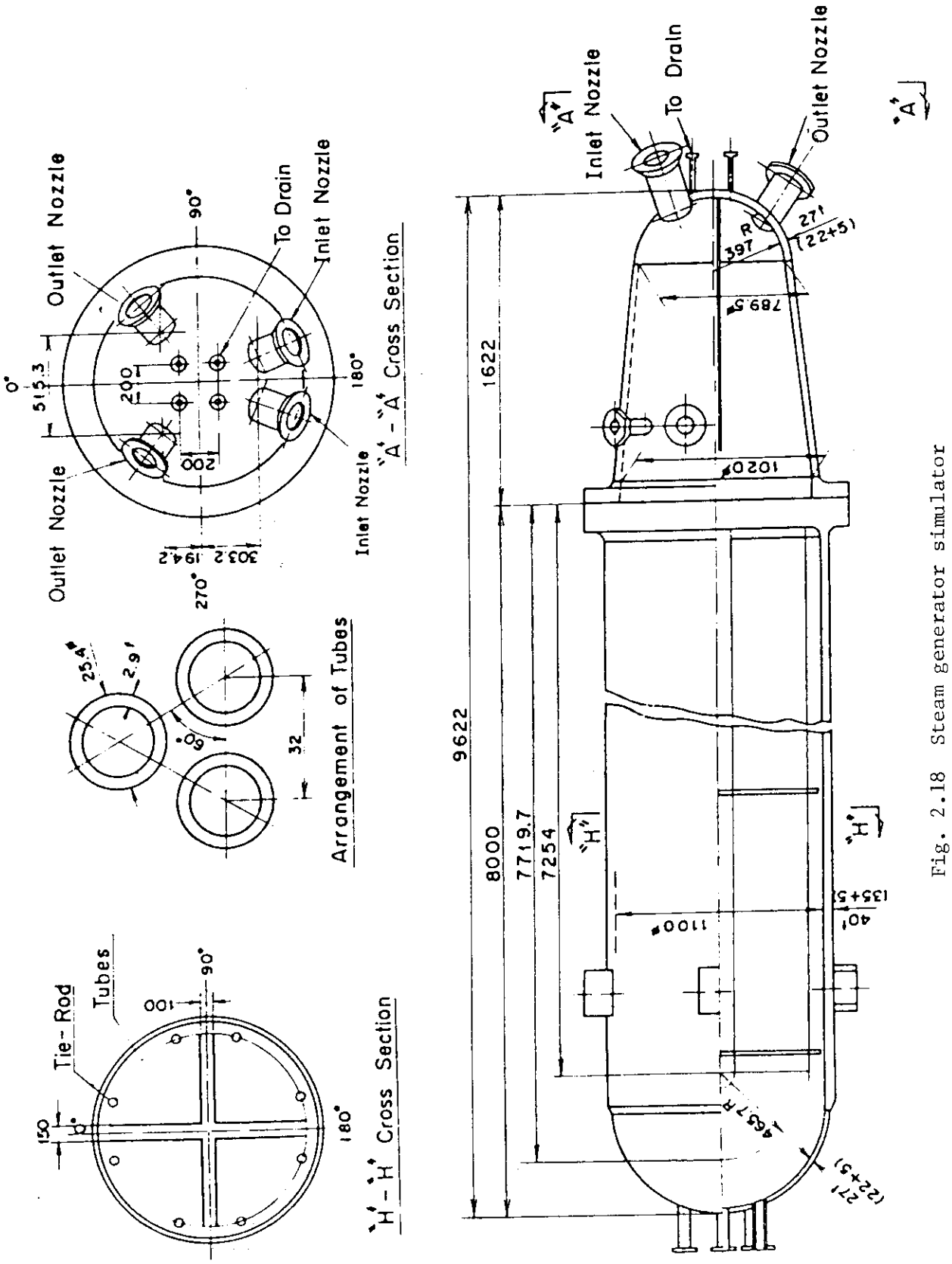

Fig. 2.18 Steam generator simulator

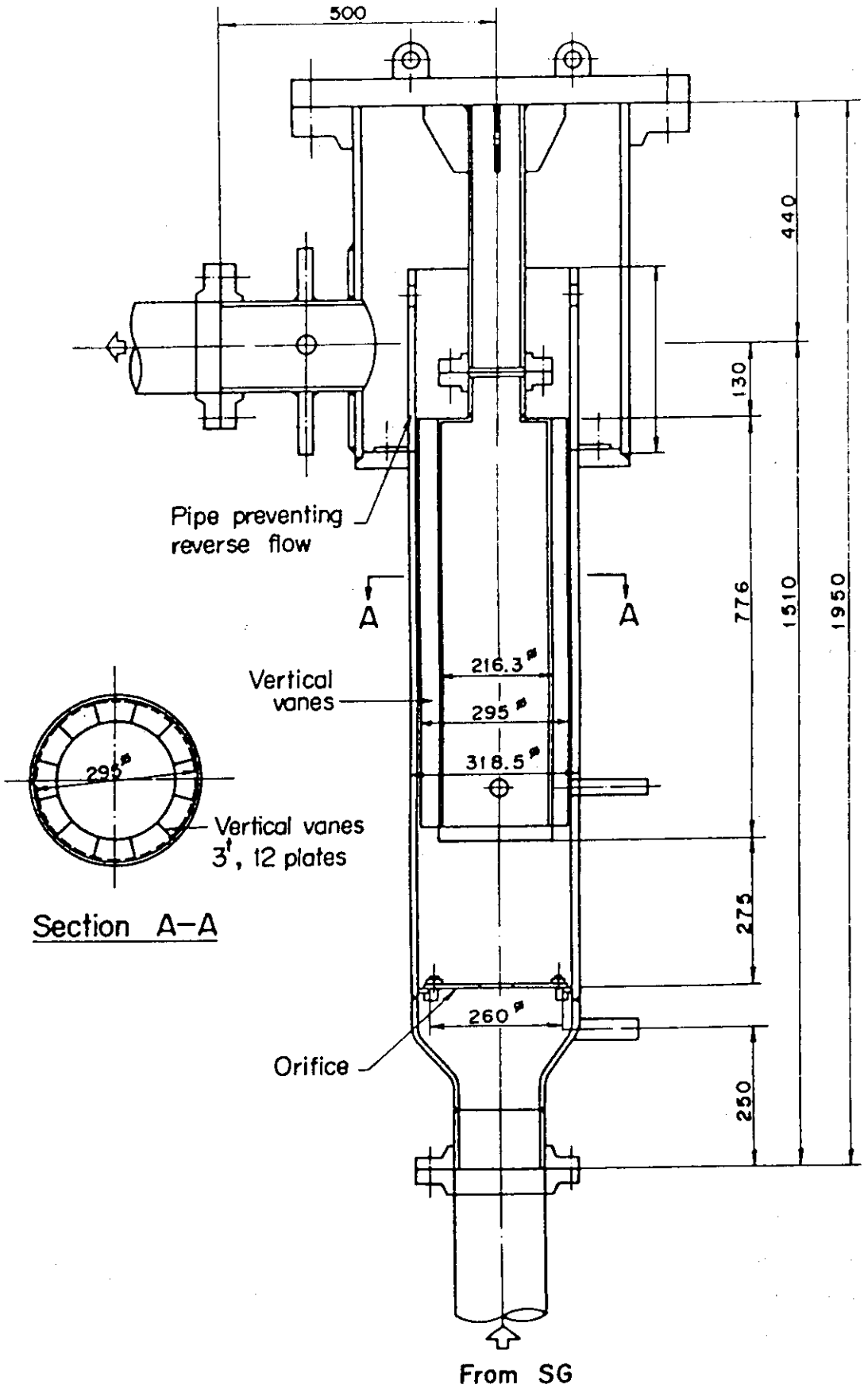

Fig. 2.19 Pump simulator

3. Discussion on Coupling Method between CCTF Test and FLECHT-SET Test

3.1 Review of CCTF Core-I FLECHT-SET Coupling Tests

In the CCTF Core-I test series, three FLECHT-SET coupling tests were performed[5] to investigate difference in thermo-hydrodynamic behavior between in the CCTF and the FLECHT-SET. Comparing these test results with those of the FLECHT-SET tests, the following differences in thermo-hydrodynamic behavior were observed in the CCTF tests[5]:

(1) Large oscillation in the system (see Fig. 3.1)
(2) Larger water head in the core and the downcomer (see Fig. 3.2)
(3) Larger broken loop pressure loss (see Fig. 3.3)
(4) Higher core flooding rate (see Fig. 3.4)
(5) Better core cooling (see Fig. 3.5)

Item (1) above is considered to be caused by overflow of the ECC water from the downcomer to the break, *i.e.* the containment tank 1, through the broken cold leg. In the FLECHT-SET Phase B experiments, the LPCI water injection rates were manually controlled to prevent the subcooled ECC water from overflowing to the break[3],[4]. However, in the CCTF tests, the LPCI water was injected with a constant rate of 0.011 m^3/s and the water overflowed.

The larger water head in the downcomer in item (2) above is considered to result from the higher LPCI injection rate in the CCTF tests, which kept the downcomer to be almost full. The larger water head in the core is considered to be caused by the higher core flooding rate mentioned in item (4).

The larger broken loop pressure loss in item (3) above is attributed to the larger broken cold leg pressure loss, which results from the larger broken cold leg pressure loss coefficient[6] of the CCTF and also the larger overflowing water mass flow rate. The larger broken cold leg pressure loss results in the higher upper plenum pressure and the higher core flooding rate.

The higher core flooding rate in item (4) above is considered to be caused by a combination of a few reasons. They are the larger downcomer water head in item (2), the higher upper plenum pressure and the larger broken cold leg pressure drop mentioned in the previous discussion on item (3).

The better core cooling in item (5) above is mainly attributed to the higher core flooding rate in item (4) and, to some extent, the higher upper plenum pressure mentioned in the previous discussion on item (3). The large oscillation also seems to be the reason[5].

From above discussion, it is concluded that the important points to achieve a better coupling with a FLECHT-SET Phase B experiment are to control the downcomer water head and the system pressure taking account of the difference in the broken cold leg pressure loss coefficient between these two facilities.

3.2 Determination of Coupling Test Conditions

3.2.1 ECC Water Injection Rate

In the FLECHT-SET experiments, the ECC water injection rate was intended to be controlled manually to keep the downcomer water level at 4.27 m (14 feet). Therefore, in the CCTF test, the ECC water injection rates were determined to be controlled manually, if necessary, to keep the downcomer water level at about 4.27 m.

On the other hand, the average core flooding rate for FLECHT-SET 2714B experiment is 1.47 cm/s[5] and this value is corresponding to the injection rate of 3.8×10^{-3} m^3/s in the CCTF. The core flooding rate of 1.47 cm/s is evaluated to produce the steam mass flow rate of 3.6 kg/s at maximum. When this amount of steam flows through the primary loops, the intact, broken and broken cold leg pressure losses are evaluated to be 28.8, 46.4 and 17.6 kPa, respectively, by solving the following equations:

$$\Delta P_B = \Delta P_I + \Delta P_{BCL} \tag{1}$$

$$\dot{m}_T = \dot{m}_B + 3\,\dot{m}_I \tag{2}$$

$$\Delta P_B = \frac{K_B}{2} \cdot \frac{\dot{m}_B^2}{\rho_g \cdot A^2} \tag{3}$$

$$\Delta P_I = \frac{K_I}{2} \cdot \frac{\dot{m}_I^2}{\rho_g \cdot A^2} \tag{4}$$

$$\Delta P_{BCL} = \frac{K_{BCL}}{2} \cdot \frac{(3\,\dot{m}_I)^2}{\rho_g \cdot A^2} \tag{5}$$

$$K_B = K_I = 25, \qquad K_{BCL} = 1.7^{[6]} \tag{6}$$

where, symbols ΔP, $\dot{m}$, K, ρ_g and A are differential pressure, mass flow rate, K-factor (pressure loss coefficient), steam density and flow area, respectively. Subscripts B, I, BCL and T mean broken loop, intact loop, broken cold leg and loop total, respectively. The downcomer water head is nearly equal to the summation of the core water head and the intact loop pressure loss (ΔP_I). Since the core water head is expected to be less than 1.2 m in the CCTF test for the above LPCI injection rate of 3.8×10^{-3} m^3/s, the downcomer water head is evaluated to be less than 4.14 m (ΔP_I = 28.8 kPa). Therefore, when the LPCI injection rate is 3.8×10^{-3} m^3/s, the downcomer water level is expected to be less than 4.27 m and the control of the injection rate is expected to be unnecessary.

Based on the above discussion, the LPCI injection rate was determined to be 3.8×10^{-3} m^3/s in the present CCTF test. Acc injection rate and duration were determined to be 0.109 m^3/s and 11 s, respectively, simulating those of the concerned FLECHT-SET experiment.

3.2.2 Containment Pressure

Since the broken cold leg pressure loss coefficients are different between the CCTF and the FLECHT-SET Phase B facility, the upper plenum pressure in the CCTF is expected to be higher for the same core outlet steam mass velocity. In the FLECHT-SET 2714B experiment, average upper plenum pressure was about 175 kPa. Therefore, the containment pressure in the CCTF test was determined to be 134 kPa, subtracting the evaluated broken loop differential pressure of 41 kPa for the steam mass flow rate of 3.42 kg/s (assuming 5% water accumulation in the system).

3.2.3 Core Power and Initial Clad Temperature

For determination of core power and initial clad temperature, the following criteria were introduced:

(1) Average linear power densities are the same in both tests

(2) Peak linear power densities are the same

(3) Initial clad temperatures at the peak power section are the same

In the FLECHT-SET 2714B experiment, the average linear power density, the peak linear power density and the initial clad temperature at the peak power section were 1.383 kW/m, 2.756 kW/m and 866 K, respectively. Therefore, in the present CCTF test, the average linear power density was determined to be 1.383 kW/m based on the criterion (1) above. The peak linear power density was determined to be 2.756 kW/m based on the criterion (2) above. The initial clad temperature at the peak power section was determined to be 823 K, which is lower by 43 K than that of FLECHT-SET value. This determination was made based on the following consideration: At the peak power section in the FLECHT-SET experiment, only two initial temperature data out of six showed 866 K, whereas the others showed the temperatures around 816 K. Furthermore, the data whose transients were shown in the data report[4] belong to the latter group. Also, in the CCTF tests, there exists usually a deviation of about 10 K in the initial clad temperatures at the peak power section. Therefore, the initial clad temperature of 823 K (550 ^{o}C) was expected to result in nearly the same initial clad temperature as those of the FLECHT-SET experiment on an average.

In the CCTF Core-II, achievable maximum linear power density is 1.067 kW/m for the lowest power rods. Therefore, the linear power densities for the high, medium and low power rods or regions became 1.969, 1.610 and 1.067 kW/m, respectively (The axial peaking factor of a CCTF Core-II rod is 1.4 as described in Section 2.1.2, whereas 1.66 for the FLECHT-SET). Therefore, the radial power distribution factors for the present test are 1.423 : 1.164 : 0.771, whereas almost flat in the FLECHT-SET experiment, although there is local power distribution of 1.2 : 0.97 : 0.92 rather than the radial power distribution in the FLECHT-SET.

3.2.4 Other Test Conditions

The other test conditions for the present test, such as the ECC water

injection location and temperature, were determined to be the same as those of the FLECHT-SET experiment. That is, the ECC water injection location was the lower plenum and the ECC water temperature was 340 K.

A comparison of the CCTF with the FLECHT-SET facility is summarized in Table 3.1. Axial power profile of a heater rod in both the facilities are compared in Fig. 3.6.

Table 3.1 Comparison of CCTF with FLECHT-SET facility

Item	CCTF	FLECHT-SET
Scaling factor of core flow area	1/21.4	1/370
Core		
Axial peaking factor	1/49	1.66
Ratio of unheated rod	0.109	0.09
Downcomer		
Configuration	Annulus	Pipe
Upper plenum		
Scaling factor of cross section	~ 1/10	~ 1/18
Internals	Simulated with 8/15 scaled internals	Extention of heated rod
Primary loops		
Quantity of loops	3 Intact+1 Broken loops	1 Intact+1 Broken loops
K-factor of pump	~ 15	~ 14.7[1)]
K-factor of other portion	~ 10	8.9[2)]
Scaling of broken cold leg nozzle	1/21.4	1/32.7

1) Including cold leg flow resistance (original value, 20.53, was devided by 1.4).

2) Excluding inlet plenum cross over.

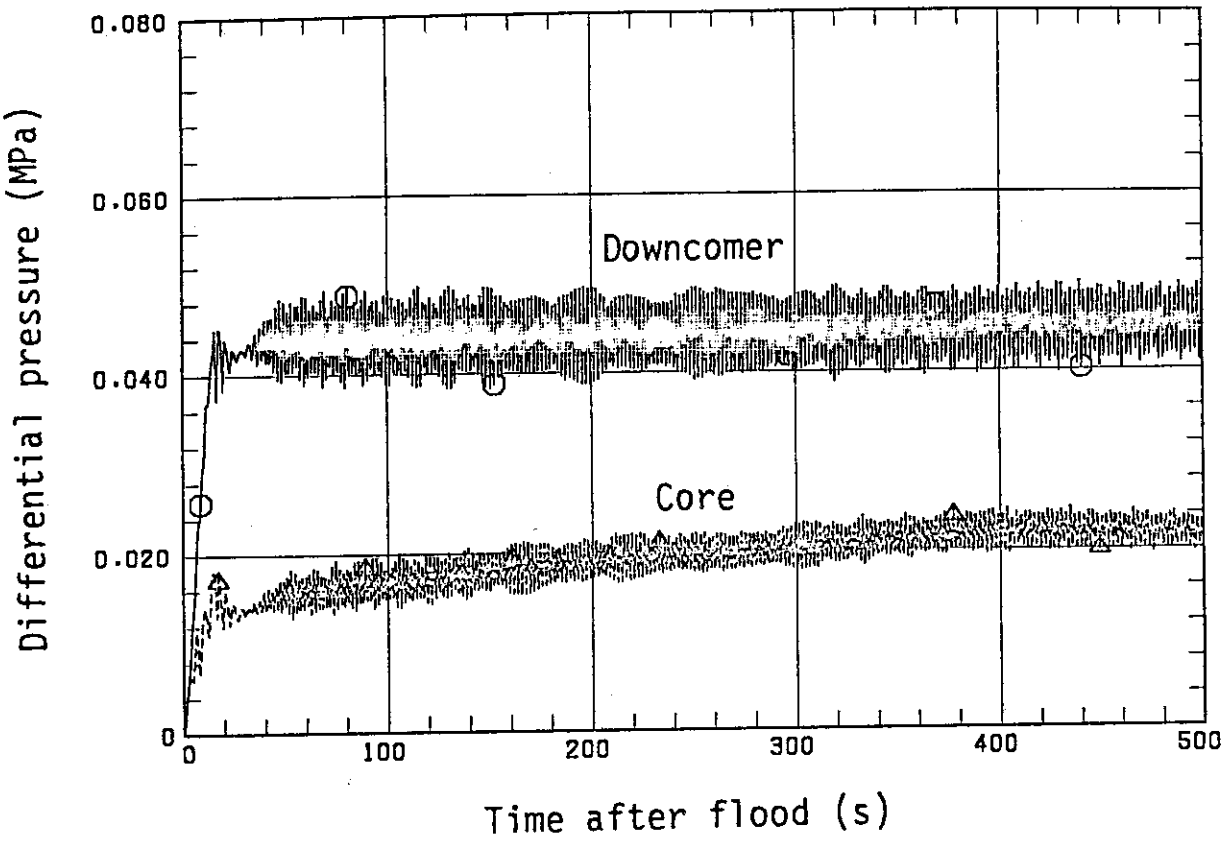

Fig. 3.1 Differential pressures in downcomer and core (ref. 5)

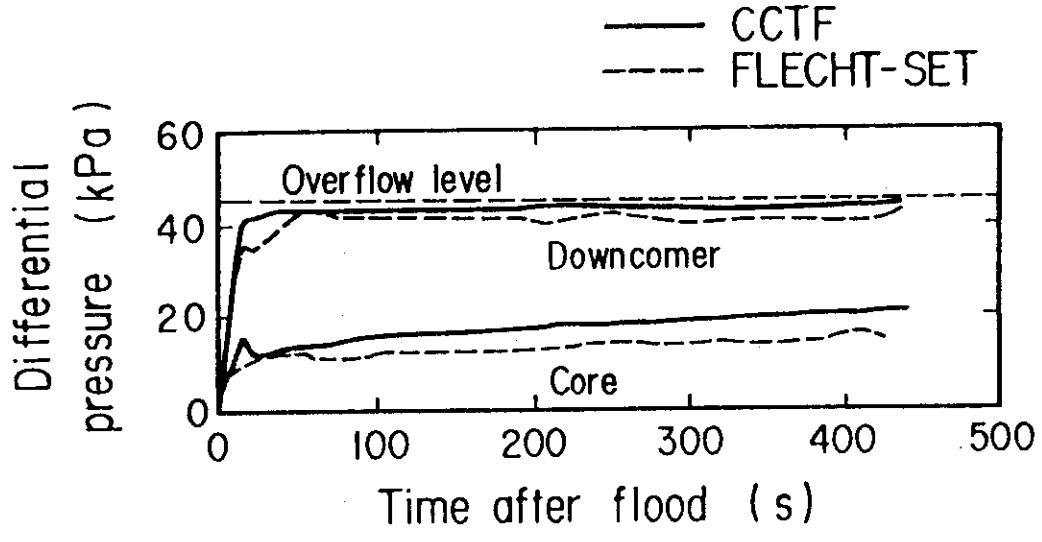

Fig. 3.2 Comparisons of core and downcomer differential pressures (ref. 5)

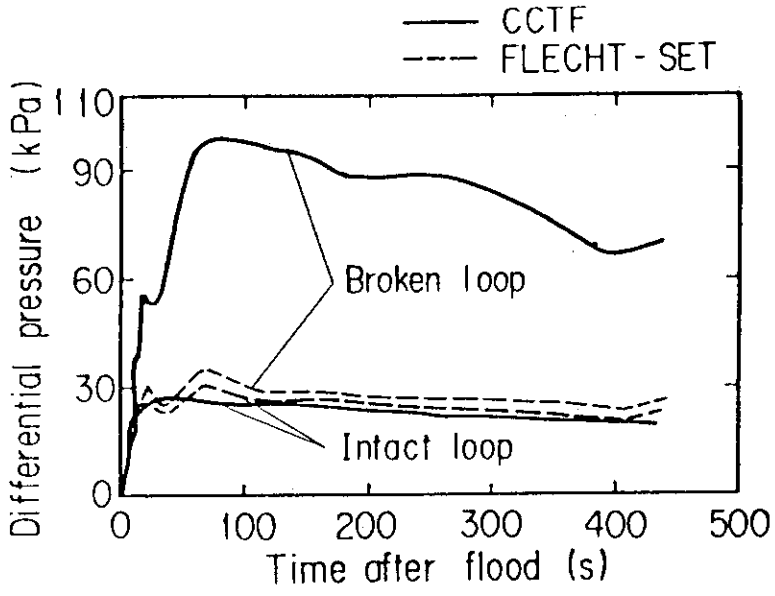

Fig. 3.3 Comparisons of intact and broken loop differential pressures (ref. 5)

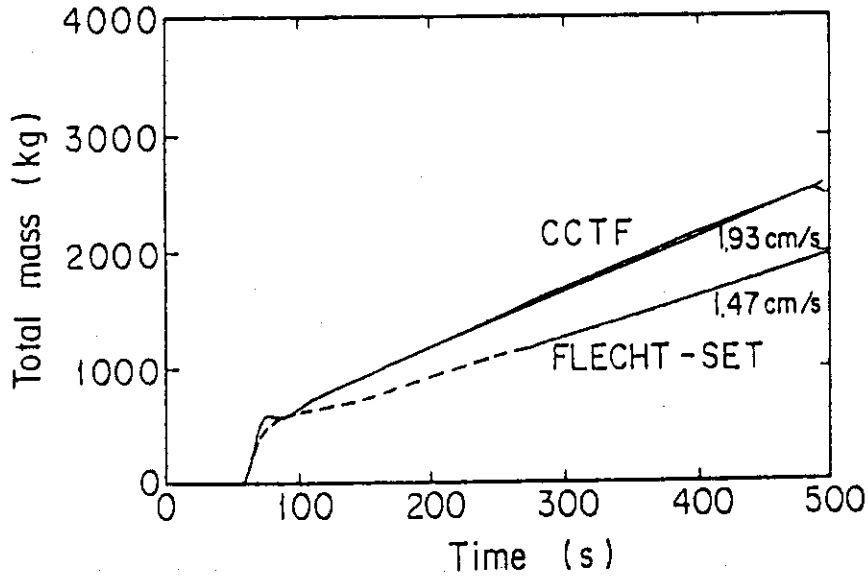

Fig. 3.4 Comparison of time-integration of core flooding mass flow rate (ref. 5)

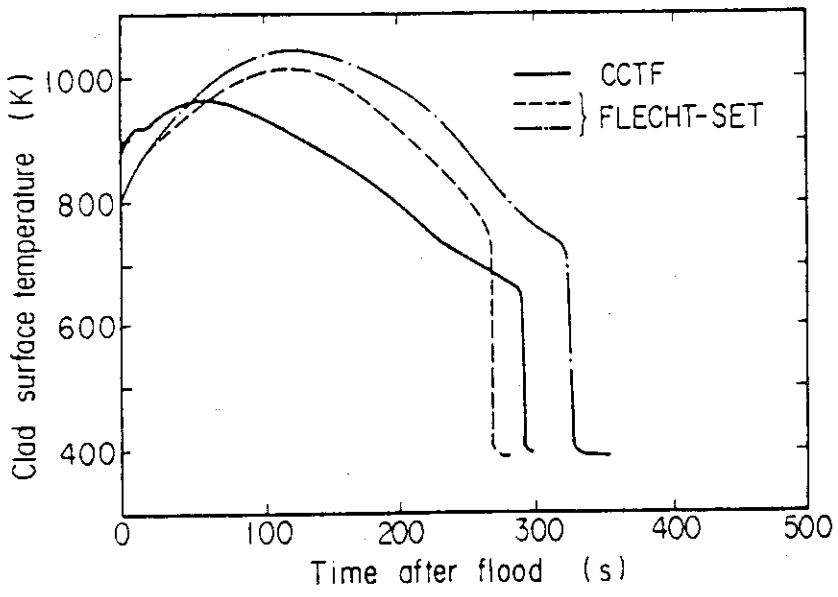

Fig. 3.5 Comparison of rod surface temperature at peak power location (ref. 5)

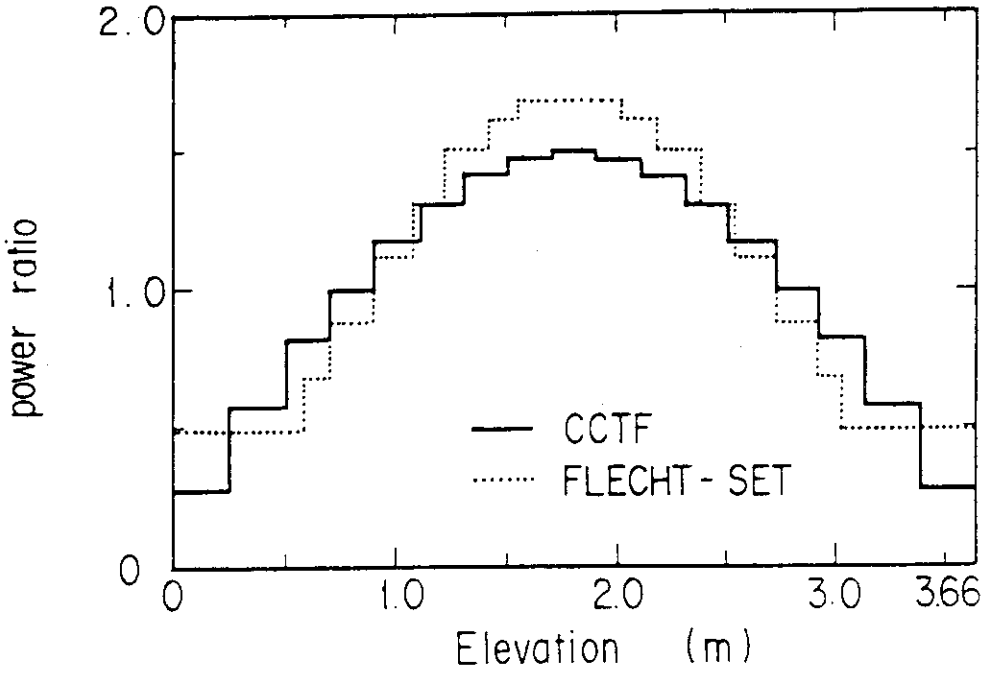

Fig. 3.6 Comparison of axial power profile of heater rod

4. Test Results and Discussion

4.1 Comparisons of Measured Test Conditions between Tests

In this section, measured test conditions of both the tests are compared and investigated as a basis of the discussion in the following sections.

Figures 4.1 and 4.2 show comparisons of the ECC water injection rate and the downcomer water head, respectively. The ECC water injection rates are normalized with each core flow area. In the CCTF test, Acc injection was longer and the duration was 21 s, whereas it was 11 s in the FLECHT-SET experiment. The longer Acc injection duration in the present test is attributed to rather long closing time of the injection line valve. This longer Acc injection resulted in the higher downcomer water head shown in Fig. 4.2, which indicates the overflow of the ECC water to the break in the initial period. To stop this overflow, LPCI injection rate was reduced till 300 s. The minimum injection rate was 1.43×10^{-3} m^3/s at around 170 s. Except for the initial period, the downcomer water head is less than the overflow level value. In both the tests, there observed oscillation of the data for the initial period of about 100 and 150 s for the CCTF and the FLECHT-SET tests, respectively. These oscillations are not drawn and only the mean values are presented in the figures of this chapter. The original data with oscillation are presented in Appendix B of this report for the CCTF test and in references 3 and 4 for the FLECHT-SET.

Figure 4.3 shows the comparison of the time-integration of core flooding rate, which is evaluated based on the mass balance. Since the evaluated core flooding rate shows the oscillatory behavior, the time-integration is presented. Gradients of these curves give average core flooding rates. This figure shows that the agreement is good except for 140 $\sim$ 250 s and after 430 s. However, judging from the core water head shown in the following section (Fig. 4.8), the core flooding rate during the initial 20 s is inferred to be much higher in the CCTF test than in the FLECHT-SET experiment. Since the accuracy of the evaluated core flooding rate is not expected to be good in the Acc injection period, the evaluated value for the CCTF test shown in Fig. 4.3 is considered to be underestimated in the initial period. The decrease of core flooding rate for 140 $\sim$ 250 s corresponds to the reduction of LPCI injection rate shown in Fig.

4.1. Therefore, the core flooding rate is considered to be higher during the initial 20 s in the CCTF test and becomes lower for 140 ∿ 250 s, but during the other time before 430 s the core flooding rate is considered to be nearly identical to that in the FLECHT-SET experiment.

Upper plenum and containment tank pressures are compared in Figs. 4.4 and 4.5, respectively. Average value of the upper plenum pressure is about 200 kPa for the CCTF, whereas it is about 175 kPa for the FLECHT-SET. The difference is caused by the higher CCTF containment tank pressure as recognized in Fig. 4.5. Although the set value was 134 kPa as described in Section 3.2.2, achieved value varies between 130 kPa and 166 kPa and is higher than the set value by about 20 kPa on an average. This higher containment tank pressure is attributed to the insufficient capability of the pressure control system of the CCTF at the low pressure. Anyway, the magnitude of difference in the pressure is considered to give a little effect on reflooding behavior.

The other test conditions are compared in Table 4.1. It shows good agreement of test conditions between the two tests except for the maximum initial clad temperature. The reason for this difference is already described in Section 3.2.3.

Although the ECC water temperatures were the same and 340 K in both the tests, core inlet fluid temperature of the CCTF test is a little higher during 20 ∿ 130 s as shown in Fig. 4.6. The difference is only 15 K at most. The core inlet fluid subcooling is shown in Fig. 4.7 for the CCTF test and that for the FLECHT-SET experiment is around 50 K. Therefore, the difference in core inlet subcooling is around 10 K, which is considered to give little effect on core cooling.

4.2 Overall System Thermo-hydrodynamic Behavior

In this section, the overall thermo-hydrodynamic behavior in the primary system is compared and discussed.

Core water heads are compared in Fig. 4.8. They are obtained by directly converting the differential pressures to the water heads. As shown in the figure, the value for the CCTF is significantly larger in the initial period. This is attributed to the higher downcomer water head (Fig. 4.2) resulted from the longer Acc injection (Fig. 4.1). However, the core water heads of both tests become close gradually and behave nearly the

same from 200 through 400 s. Therefore, if the Acc injection duration for the CCTF test were the same as for the FLECHT-SET, the core water heads are expected to be nearly identical in both the tests through the whole transient.

Figures 4.9 and 4.10 show the intact and broken loop differential pressures, respectively. The intact loop differential pressures are nearly the same except for the initial period. The broken loop differential pressure is higher in the CCTF test. This is attributed to the higher pressure loss in the broken cold leg of the CCTF, as described in Sections 3.1 and 3.2. Expected intact and broken loop differential pressures are 28.8 and 46.4 kPa at maximum, respectively, as presented in Section 3.2.1. They are in good agreement with the experimental results of Figs. 4.9 and 4.10, except for the period till 100 s for the broken loop differential pressure. The significantly large broken loop differential pressure in this period is attributed to the significantly large broken cold leg pressure loss caused by overflow of downcomer water to the break[6].

Therefore, overall system thermo-hydrodynamic behavior in the present CCTF test is considered to be similar to that for the FLECHT-SET 2714B experiment except for the initial period.

4.3 Core Thermo-hydrodynamic Behavior

The core water heads are presented in Fig. 4.8 and explained in the previous section. In order to investigate the axial core water distribution, void fractions at six sections of the core are compared in Fig. 4.11. They are obtained from the differential pressure data neglecting frictional and accelerational losses for both the CCTF and the FLECHT-SET. Void fractions in the initial period of about 20 s are significantly lower in the CCTF test at every section. This behavior is corresponding with those of the ECC water injection rates (Fig. 4.1) and the core water heads (Fig. 4.8).

Difference in axial void fraction distribution is observed between the two tests above 1.83 m. That is, the void fractions above 1.83 m elevation are nearly the same in the CCTF, whereas it becomes higher at the higher section in the FLECHT-SET. This difference of characteristic is typical one between the CCTF test and the FLECHT series experiments and is described more in detail in Ref.11. The reason for this difference has not

clarified yet and is under investigation. However, the other typical characteristic observed in the CCTF tests, that the void fractions start to decrease at the upper part of the core from the beginning of the transient, is also observed in the FLECHT-SET. Since this characteristic has more influence on core cooling than the other, the core cooling behavior of the FLECHT-SET experiment is expected to be more similar to that of the CCTF test than that of the FLECHT series experiments.

Rod surface temperatures are compared in Figs. 4.12 and 4.13 for 1.83 and 2.44 m elevations, respectively. At 1.83 m, data for the peak power rods are shown and their peak linear power densities are the same (2.76 kW/m). At 2.44 m, the linear power density for the CCTF test is 2.02 kW/m, whereas 2.16 kW/m for the FLECHT-SET. The heat transfer coefficients for the rod surface temperatures shown in Figs. 4.12 and 4.13 are presented in Figs. 4.14 and 4.15, respectively.

As recognized from Figs. 4.12 and 4.14, the core cooling is significantly better in the CCTF test at 1.83 m elevation. The reasons for this better core cooling is considered to be the heat transfer enhancement in the higher power region of the core, which has been observed in the tests[7],[8] with the CCTF and the Slab Core Test Facility (SCTF)[1]. In these tests, it has been observed that the heat transfer coefficient in the higher power region is higher when the core radial power distribution exists. For the present CCTF test, there exists a considerable steep radial core power distribution (1.42 : 1.16 : 0.77). The heat transfer enhancement in the higher power region is shown in Figs. 4.16 and 4.17 for 1.83 and 2.44 m elevations, respectively. The heat transfer enhancement is observed to be much more at 1.83 m elevation than at 2.44 m elevation. This tendency is the same as observed in other CCTF tests[7]. The enhancement is no longer noticeable at 3.05 m elevation.

Since the effect of the core radial power distribution is small above 2.44 m elevation, the direct comparison of core cooling between the CCTF and the FLECHT-SET tests is to be performed above 2.44 m elevation. Figures 4.13 and 4.15 show this direct comparison at 2.44 m elevation. Figure 4.15 shows that the heat transfer coefficients are nearly identical between the two tests. It should be noted that the effect of the difference in the Acc injection is also small at this elevation. Therefore, it is suggested that the core cooling is expected to be almost the same in the two tests, if there is no difference in the core boundary conditions

and the core radial power distribution between them.

On the other hand, in the FLECHT-SET experiment, this kind of heat transfer enhancement was neither reported[3] nor found[4]. This is considered to be due to the difference in the core radial power distribution between the two tests. In the CCTF test, the radial power distribution is achieved in bundle-wise and also the power profile is steep (1.42 : 1.16 : 0.77), whereas in the FLECHT-SET the distribution is rather local one in rod-wise manner and the power profile is not so steep (1.2 : 0.97 : 0.92)[3].

Figure 4.18 shows the quench front envelopes. In this figure, CCTF data are shown for two different power rods. One is the peak power rod with the rod average linear power density of 1.97 kW/m. The other is 1.61 kW/m, which is close to the peak power rod of the FLECHT-SET, *i.e.* 1.66 kW/m. This figure indicates that the quench front propagates faster in the CCTF up to about 2.5 m.

Since the boundary conditions for the core thermo-hydrodynamic behavior are not identical in the two tests, the heat transfer coefficients of the core are compared with the calculated results of a heat transfer coefficient correlation, in addition to the direct comparison previously performed. The heat transfer coefficient correlation used here was developed for the saturated film boiling flow by Murao and Sugimoto[9] and has the form of:

$$h = 0.94\ [\lambda_g^3\ \rho_g\ \rho_\ell\ H_{fg}\ g_o/L_q\ \mu_g\ \Delta T_{sat}]^{1/4}(1-\alpha)^{1/4}$$

$$+ E\ \varepsilon\ (1-\alpha)^{1/2}\ (T_w^4 - T_{sat}^4)/\Delta T_{sat} \qquad (7)$$

where, $\Delta T_{sat} = T_w - T_{sat}$ and the emissibity E is set to 0.65 based on reference 9. This correlation is used in the REFLA code[10], which analyzes a reflooding behavior during a PWR-LOCA, and the calculational results with this code are reported to be in good agreement with the average power rod data of many CCTF tests[11].

In Fig. 4.19, the measured and the calculated results are presented for both the tests at 1.83 m of the peak power rods. The measured and the calculated results are in good agreement for the FLECHT-SET experiment, whereas the CCTF measured value is about 50% higher than the calculated through the whole transient. As pointed out in reference 7, the correla-

tion cannot take account of the heat transfer enhancement due to the radial power distribution, and this is considered to be the reason for the large difference above.

Figure 4.20 shows the comparison of the measured and calculated heat transfer coefficients at 2.44 m. For this elevation, the correlation gives good agreement with both the CCTF and the FLECHT-SET data. As already discussed above, both the effects of the difference in the Acc injection and the core radial power distribution become small at 2.44 m. Therefore, it is concluded that the core heat transfer is expected to be close to each other for the CCTF and the FLECHT-SET tests, if there is no difference in the core boundary conditions and the core radial power distribution, and Murao-Sugimoto correlation gives good prediction for them.

Table 4.1 Comparison of measured test conditions

Item	CCTF	FLECHT-SET
ECC water temperature (K)	340	340
Average linear power density (kW/m)	1.385	1.383
Peak linear power density (kW/m)	2.76	2.76
Maximum initial clad temperature (K)	827	866

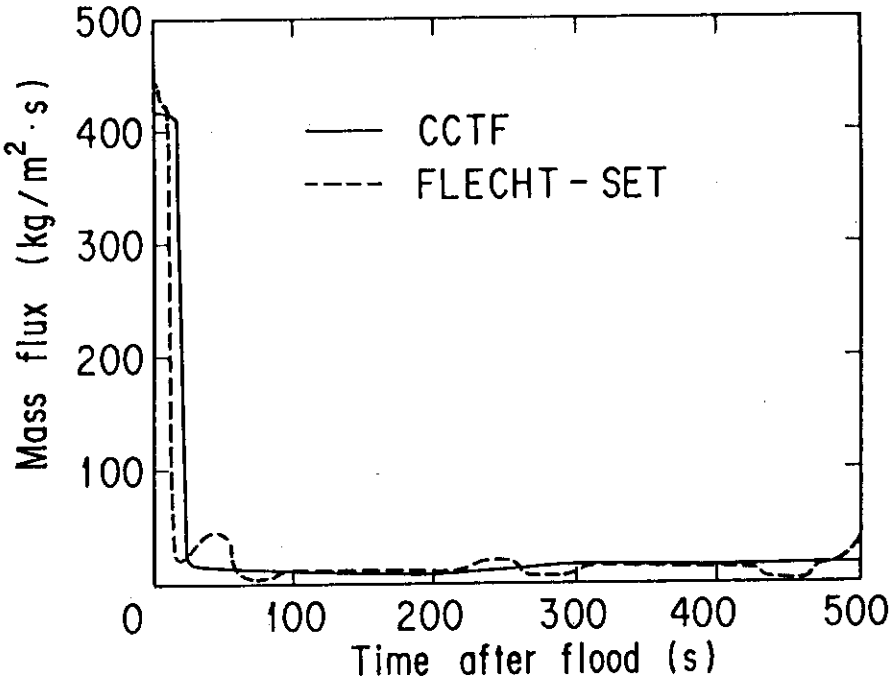

Fig. 4.1 Comparison of ECC water injection rate

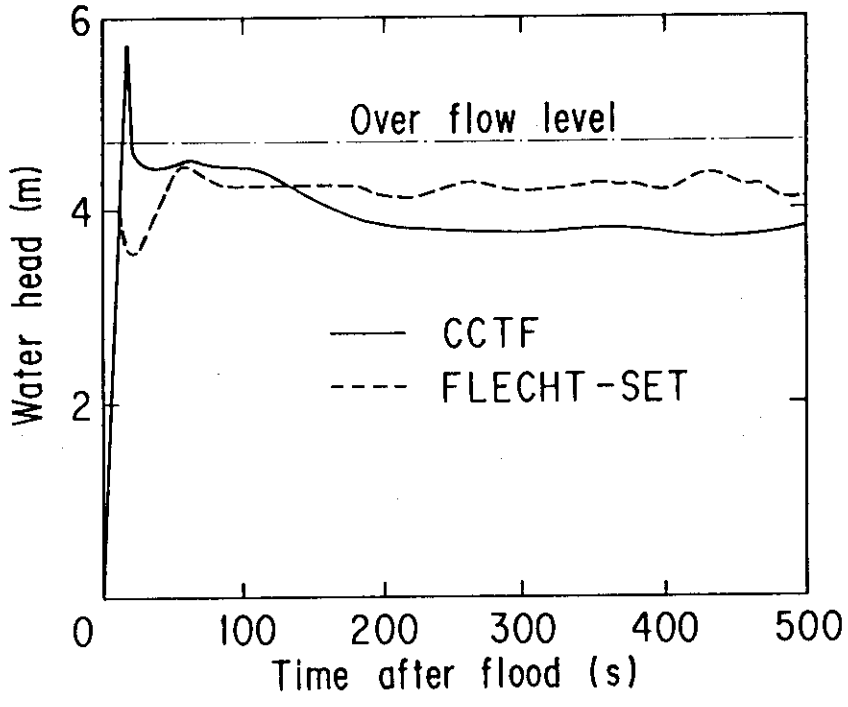

Fig. 4.2 Comparison of downcomer water head

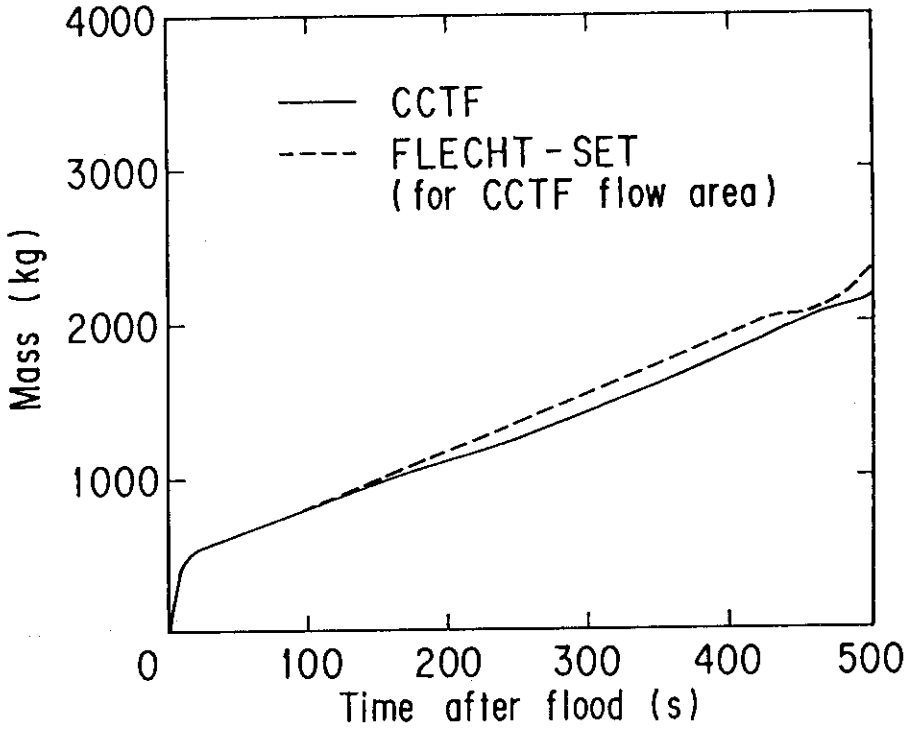

Fig. 4.3 Comparison of time-integration of core flooding mass flow rate

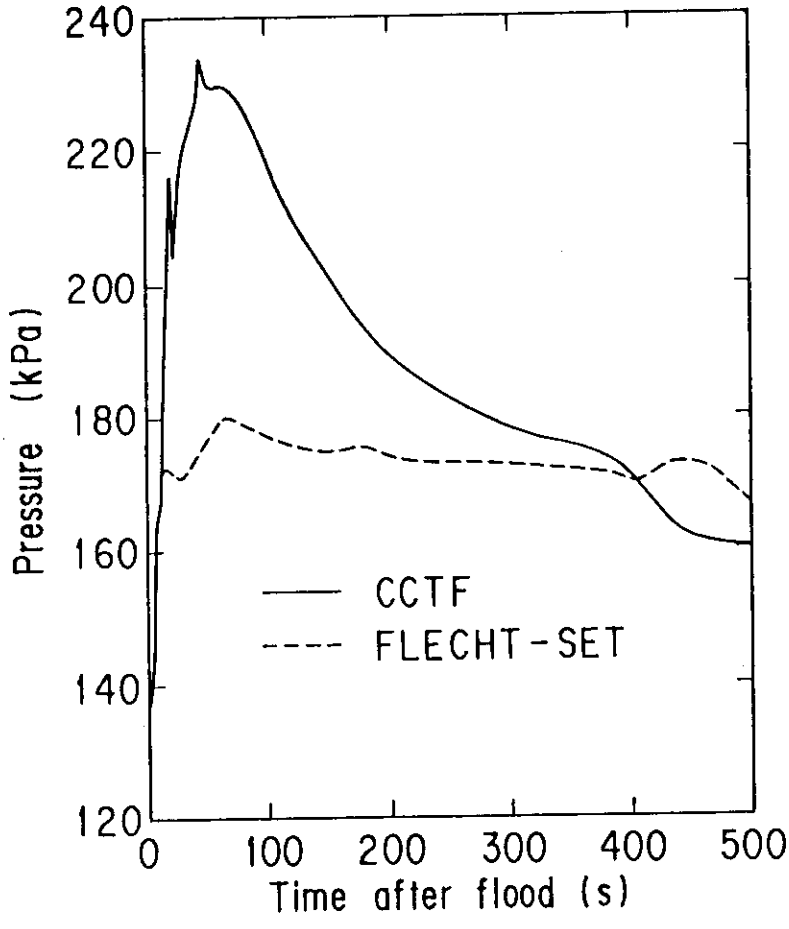

Fig. 4.4 Comparison of upper plenum pressure

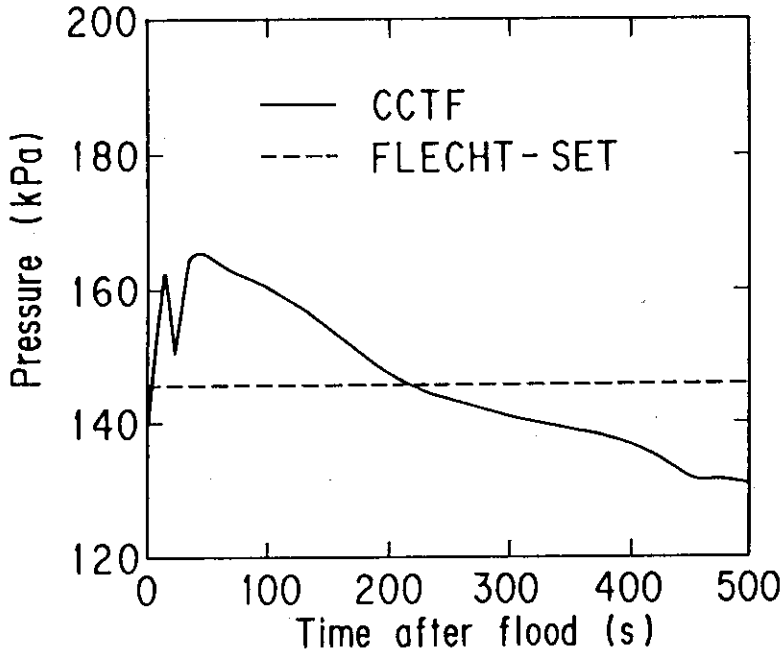

Fig. 4.5 Comparison of containment tank pressure

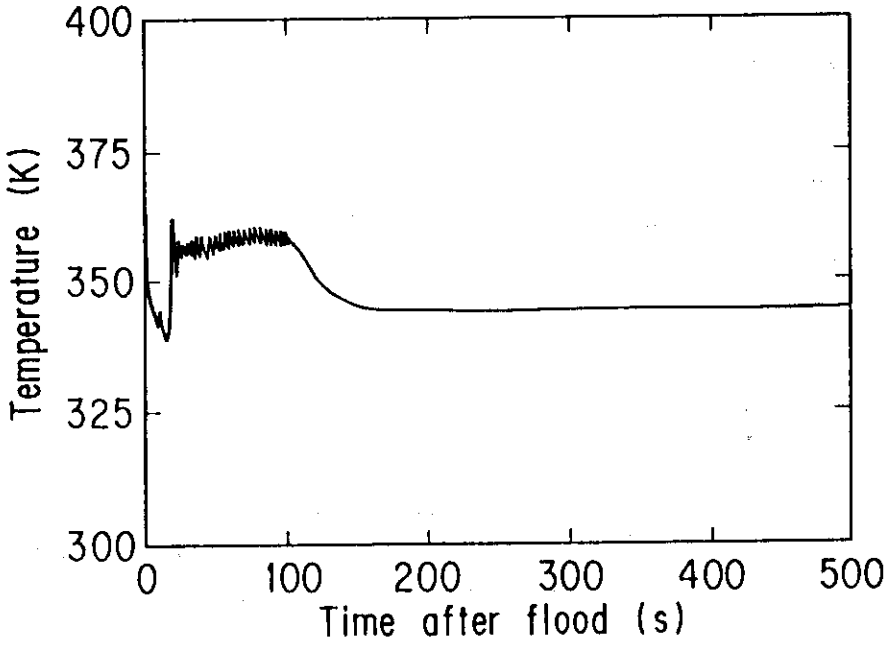

Fig. 4.6 Core inlet fluid temperature

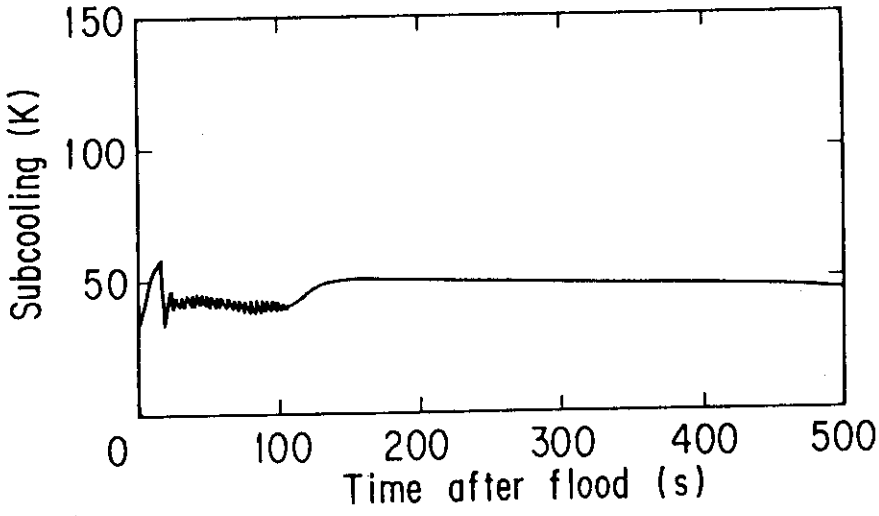

Fig. 4.7 Core inlet fluid subcooling

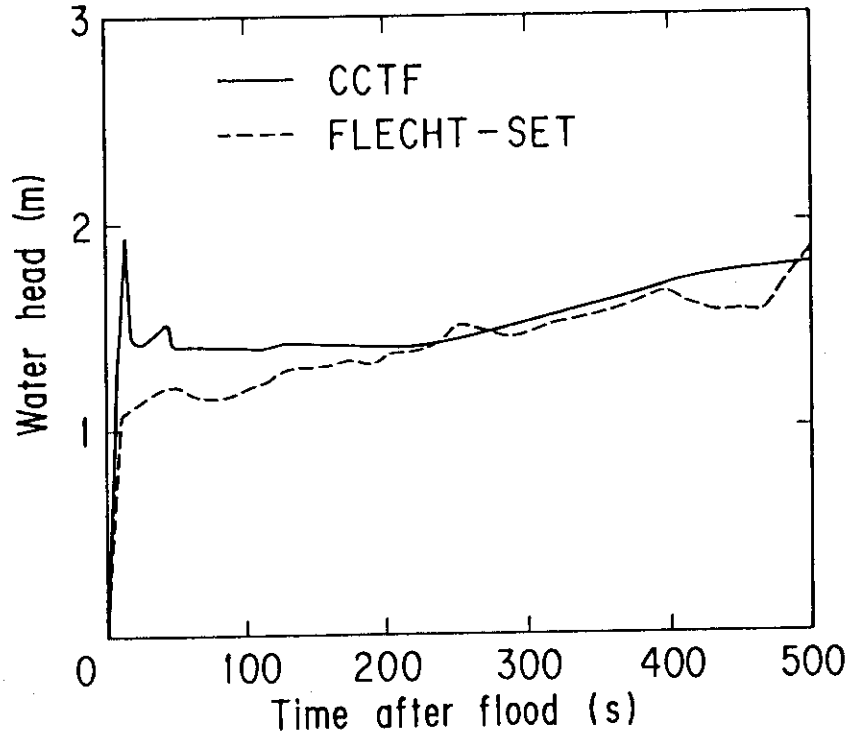

Fig. 4.8 Comparison of core water head

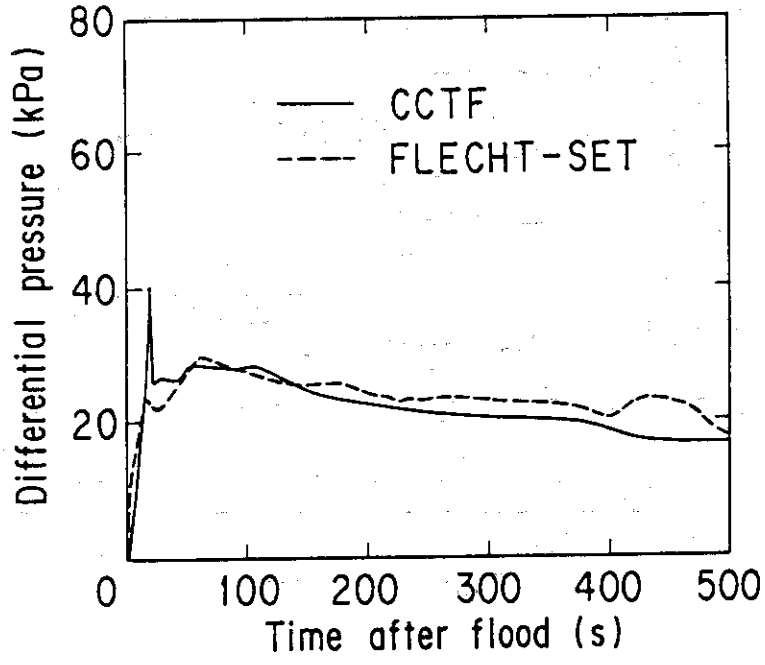

Fig. 4.9 Comparison of intact loop differential pressure

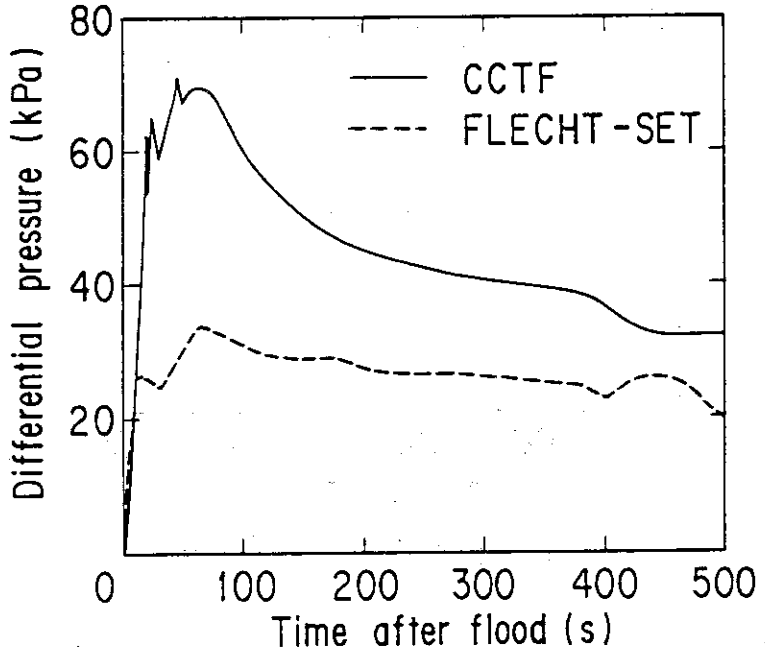

Fig. 4.10 Comparison of broken loop differential pressure

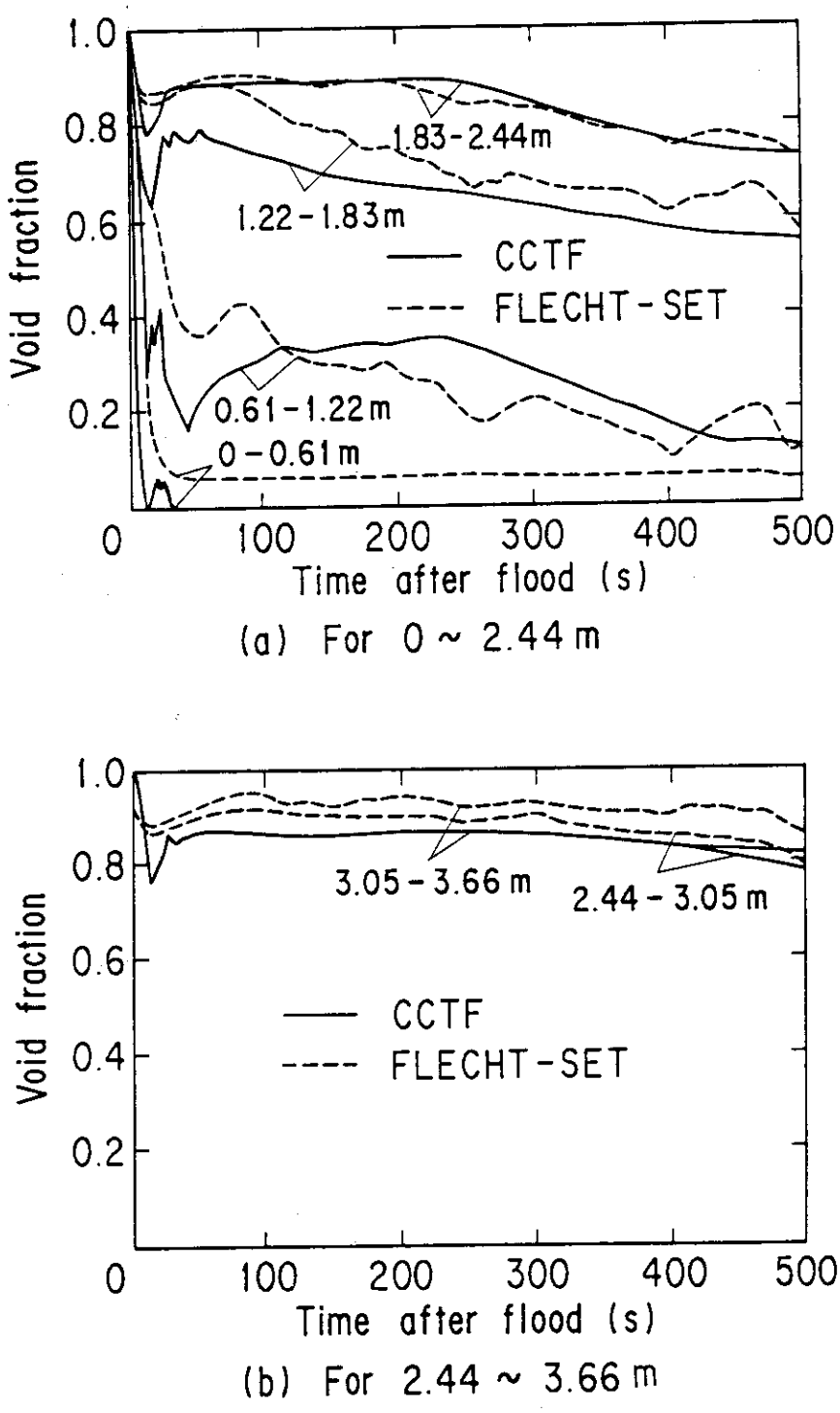

Fig. 4.11 Comparisons of core sectional void fractions

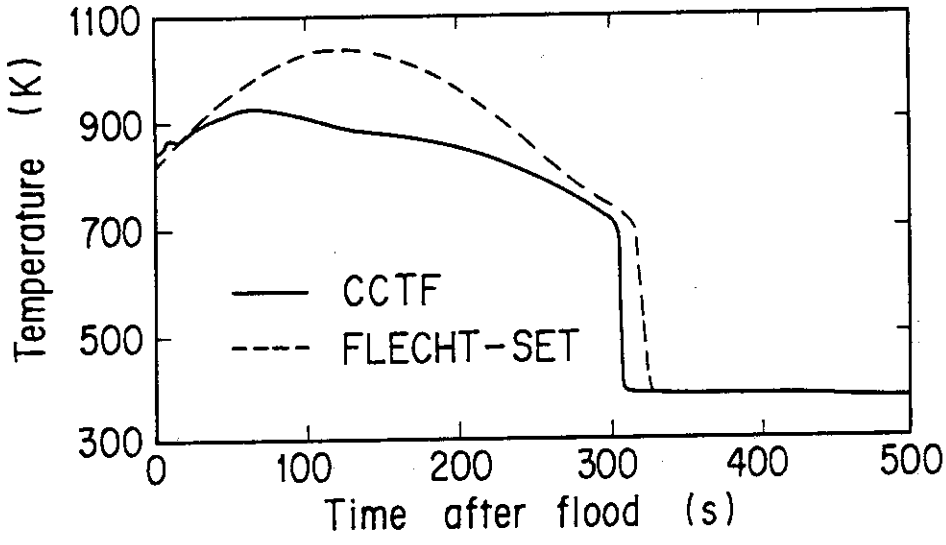

Fig. 4.12 Comparison of rod surface temperature at 1.83 m

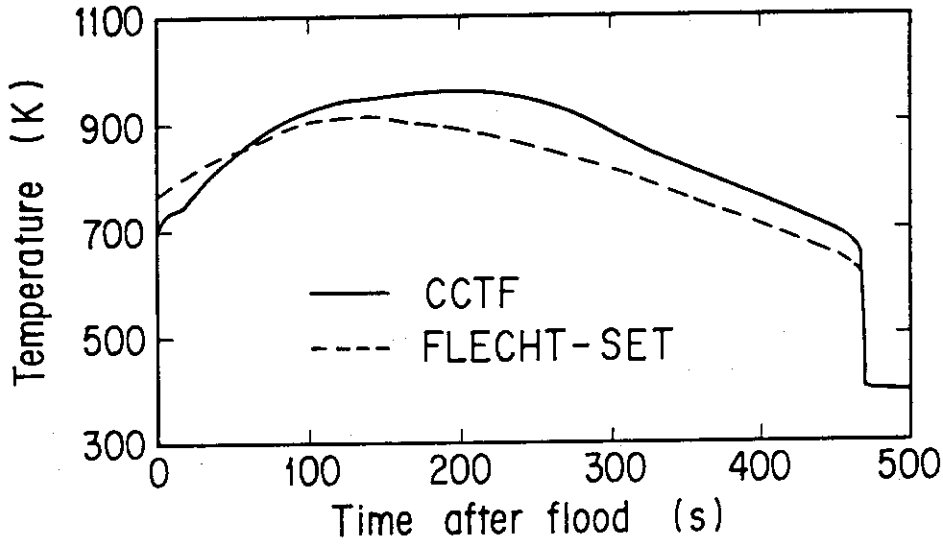

Fig. 4.13 Comparison of rod surface temperature at 2.44 m

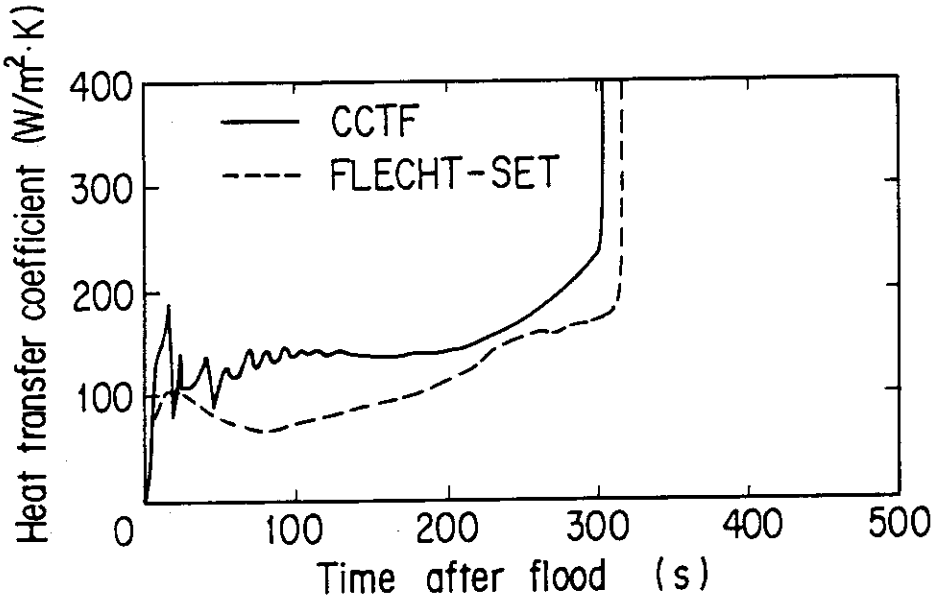

Fig. 4.14 Comparison of heat transfer coefficient at 1.83 m

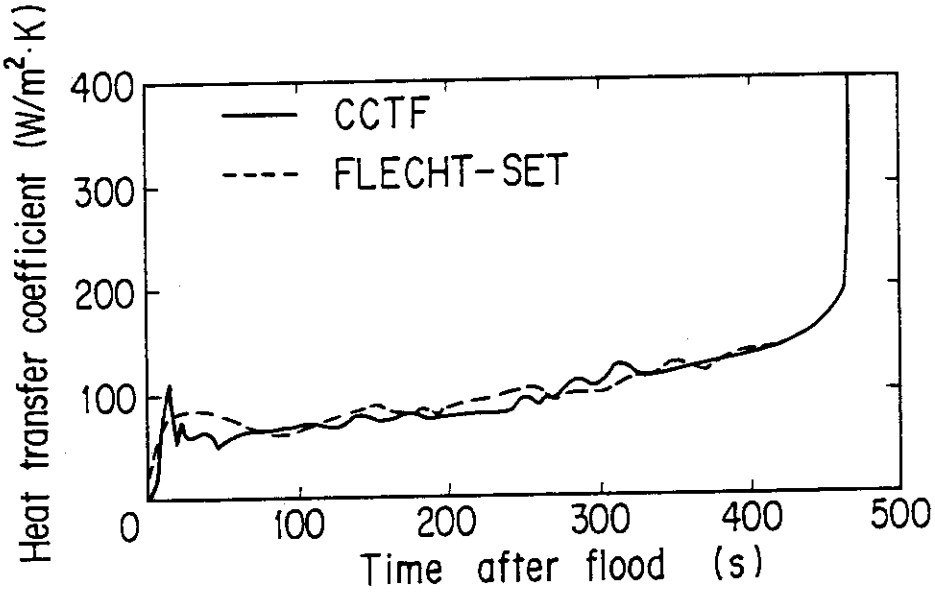

Fig. 4.15 Comparison of heat transfer coefficient at 2.44 m

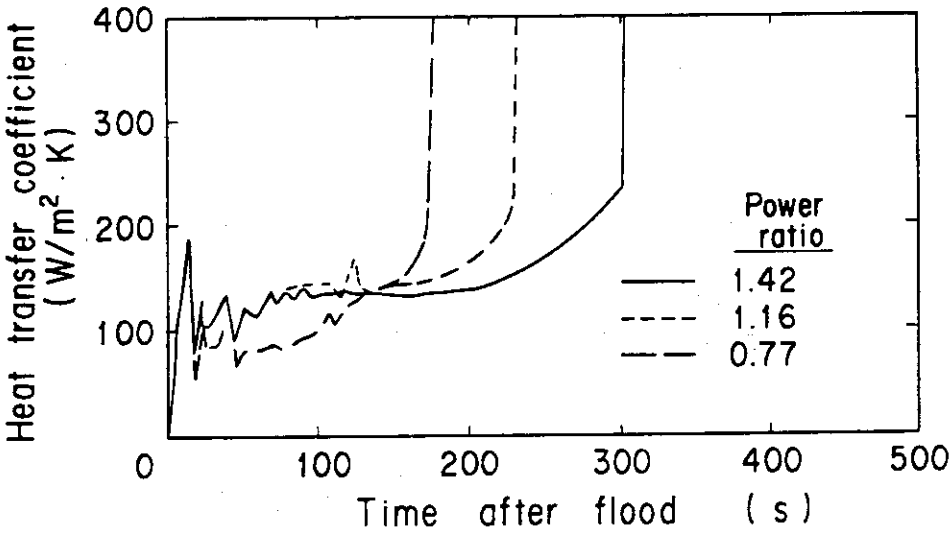

Fig. 4.16 Heat transfer coefficients at 1.83 m

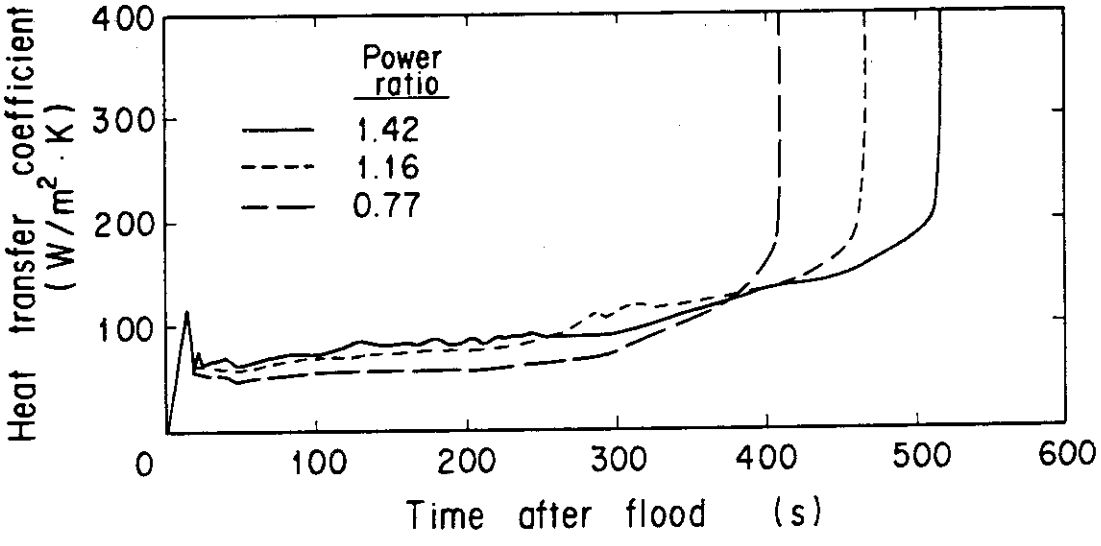

Fig. 4.17 Heat transfer coefficients at 2.44 m

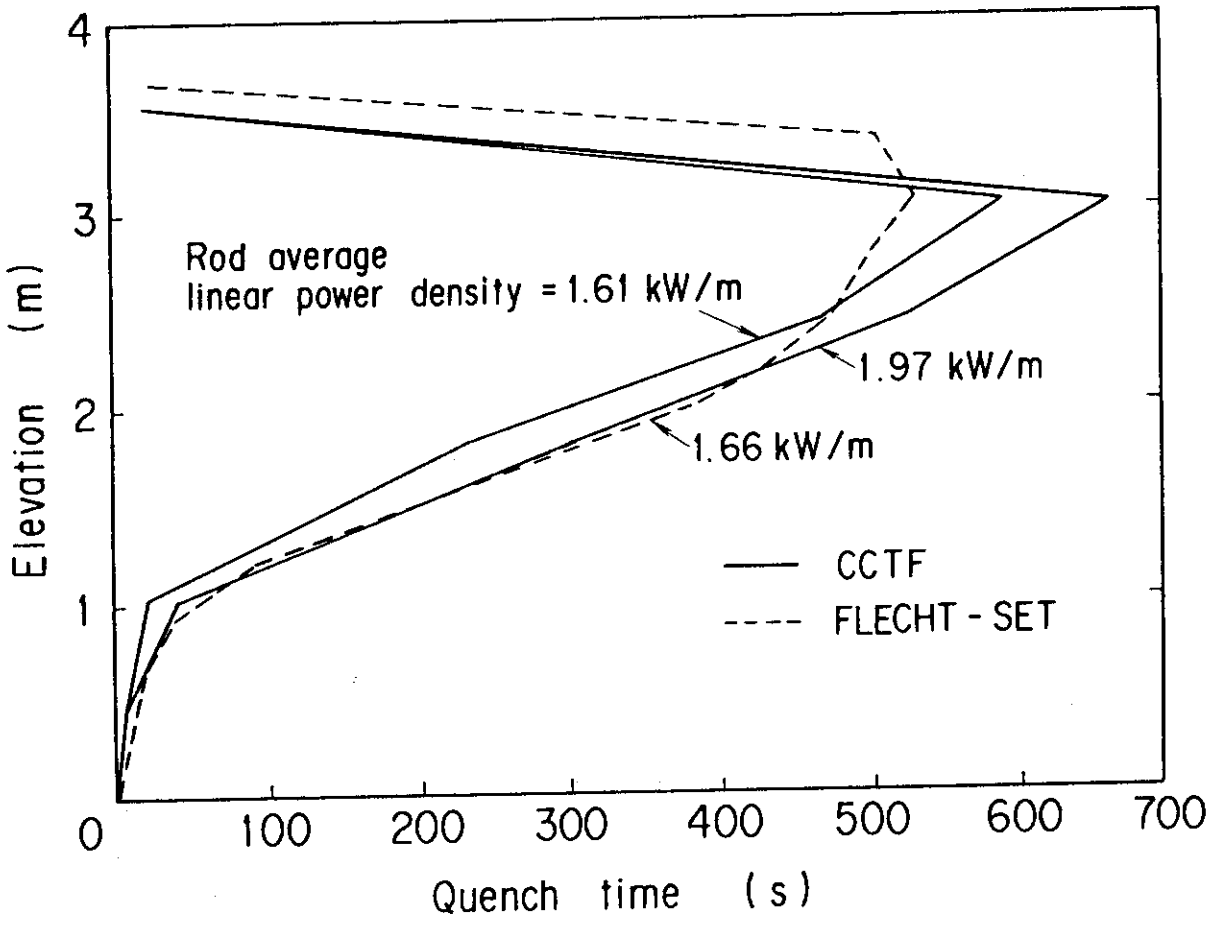

Fig. 4.18 Comparison of quench front envelope

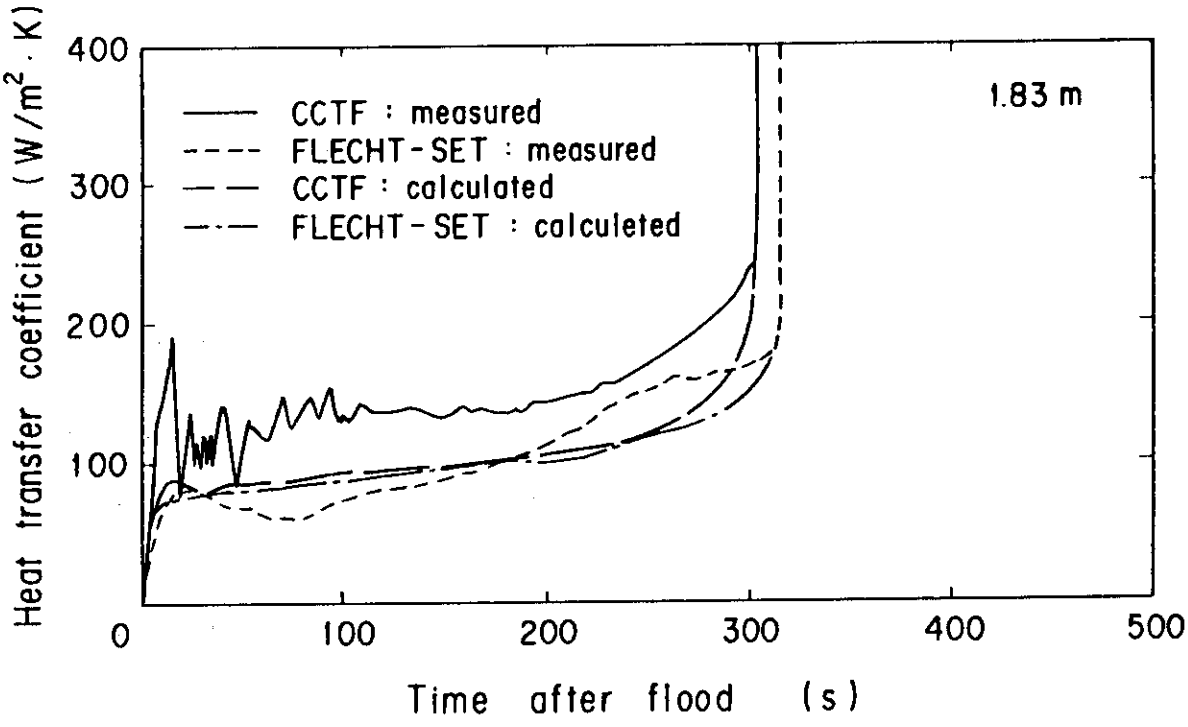

Fig. 4.19 Comparisons of heat transfer coefficients between measured and calculated with a correlation at 1.83 m

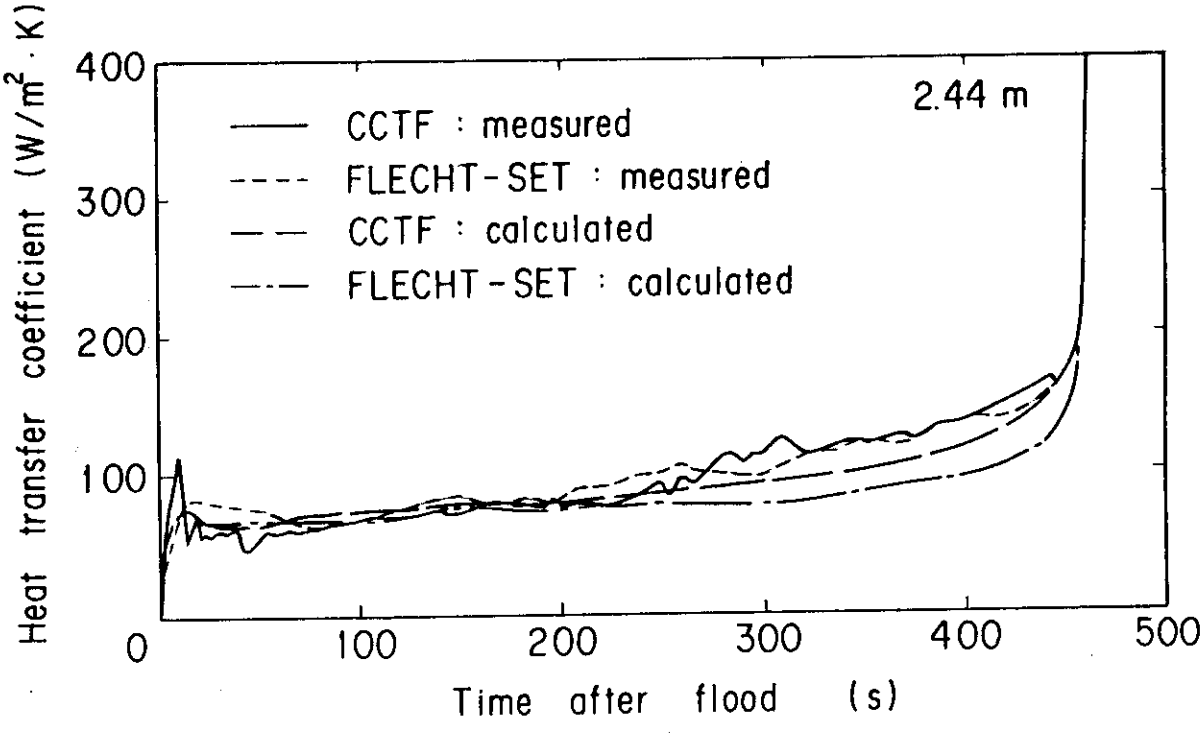

Fig. 4.20 Comparison of heat transfer coefficients between measured and calculated with a correlation at 2.44 m

5. Conclusions

In order to investigate whether the thermo-hydrodynamic behavior is different between the CCTF and the FLECHT-SET tests, a FLECHT-SET coupling test is performed with the CCTF. Investigating results of both the CCTF and the FLECHT-SET tests, the following conclusions are obtained:

(1) Some discrepancies were observed in the measured test conditions between the two tests. Out of them, difference in the Acc injection duration was large and affected test results, such as the water accumulation in the downcomer and the core and the core cooling, during the initial period. However, this effect was found to become small with time.

(2) Taking account of this difference and the difference in the broken cold leg pressure loss coefficient between the two facilities, the overall reflooding behavior is judged to be similar in the two facilities.

(3) The CCTF test results showed the core heat transfer enhancement in the higher power region due to its steep radial power distribution, whereas the FLECHT-SET did not due to its rather flat radial power distribution. This enhancement was observed significantly at 1.83 m but was smaller at the higher elevation.

(4) The heat transfer was nearly identical between the two tests and an existing correlation could well predict the heat transfer coefficients of both the tests at the location where the heat transfer enhancement mentioned above (3) were small, during the time period when the effect of the difference in the Acc injection mentioned above (1) were small.

(5) Therefore, the core cooling is expected to be almost the same in the CCTF and the FLECHT-SET under the same core boundary conditions and core radial power distribution.

Acknowledgments

The authors are indebted to Mr. T. Hojo of Mitsubishi Atomic Power Industries, Inc. (MAPI) for his valuable suggestions.

They are deeply indebted to Messrs. I. Arase, T. Oyama, T. Wakabayashi, Y. Niitsuma, K. Nakajima, T. Chiba, K. Komori, H. Sonobe and A. Owada of JAERI for their contribution to the test conduction.

5. Conclusions

In order to investigate whether the thermo-hydrodynamic behavior is different between the CCTF and the FLECHT-SET tests, a FLECHT-SET coupling test is performed with the CCTF. Investigating results of both the CCTF and the FLECHT-SET tests, the following conclusions are obtained:

(1) Some discrepancies were observed in the measured test conditions between the two tests. Out of them, difference in the Acc injection duration was large and affected test results, such as the water accumulation in the downcomer and the core and the core cooling, during the initial period. However, this effect was found to become small with time.

(2) Taking account of this difference and the difference in the broken cold leg pressure loss coefficient between the two facilities, the overall reflooding behavior is judged to be similar in the two facilities.

(3) The CCTF test results showed the core heat transfer enhancement in the higher power region due to its steep radial power distribution, whereas the FLECHT-SET did not due to its rather flat radial power distribution. This enhancement was observed significantly at 1.83 m but was smaller at the higher elevation.

(4) The heat transfer was nearly identical between the two tests and an existing correlation could well predict the heat transfer coefficients of both the tests at the location where the heat transfer enhancement mentioned above (3) were small, during the time period when the effect of the difference in the Acc injection mentioned above (1) were small.

(5) Therefore, the core cooling is expected to be almost the same in the CCTF and the FLECHT-SET under the same core boundary conditions and core radial power distribution.

Acknowledgments

The authors are indebted to Mr. T. Hojo of Mitsubishi Atomic Power Industries, Inc. (MAPI) for his valuable suggestions.

They are deeply indebted to Messrs. I. Arase, T. Oyama, T. Wakabayashi, Y. Niitsuma, K. Nakajima, T. Chiba, K. Komori, H. Sonobe and A. Owada of JAERI for their contribution to the test conduction.

This work was performed under contract with the Atomic Energy Bureau of Science and Technology Agency of Japan.

References

1. Hirano, K. and Murao, Y.: "Large Scale Reflood Test". Nihon-Genshiryoku-Gakkai Shi (J. At. Energy Soc. Jpn.), 22 [10], 681 (1980) [in Japanese].
2. Murao, Y. et al.: "Analysis Report on CCTF Core-I Reflood Test", to be published as a JAERI-M report.
3. Waring, J.P. and Hochreiter L.E.: "PWR FLECHT-SET Phase B1 Evaluation Report", WCAP-8583 (1975).
4. Waring J.P. et al.: "PWR FLECHT-SET Phase B1 Data Report", WCAP-8431 (1974).
5. Murao, Y. et al.: "Evaluation Report on CCTF Core-I Reflood Tests C1-16 (Run 25), C1-21 (Run 40) and C1-22 (Run 41) -- Comparison of Results between FLECHT Coupling Tests and FLECHT-SET Tests --, JAERI-M 83-065 (1983).
6. Akimoto, H. et al.: "Pressure Drop through Broken Cold Leg during Reflood Phase of Loss-of-Coolant Accident of Pressurized Water Reactor", J. Nucl. Sci. Technol., 21 [6], 450 (1984).
7. Akimoto, H. et al.: "Core Radial Power Effect on System and Core Cooling Behavior during Reflood Phase of PWR-LOCA with CCTF Data", ibid., 22 [7], 538 (1985).
8. Iwamura, T. et al.: "Effect of Radial Core Power Profile on Core Thermo-Hydraulic Behavior during Reflood Phase in PWR-LOCAs", ibid., 20 [9], 743 (1983).
9. Murao, Y. and Sugimoto, J.: "Correlation of Heat Transfer Coefficient for Saturated Film Boiling during Reflood Phase Prior to Quenching", ibid., 18 [4], 275 (1981).
10. Murao, Y. et al.: "REFLA-1D/MODE3: A Computer Code for Reflood Thermo-hydrodynamic Analysis during PWR-LOCA -- User's Manual --", JAERI-M 84-243 (1985).
11. Okubo, T. and Murao, Y.: "Assessment of Core Thermo-hydrodynamic Models of REFLA-1D Code with CCTF Data for Reflood Phase of PWR-LOCA", J. Nucl. Sci. Technol., 22[12], 983 (1985).

Appendix A

Definitions of Tag IDs

Figure List

1. Definition of Tag. ID for clad surface temperatures and heat fransfer coefficients

Notation : TEnnYlm (temperature)

HTEmmYlm (heat transfer coefficient)

nn : Bundle number (see Fig. A.1)

m : Elevation number

	Elevation (m)	Axial power factor
3	0.38	0.651
5	1.015	1.147
7	1.83	1.40
9	2.44	1.256
A	3.05	0.854

2. Definition of power zone and boundle number

See Fig. A.1

3. Definition of Tag. ID for void fraction

See Fig. A.2

4. Definition of Tag. ID for average linear power of heater rod in each power unit zone

See Fig. A.3

5. Definition of Tag. ID for differential pressure through downcomer, upper plenum, core and lower plenum

See Fig. A.4

6. Definition of Tag. ID for differential pressure through intact and broken loop and broken cold leg nozzle

See Fig. A.5

7. Definition of Tag. ID for fluid temperature in inlet and outlet plenum and secondary side of steam generator

See Fig. A.6

8. Definition of Tag. ID for ECC water injection rate, ECC water temperature and vented steam flow rate

See Fig. A.7

9. Definition of initial temperature, turnaround temperature quench temperature, temperature rise, turnaround time and quench time. (See Fig. A.8)

T_i : Initial temperature (Clad surface temperature at reflood initiation)

T_t : Turnaround temperature (Maximum clad surface temperature in each temperature history)

ΔT_r : Temperature rise ($= T_t - T_i$)

T_q : Quench temperature (Clad surface temperature at quenching)

10. Definition of quenching

See Fig. A.8

Quench time t_t is determined as

$$t_t = i \times \Delta t - \text{(reflood initiation time)}$$

In above equation, i is determined by the following criteria.

(1) Clad surface temperature is high, compared with the saturation temperature.

$$T_i > T_{sat} + \Delta T_1$$

(2) Decreasing rate of clad surface temperature is large.

$$\frac{T_{i+1} - T_i}{\Delta t} < - C_{st}$$

(3) Clad surface temperature falls around the saturation temperature.

$$T_{i + k_1} \leq T_{sat} + \Delta T_1$$

(4) If the determined i is inadequate, the value i is manually re-determined.

Δt : Data sampling period (s)

T_i : Clad surface temperature (K)

T_{sat} : Saturation temperature at the pressure in upper plenum (K)

ΔT_1 : Temperature discrepancy (K)
Default value = 50.0

C_{st} : Decreasing rate of clad surface temperature (K/S)
Default value = 25.0

k_1 : Number of referred data (-)
Default value = 6

11. Definition of Tag. ID for core inlet mass flow rate, time-integral core inlet mass flow rate and carry-over rate fraction

(1) Core inlet mass flow rate : $\dot{m}_F$
Notation : MLCRI□ (□ = N, 1 or 11)

(2) Time-intefral core inlet mass flow rate : $\int \dot{m}_F dt$
Notation : IMLCRI□ (□ = N, 1 or 11)

(3) Carry-over rate fraction : $(\dot{m}_F - \dot{m}_{CR})/\dot{m}_F$
Natation : CRF□ (□ = N, 1 or 11)

where $\dot{m}_F$: Core inlet mass flow rat (See item 12)

$\dot{m}_{CR}$: Water accumulation rate in core

Suffix	$\dot{m}_F$ based on
N	Eq.(A.2)
1	Eq.(A.1) with K=15
11	Eq.(A.1) with K=20

12. Evaluation of core inlet mass flow rate

The reflood phenomena is a relatively slow transient and a steady state condition can be applied. In a steady state condition, based on the mass balance relations of the system, the core flooding mass flow rates $\dot{m}_F$s can be written as follows:

By using the data measured at the downstream of the core inlet, $\dot{m}_F$ is derived as,

$$\dot{m}_F = \dot{m}_C + \dot{m}_U + \dot{m}_B + \Sigma \dot{m}_I \quad , \qquad (A.1)$$

where $\dot{m}_C$ and $\dot{m}_U$ are the mass accumulation rates in the core and the upper plenum respectively. The $\dot{m}_B$ and $\dot{m}_I$ are the mass flow rates in the broken loop and the intact loop, respectively.

By using the data measured at the upstream of the core inlet, $\dot{m}_F$ is derived as,

$$\dot{m}_F = \Sigma \dot{m}_{DL} - \dot{m}_D - \dot{m}_O + \dot{m}_{ECC/LP} \quad , \tag{A.2}$$

where $\dot{m}_{DL}$ and $\dot{m}_O$ are the mass flow rates of the water flowing into and overflowing from the downcomer, $\dot{m}_{ECC/LP}$ and $\dot{m}_D$ are the mass flow rate of the ECC water injected into the lower plenum and the water accumulation rate in the dowmcomer respectively.

The $\dot{m}_I$s and $\dot{m}_B$ can be obtained from the pressure drops at the pump simulators with orifices by assuming the K-factor of the orifice is constant. The values of $\dot{m}_C$, $\dot{m}_D$ and $\dot{m}_U$ can be evaluated with the differential pressure ΔP_C, ΔP_D and ΔP_U, respectively, as follows:

$$\dot{m}_n = d(\Delta P_n S_n/g)/dt \quad (n : C, D, U) \quad , \tag{A.3}$$

where g is the gravitational acceleration and S_n is the cross sectional area. The value of $\dot{m}_O$ can be obtained from the liquid level X in the Containment tank 1 as,

$$\dot{m}_O = d(X\rho_\ell S_o)/dt \quad , \tag{A.4}$$

where ρ_ℓ is the liquid density and S_o is the cross sectional area of the containment tank 1.

The value of $\dot{m}_{DL}$, $\dot{m}_{DV}$ and h, which are liquid flow rate, steam flow rate and enthalpy of two phase mixture downstream each ECC port respectively, are obtained from the following mass and energy balance relations at each ECC port under the assumption of thermal equilibrium:

$$\dot{m}_{DV} + \dot{m}_{DL} = \dot{m}_{ECC} + \dot{m}_I \quad , \tag{A.5}$$

$$(\dot{m}_{DV} + \dot{m}_{DL})i = \dot{m}_{ECC} h_{ECC} + \dot{m}_I h_I \quad , \tag{A.6}$$

$$\begin{aligned} &\text{if} \quad h_g \geq h \geq h_\ell \ , \ (\dot{m}_{DV} + \dot{m}_{DL})h = \dot{m}_{DV} h_g + \dot{m}_{DL} h_\ell \\ &\text{if} \quad h \geq h_g \ , \ \dot{m}_{DL} = 0 \quad , \\ &\text{if} \quad h \geq h_\ell \ , \ \dot{m}_{DV} = 0 \end{aligned} \tag{A.7}$$

where h is enthalpy of fluid and h_ℓ and h_g are enthalpies of liquid and steam at the saturation temperature, respectively.

The fluid temperatures can be measured with thermocouples immersed in the fluid and the enthalpies h_I and h_{ECC} can be estimated.

Mass balance calculations were performed with Eqs. (A.1) and (A.2). The K-factor of the orifice in the pump simulator was evaluated in the following two ways.

The K-factor of 20 was obtained with the steam and water single phase calibration tests using the flow meter and spool piece data. The K-factor of 15 was obtained with the Pitot tube measurement in a typical reflood condition assuming the flat velocity profile in the pipings. In the differentiation, higher frequency components of the data tends to be amplified more. Therefore, in the differentiation of the differential pressure data, the smoothing procedure was used to uppress the high frequency components of the data.

In the Acc injection period, the calculated $\dot{m}_F$s with Eqs. (A.1) and (A.2) are significantly different from each other. This discrepancy may be caused by inaccuracy of the mass flow rate injected into the system and by the unaccounting of the storage of water in the cold leg pipe. The former might be introduced from the slow time response of the flow meter (time constant 1 second) and the change of the gas volume in the injection line. In this period, especially before the steam generation from the core becomes noticeable, the mass flow rate, $\dot{m}_F$, calculated with Eq. (A.1) is probably reasonable, since the calculation uses the increasing rates of the masses in the core and the upper plenum and their accuracy is good enough for our estimation.

In the LPCI injection period, the calculated $\dot{m}_F$s are slightly different from each other. Judging from the time-integral values of both $\dot{m}_F$s, their average values are nearly proportional. The discrepancy was inferred to be caused by the disregard of the bypass of steam and liquid from the upper plenum without going through the hot legs in the calculation with Eq. (A.1). And additionally the discrepancy was caused by the disregard of the steam generation in the downcomer due to the hot wall of the pressure vessel in the calculation with Eq. (A.2). It was estimated that the disregard of the downcomer steam generation causes the error of 0.25 kg/s on predicted $\dot{m}_F$. The estimation was made by comparing the results of the tests with hot and cold downcomer conditions.

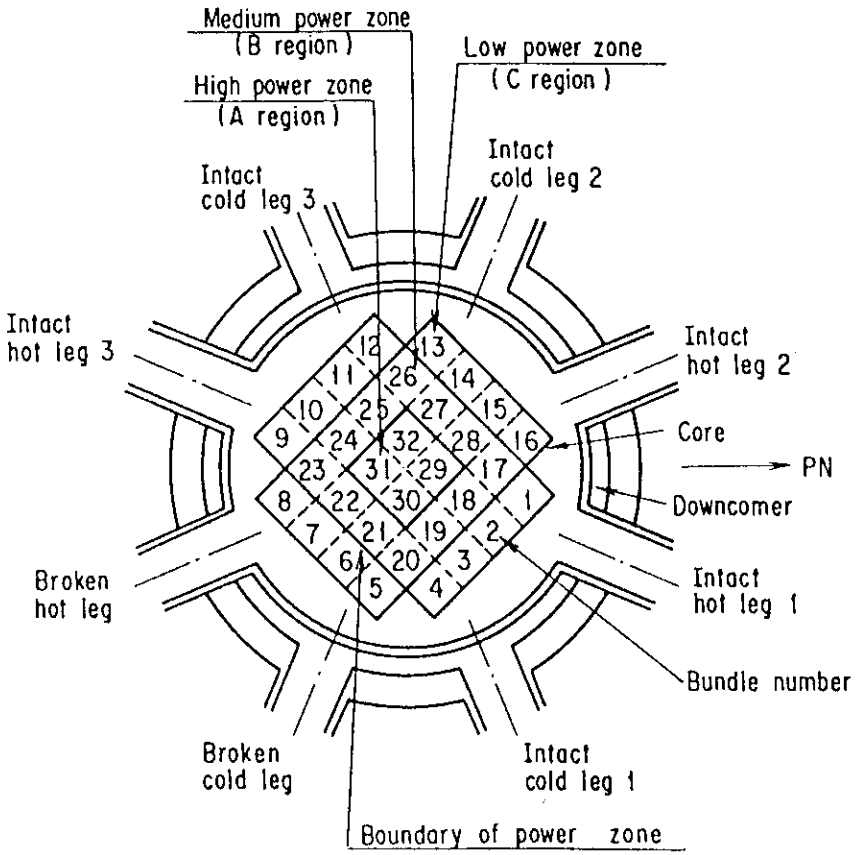

Fig. A.1 Definition of power zones and bundle numbers

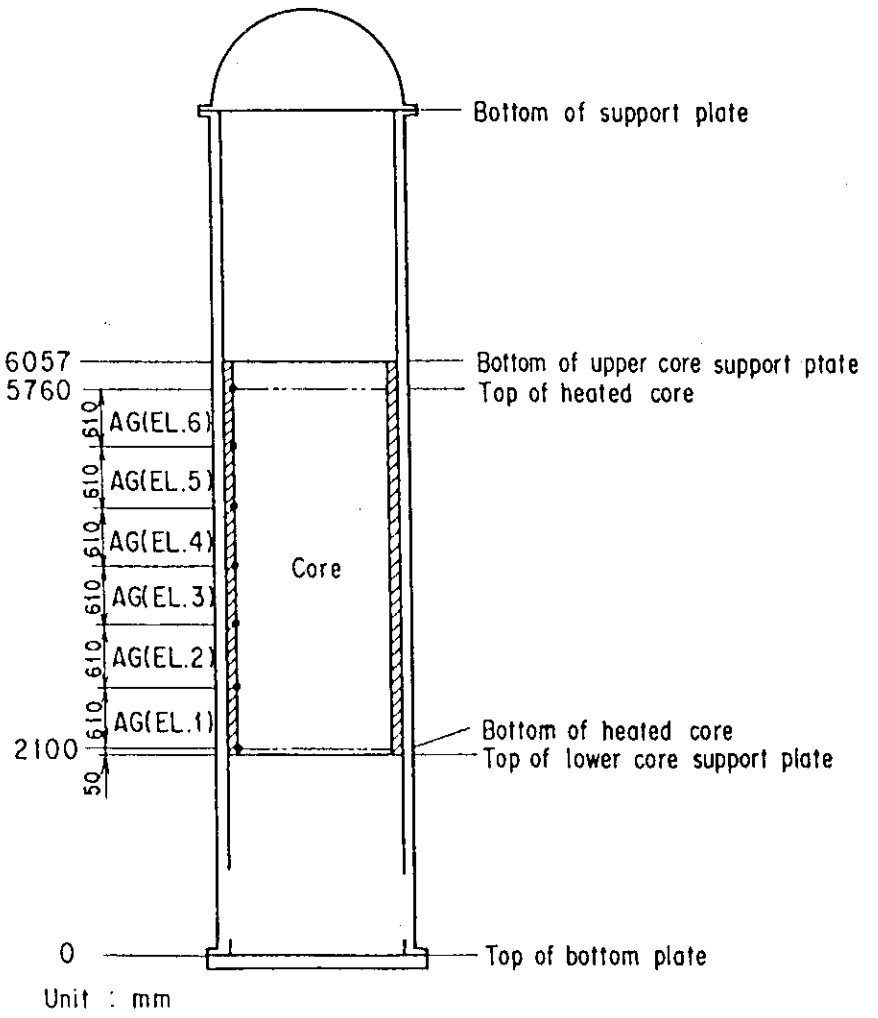

Fig. A.2 Definition of Tag. ID for void fraction (AG(EL.1) ~ AG(EL.6))

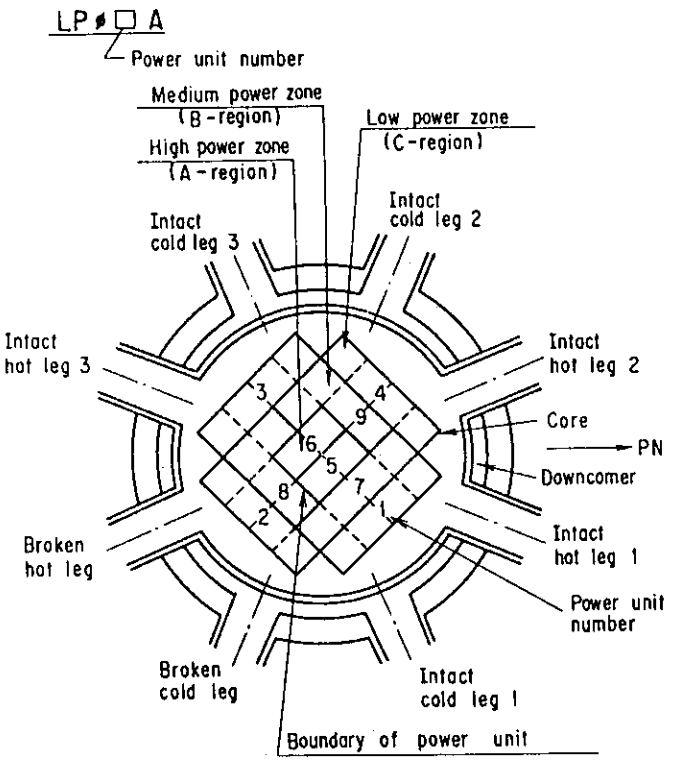

Fig. A.3 Definition of Tag. ID for average linear power of heater and in each power unit zone (LP01A ~ LP09A)

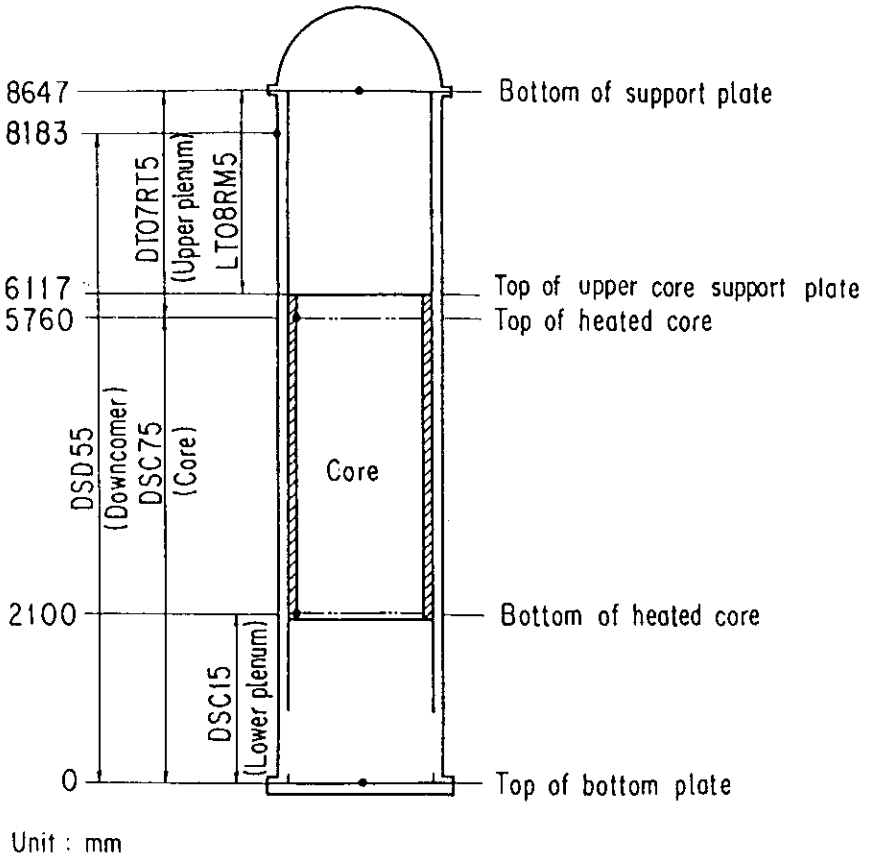

Fig. A.4 Definition of Tag. ID for differential pressure through downcomer, upper plenum, core, and lower plenum (DSD55, DTO7RT5, LTO8RM5, DSC75, DSC15)

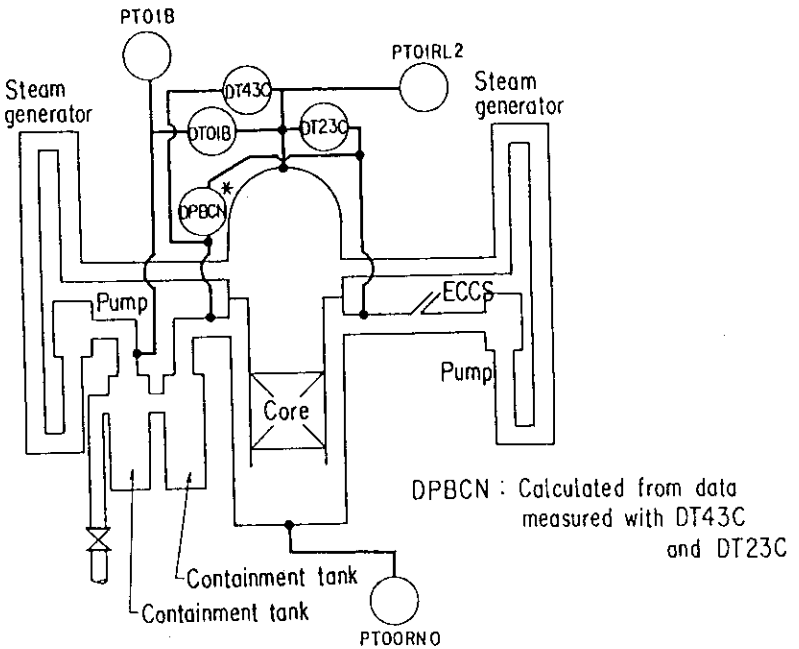

Fig. A.5 Definition of Tag. ID for differential pressure through intact and broken loop and broken cold leg nozzle (DT23C, DT01B, DPBCN)

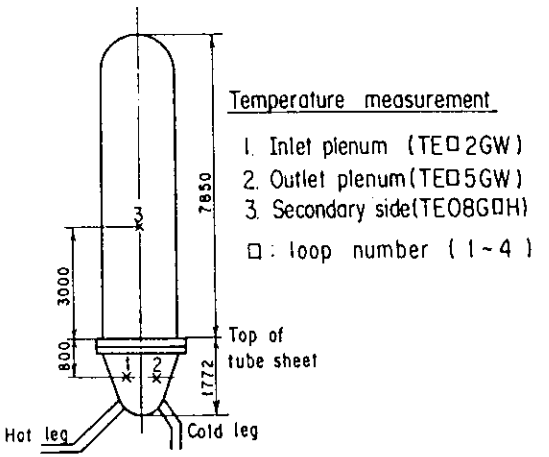

Fig. A.6 Definition of Tag. ID for fluid temperature in inlet and outlet plenum and secondary of steam genrator (TE□2GW, TE□5GW, TE08G□H)

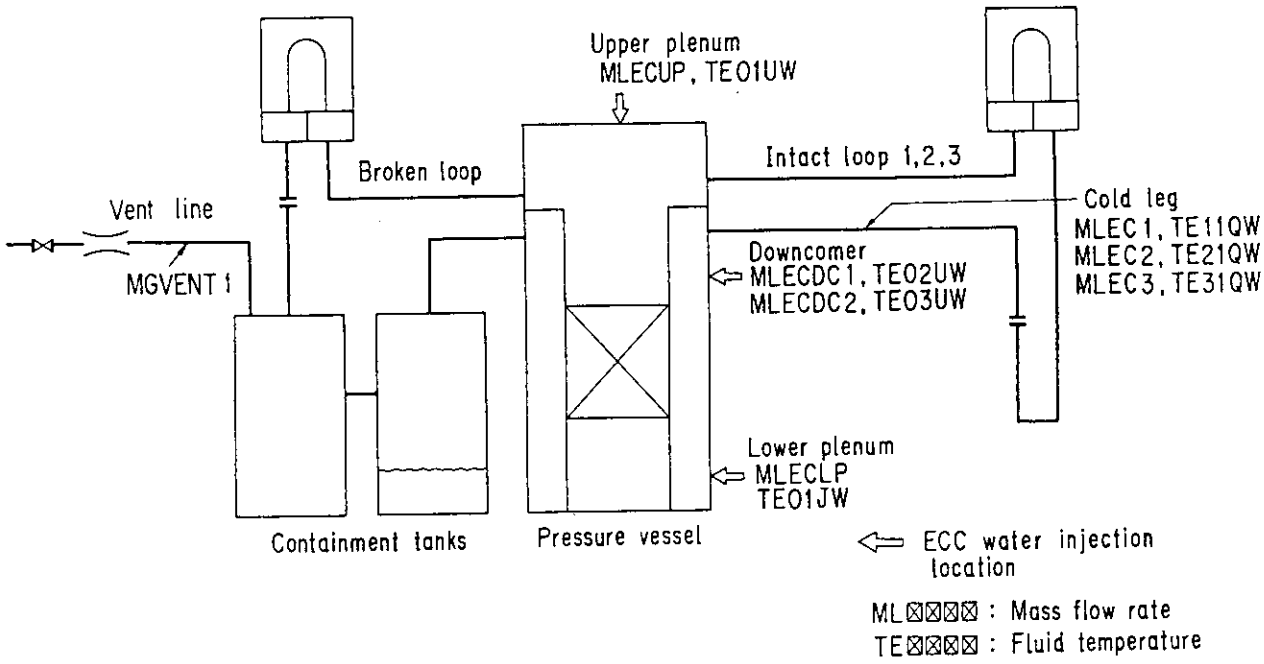

Fig. A.7 Definition of Tag. ID for ECC water injection rate, ECC water temperature and vented steam flow rate (MLEC1, MLEC2, MLEC3, MLECLP, MLECUP, MLECDC1, MLECDC2, TE11QW, TE21QW, TE01JW, TE01UW, TE02UW, TE03UW, MGVENT1)

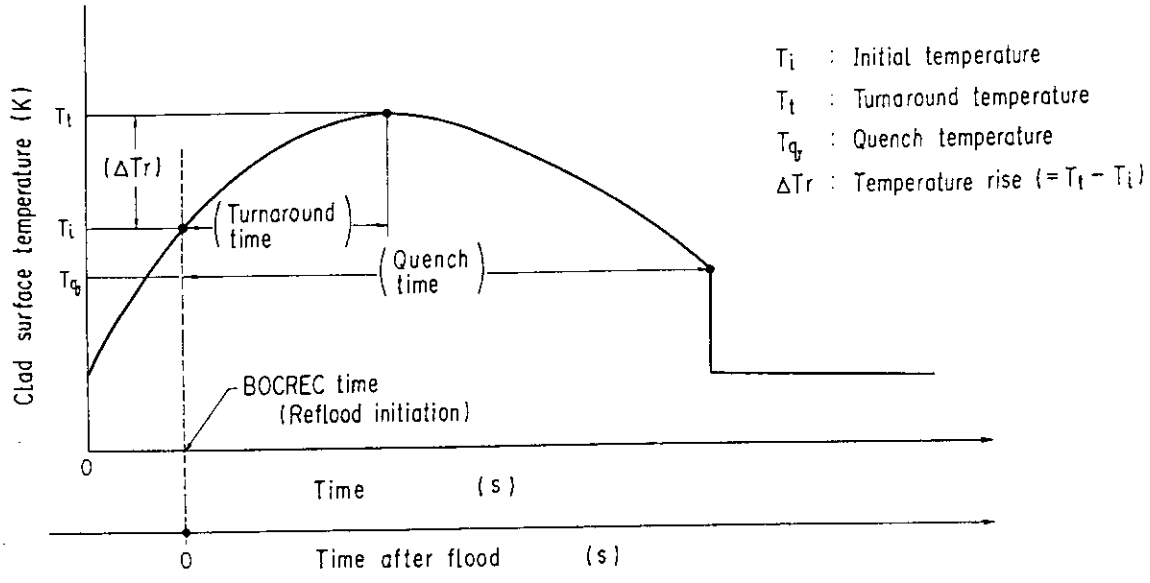

Fig. A.8 Definition of initial temperature, turnaround temperature, quench temperature, temperature rise, turnaround time and quench time

Appendix B

Selected data of CCTF Test C2-15 (Run 75)

Figure List

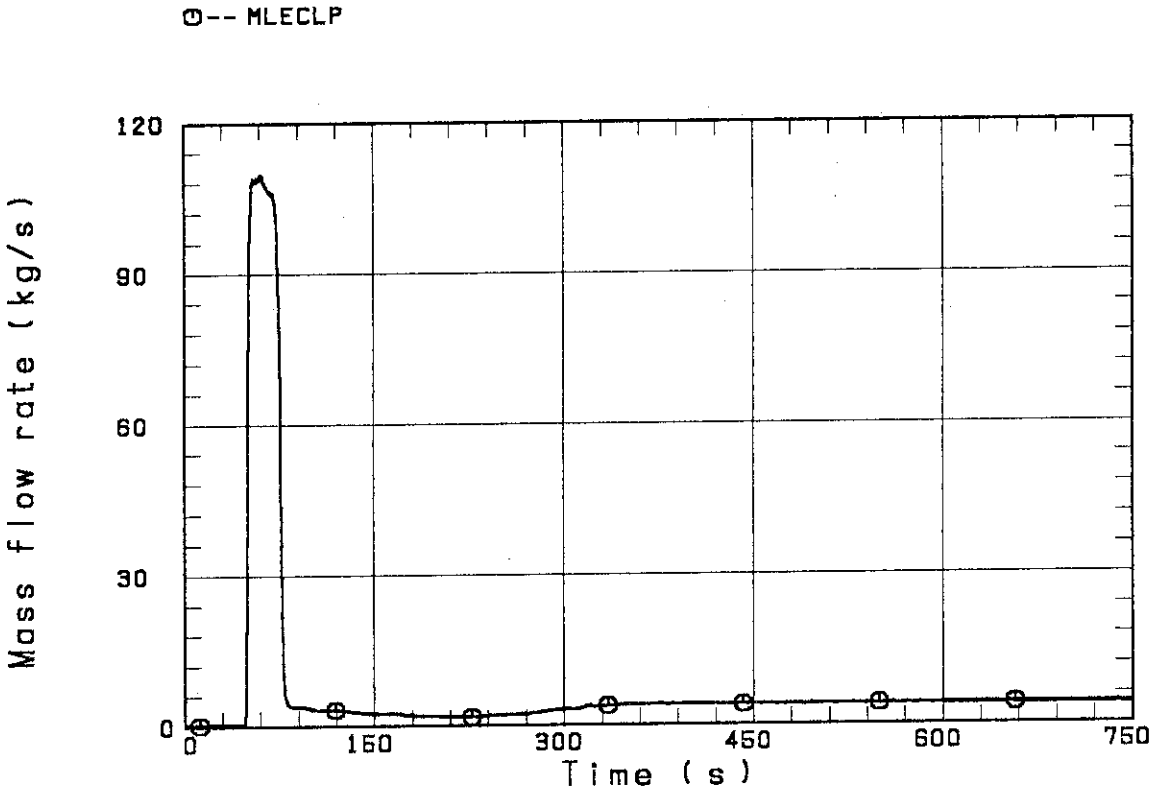

Fig. B.1 ECC water injection rates into the primary system

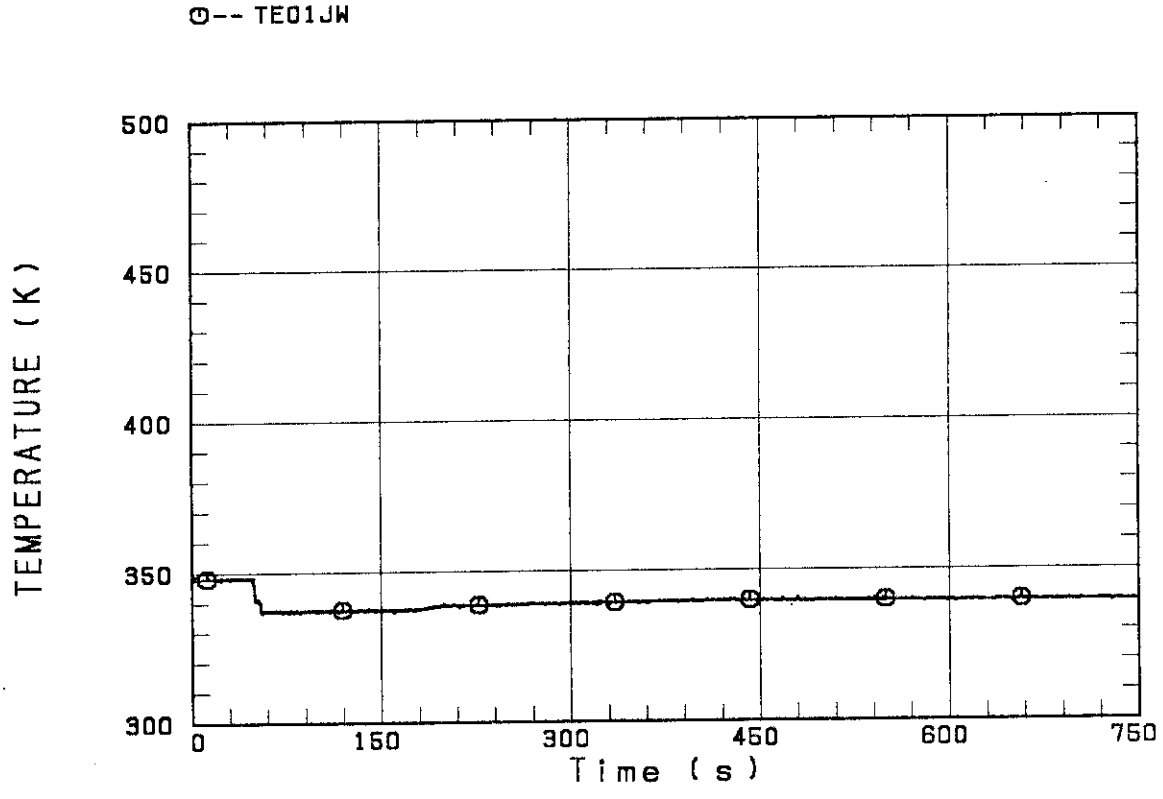

Fig. B.2 ECC water temperature

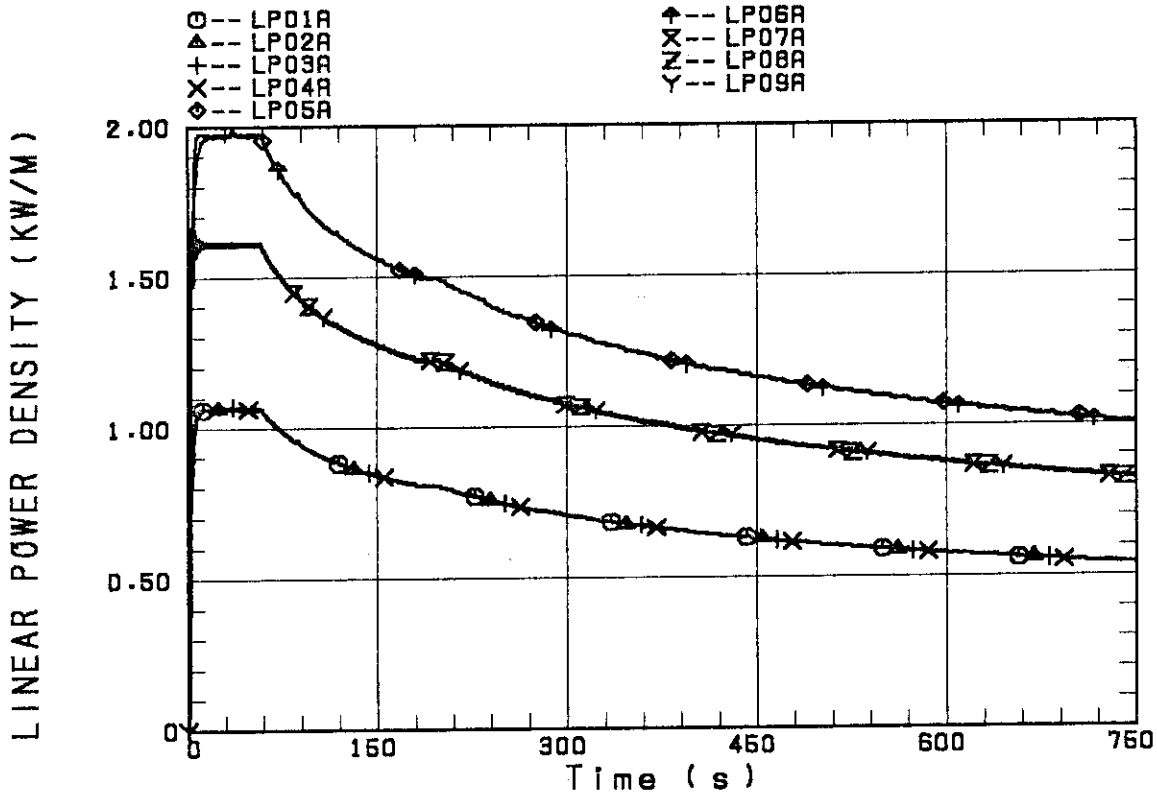

Fig. B.3 Average liner power of heater rod in each power unit zone

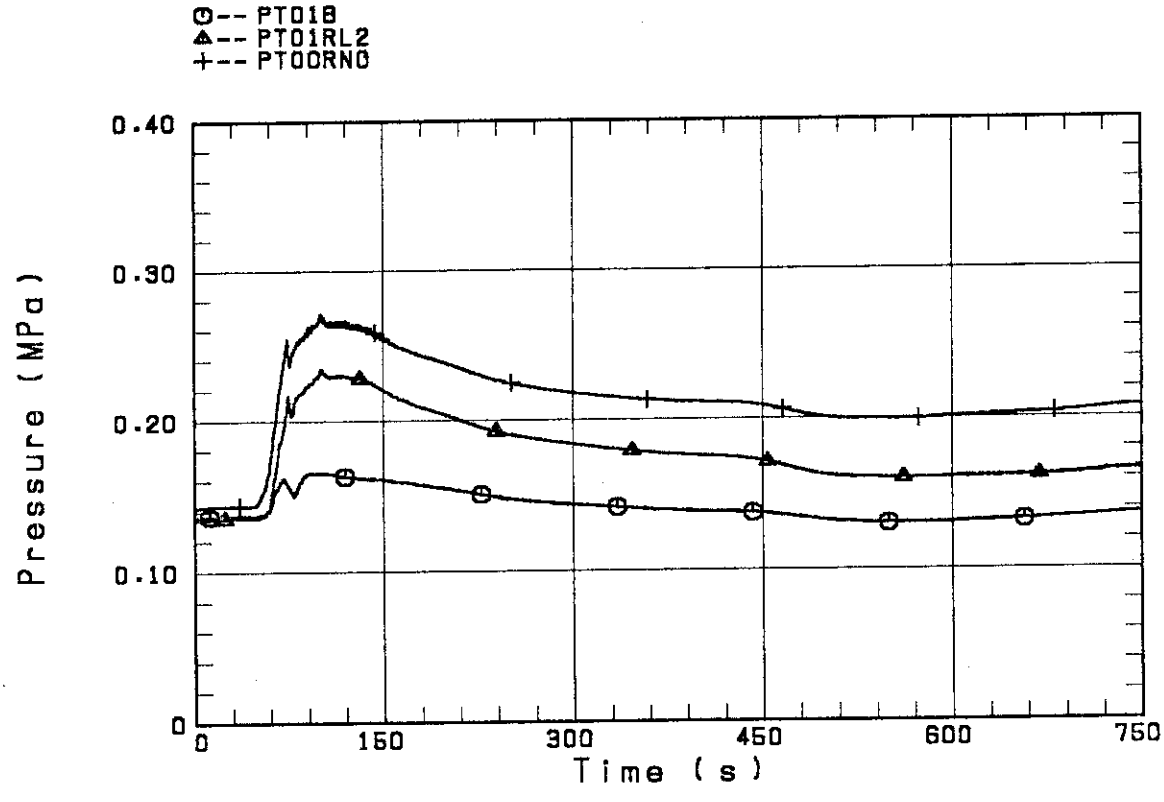

Fig. B.4 Pressure history in containment tank 2, upper plenum and lower plenum

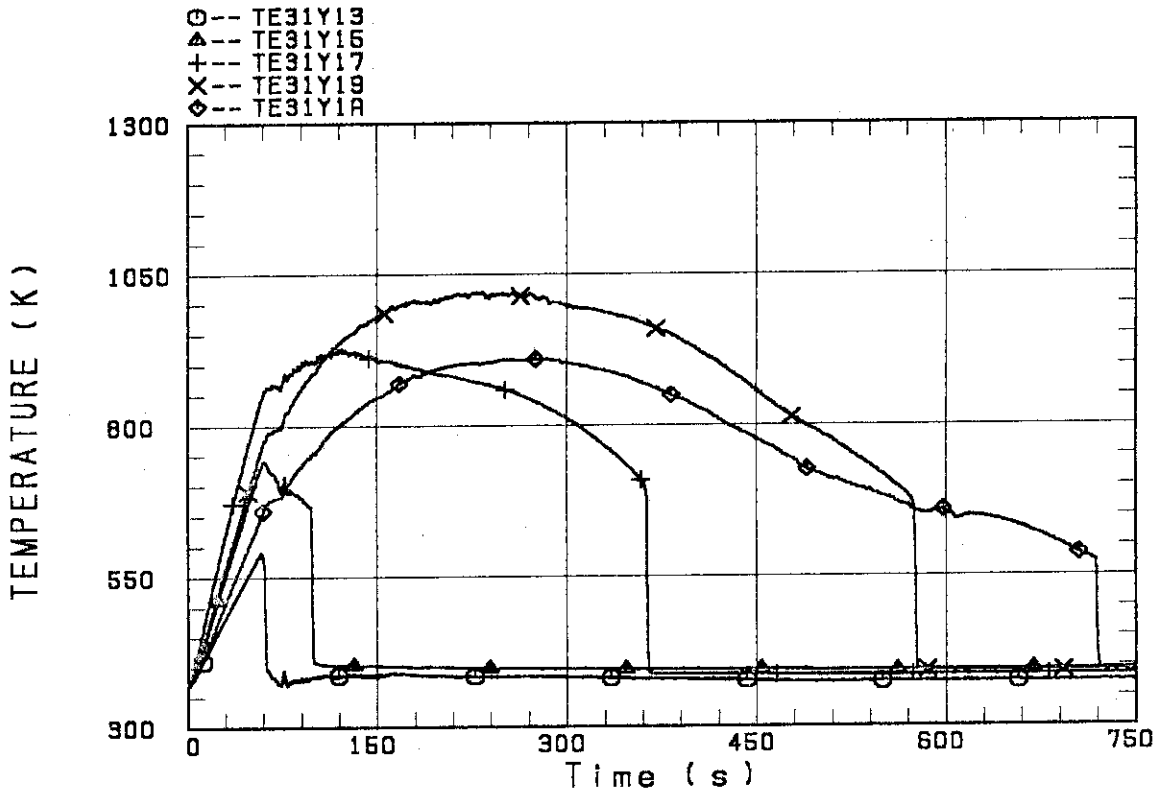

Fig. B.5 Clad surface temperature at various elevations along a heater rod in high power region (A region)

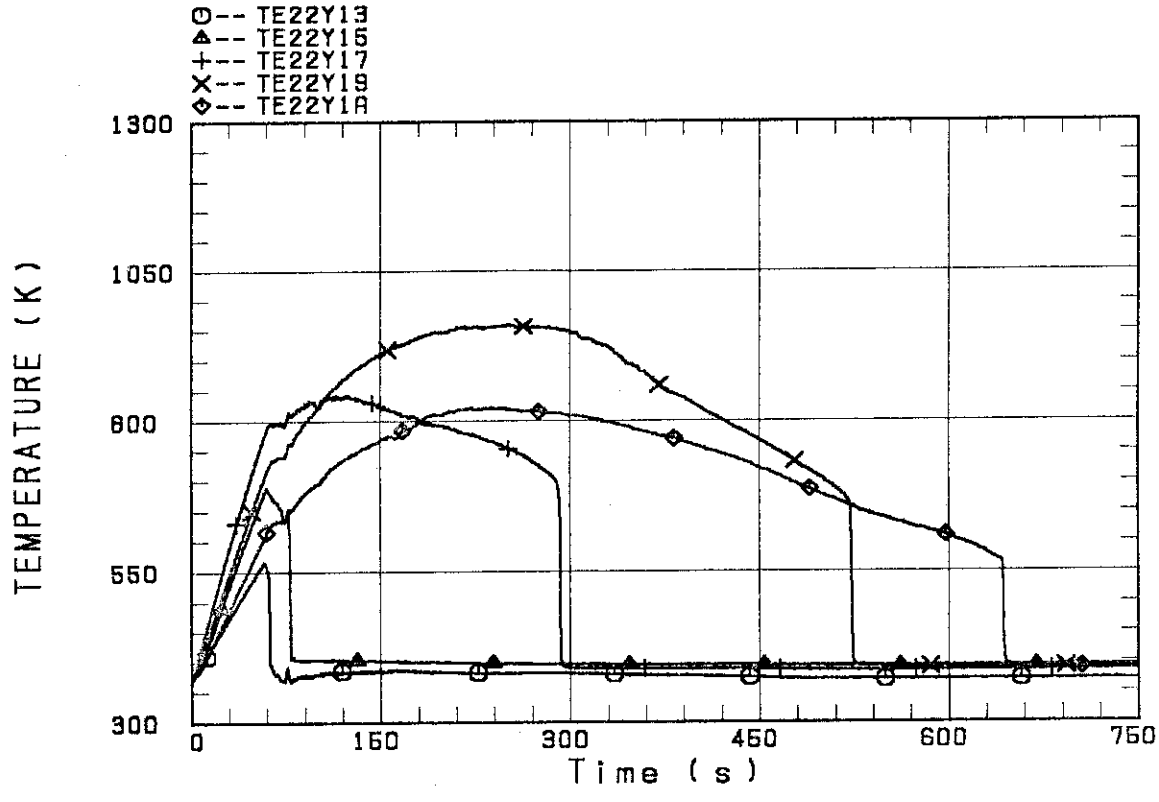

Fig. B.6 Clad surface temperature at various elevations along a heater rod in medium power region (B redion)

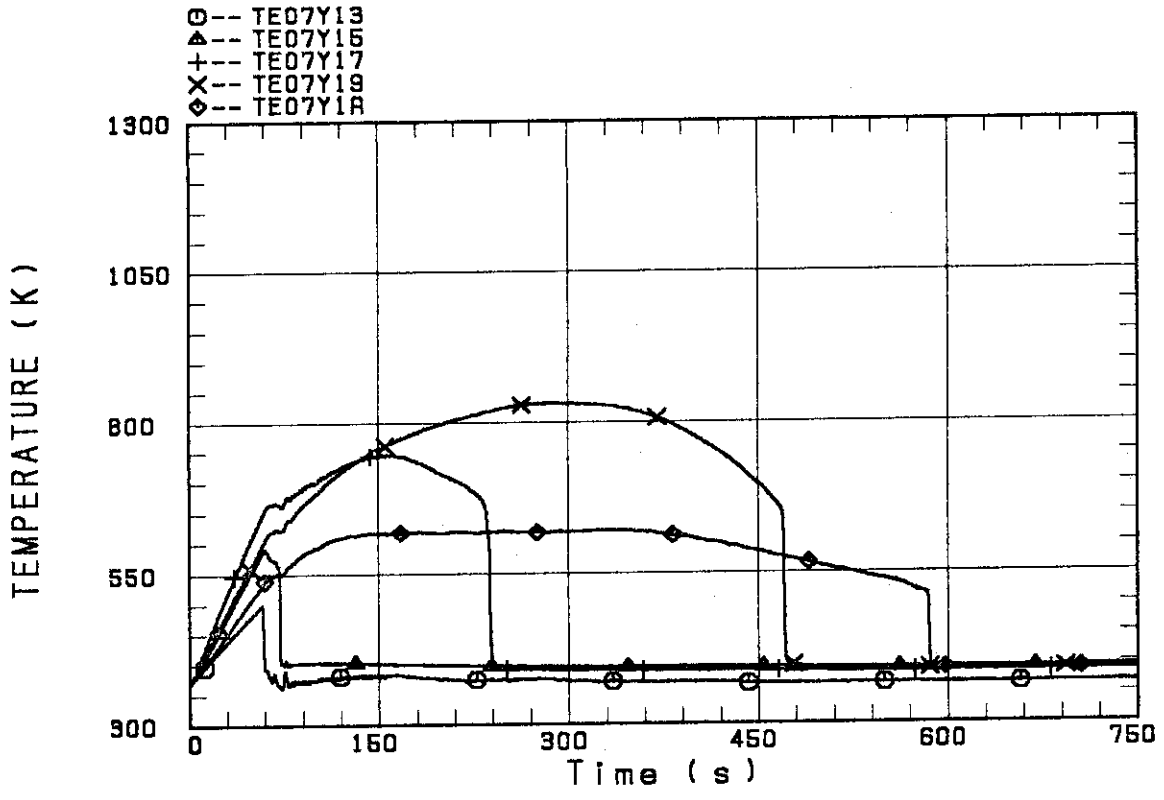

Fig. B.7 Clad surface temperature at various elevations along a heater rod in low power region (C region)

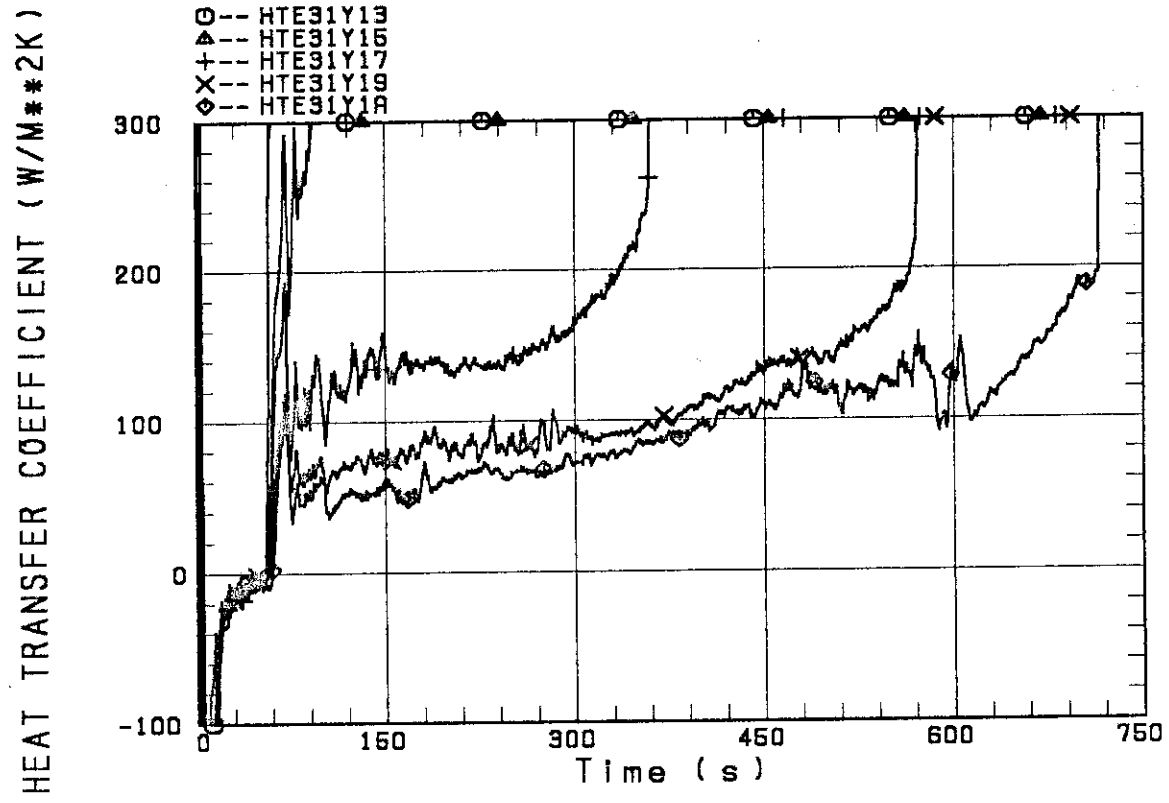

Fig. B.8 Heat transfer coefficient at various elevations along a heater rod in high power region (A region)

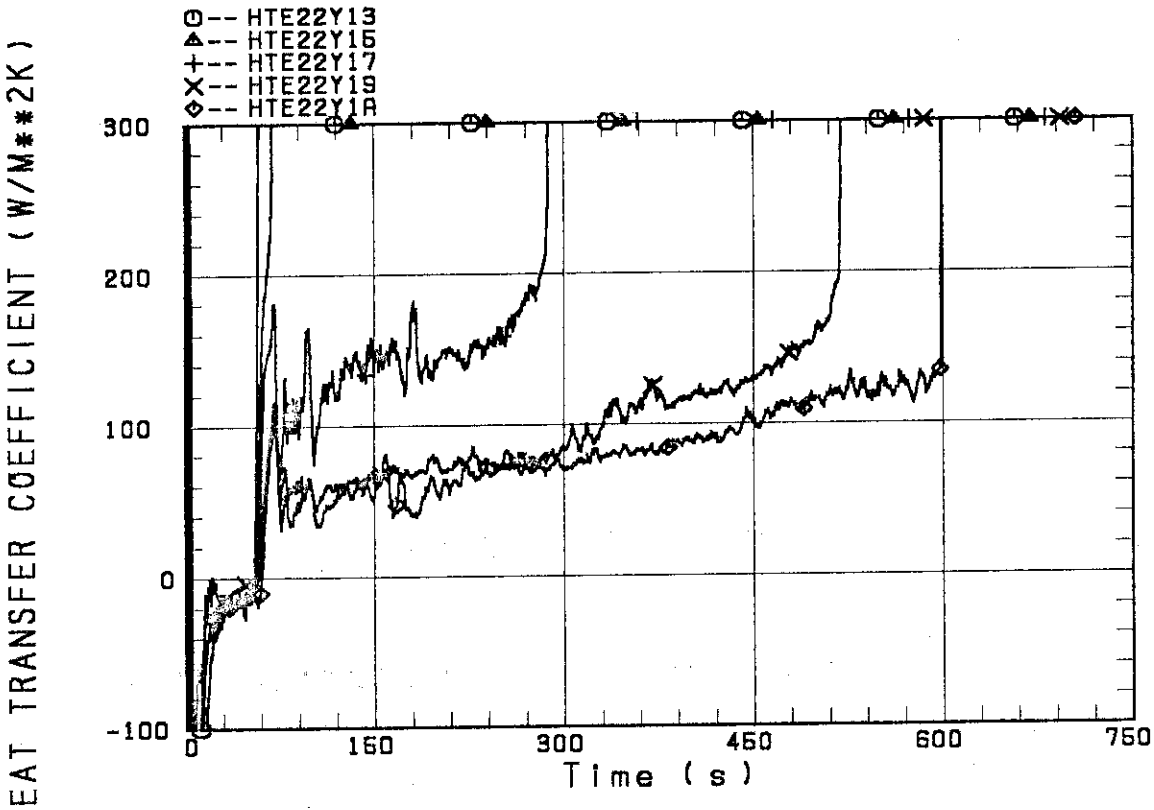

Fig. B.9 Heat transfer coefficient at various elevations along a heater rod in medium power region (B region)

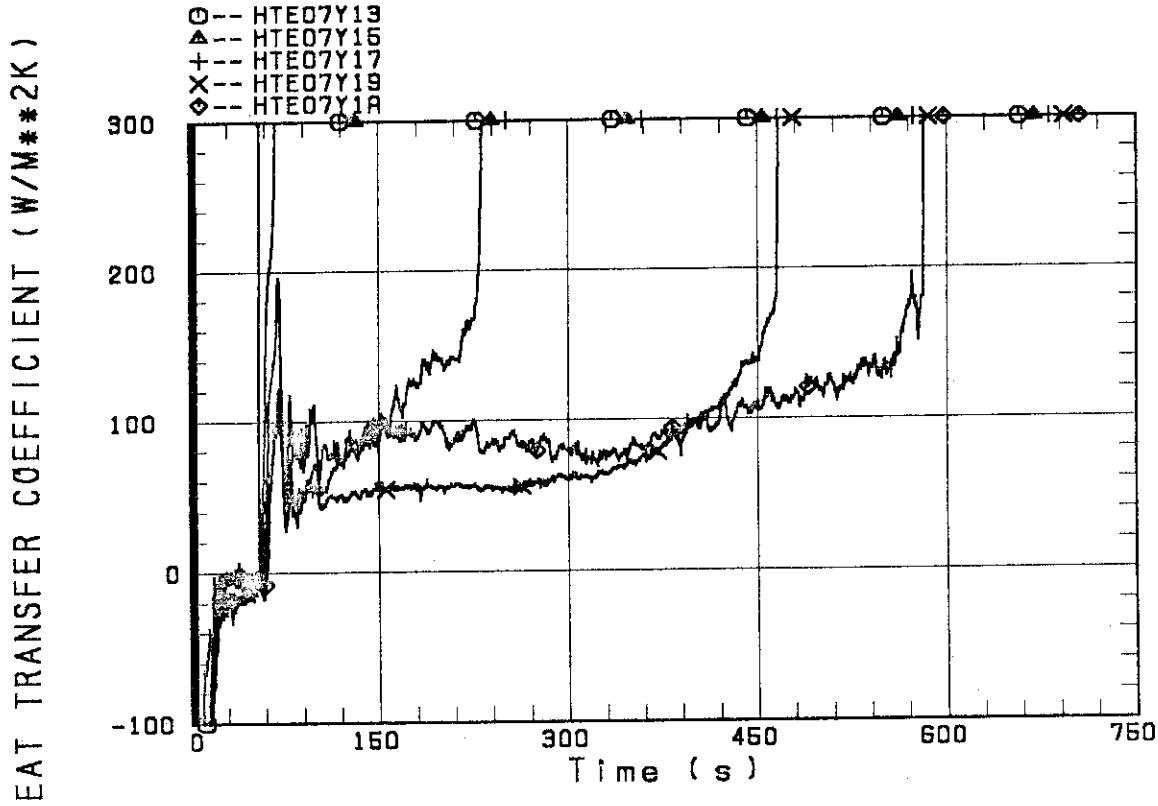

Fig. B.10 Heat transfer coefficient at various elevations along a heater rod low power region (C region)

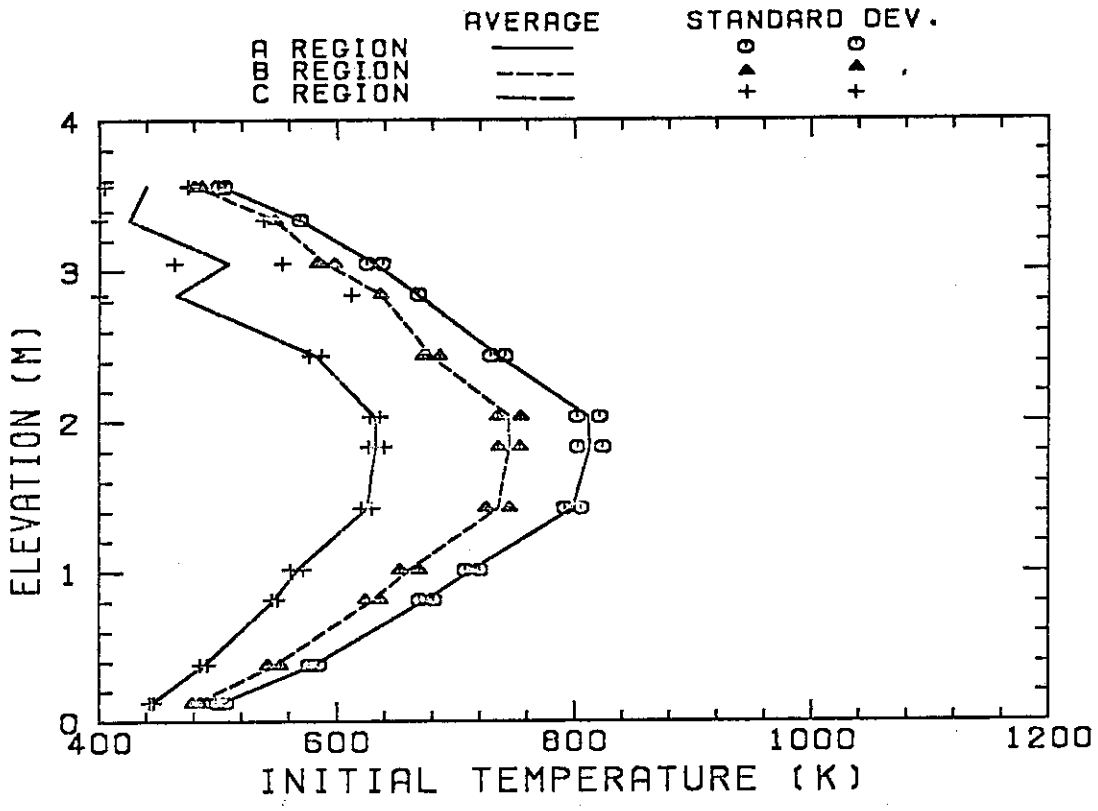

Fig. B.11 Initial clad suface temperature

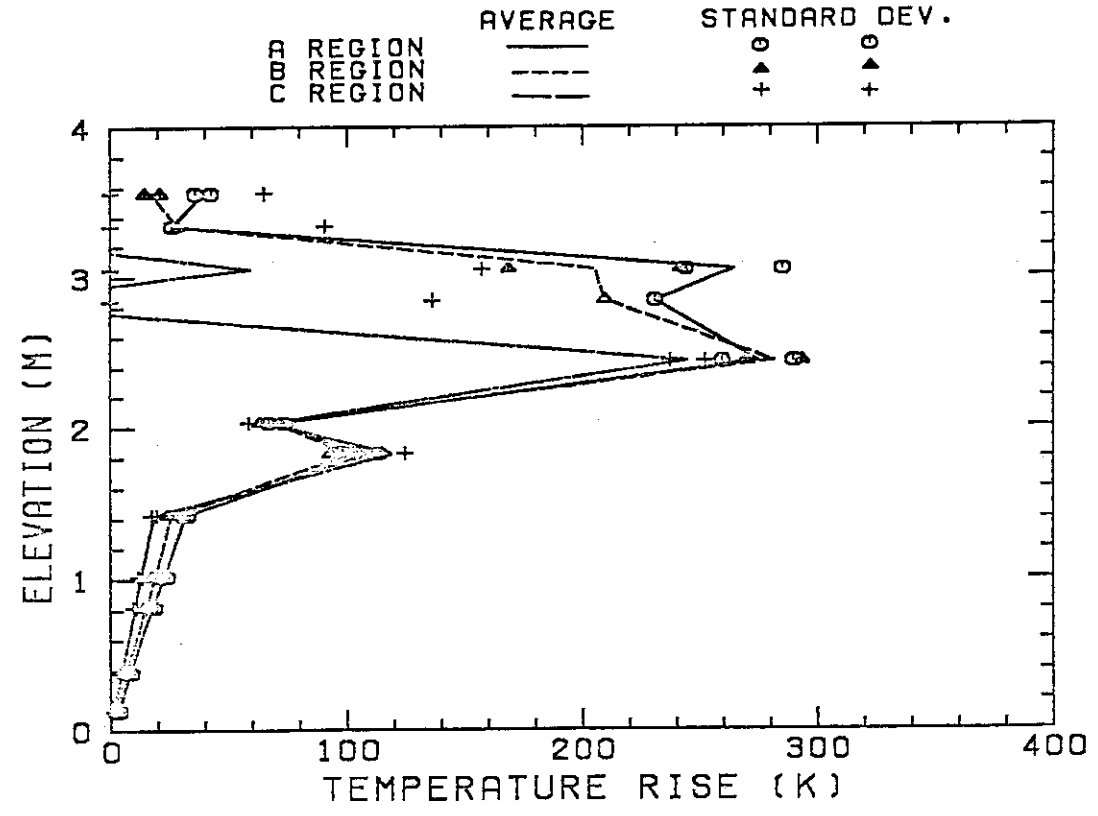

Fig. B.12 Temperature rise

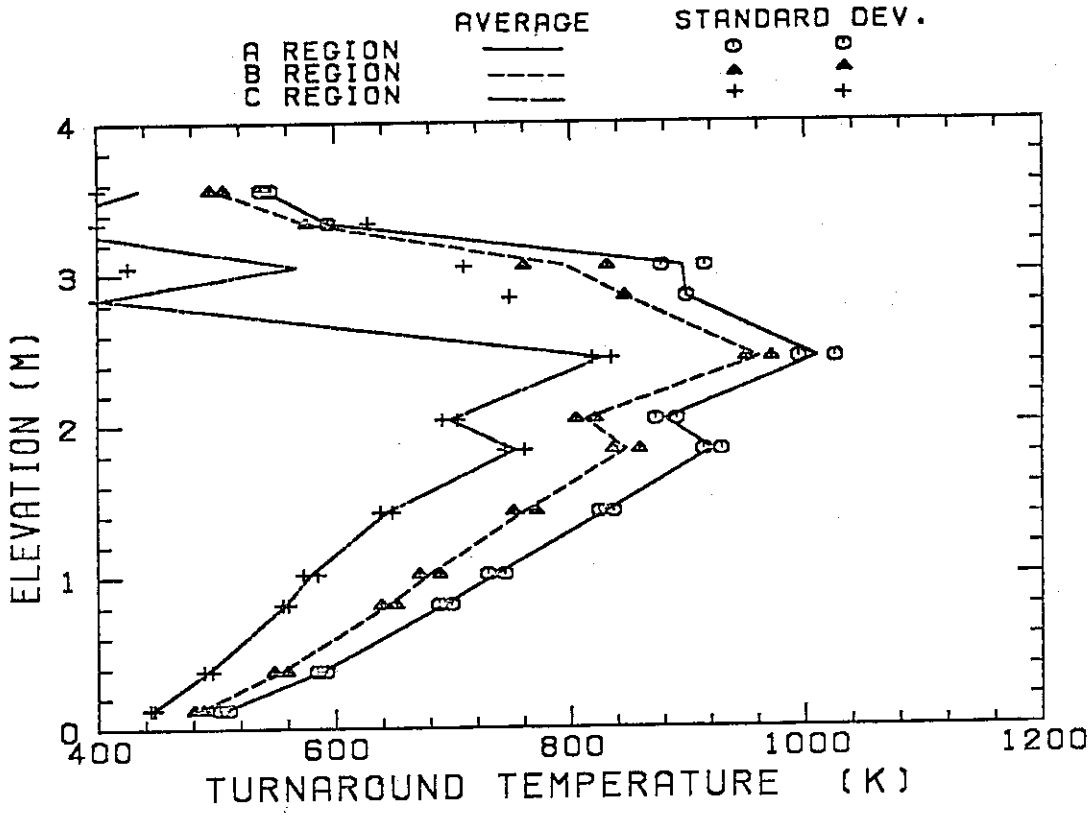

Fig. B.13 Turnaround temperature

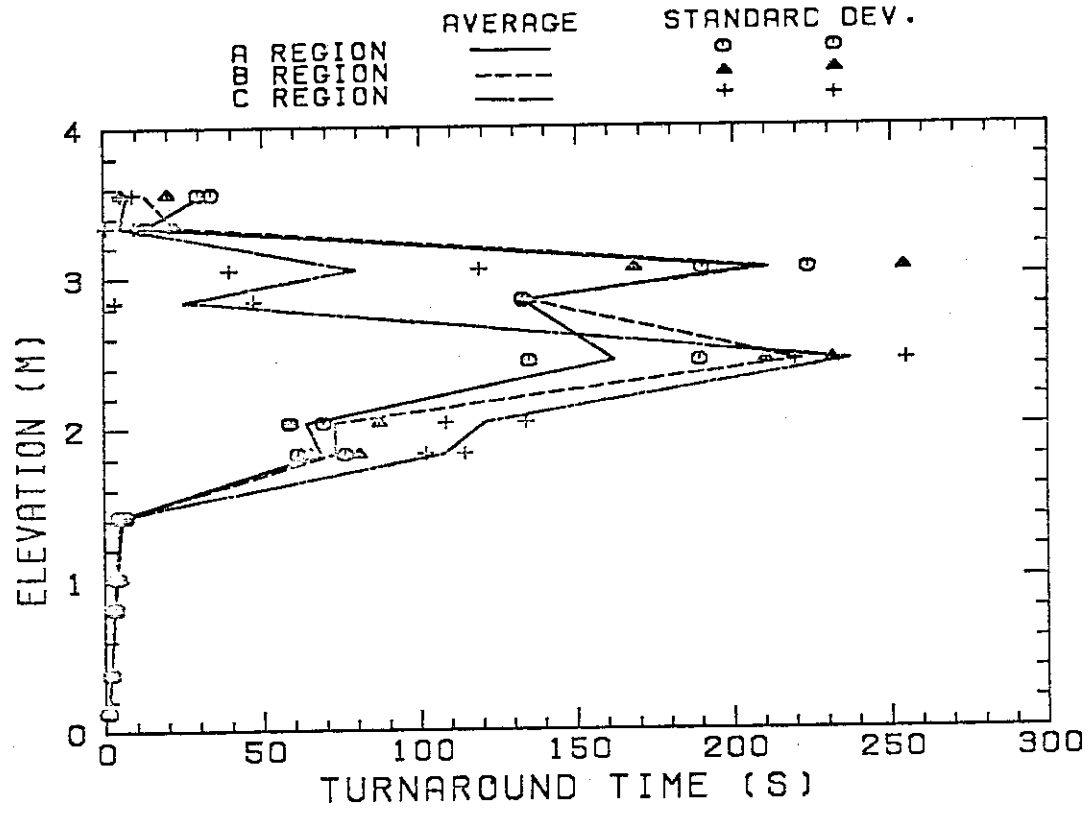

Fig. B.14 Turnaround time

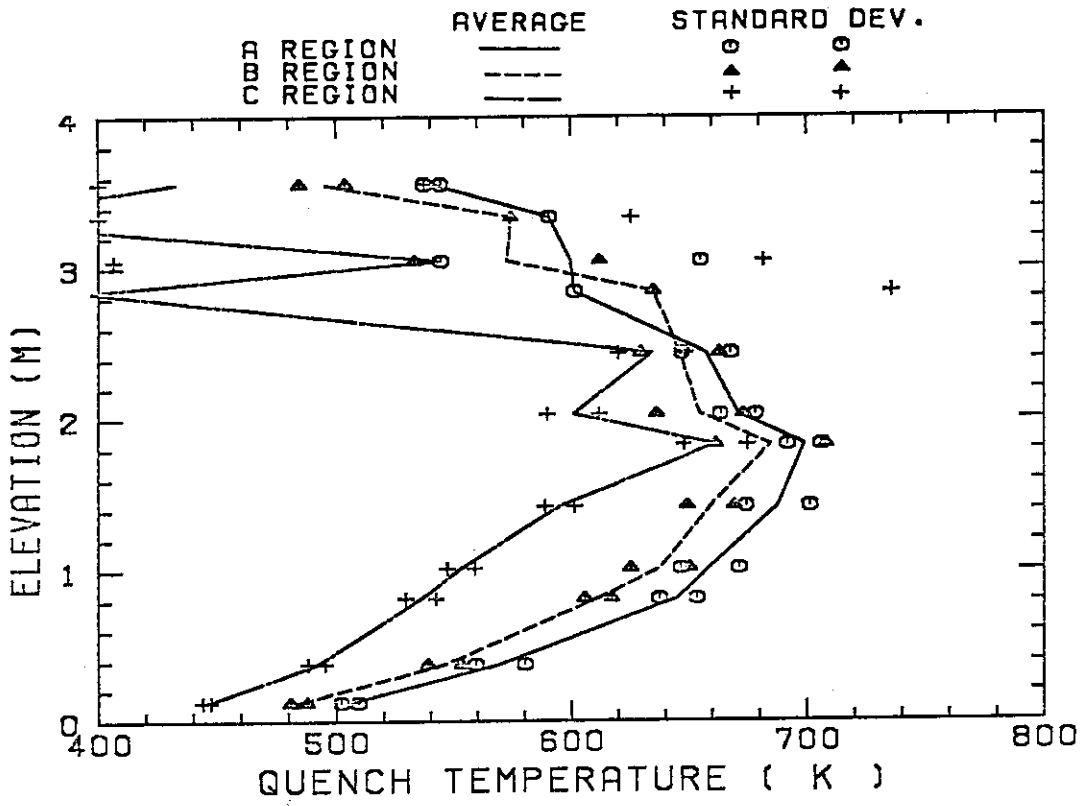

Fig. B.15 Quench temperature

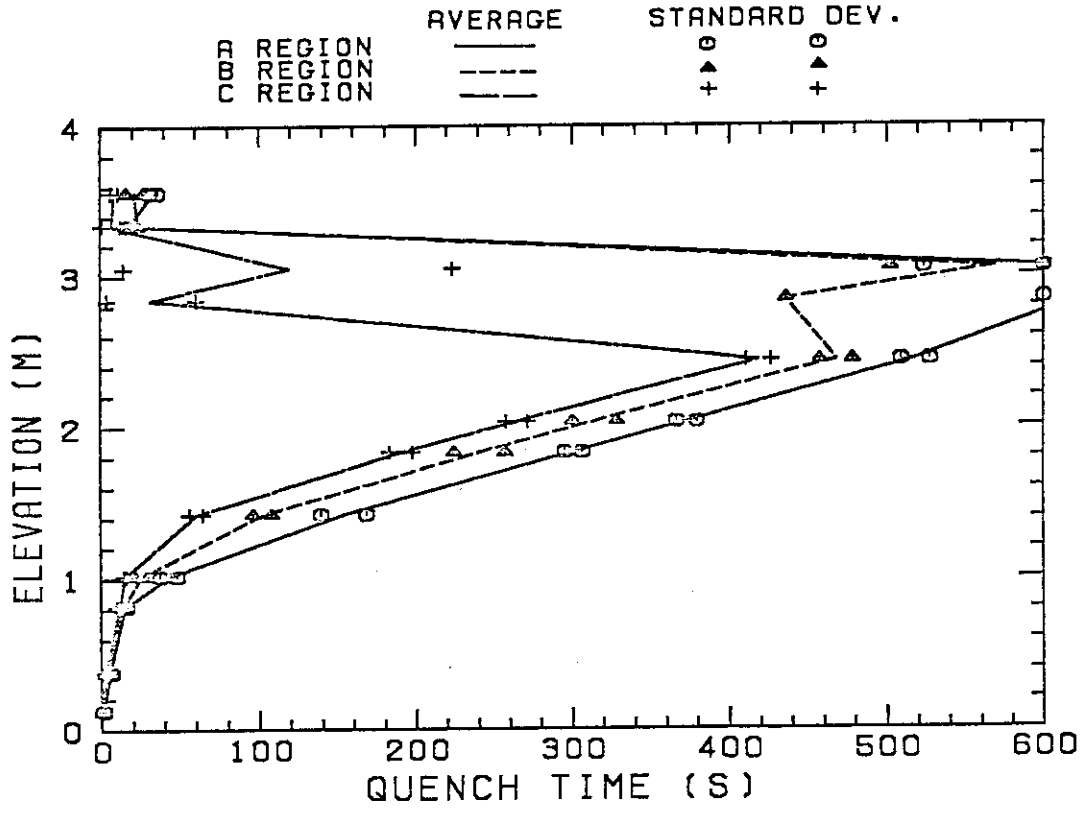

Fig. B.16 Quench time

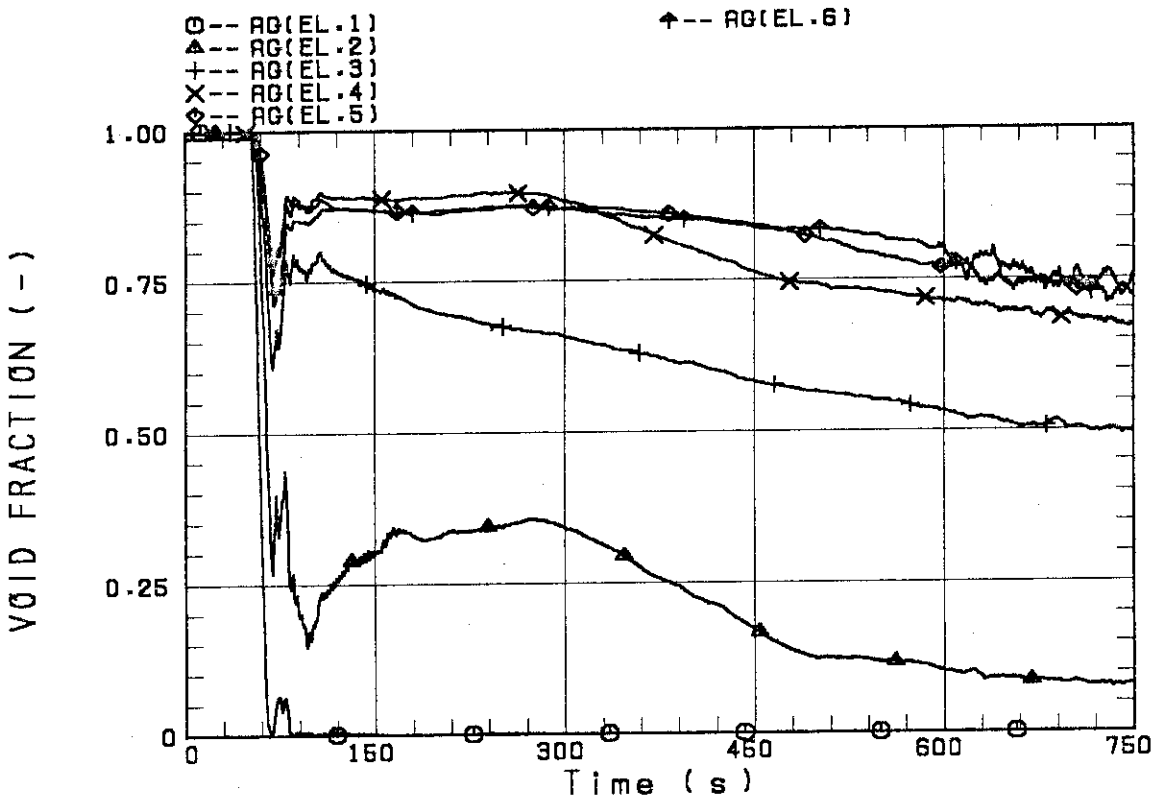

Fig. B.17 Void fraction in core

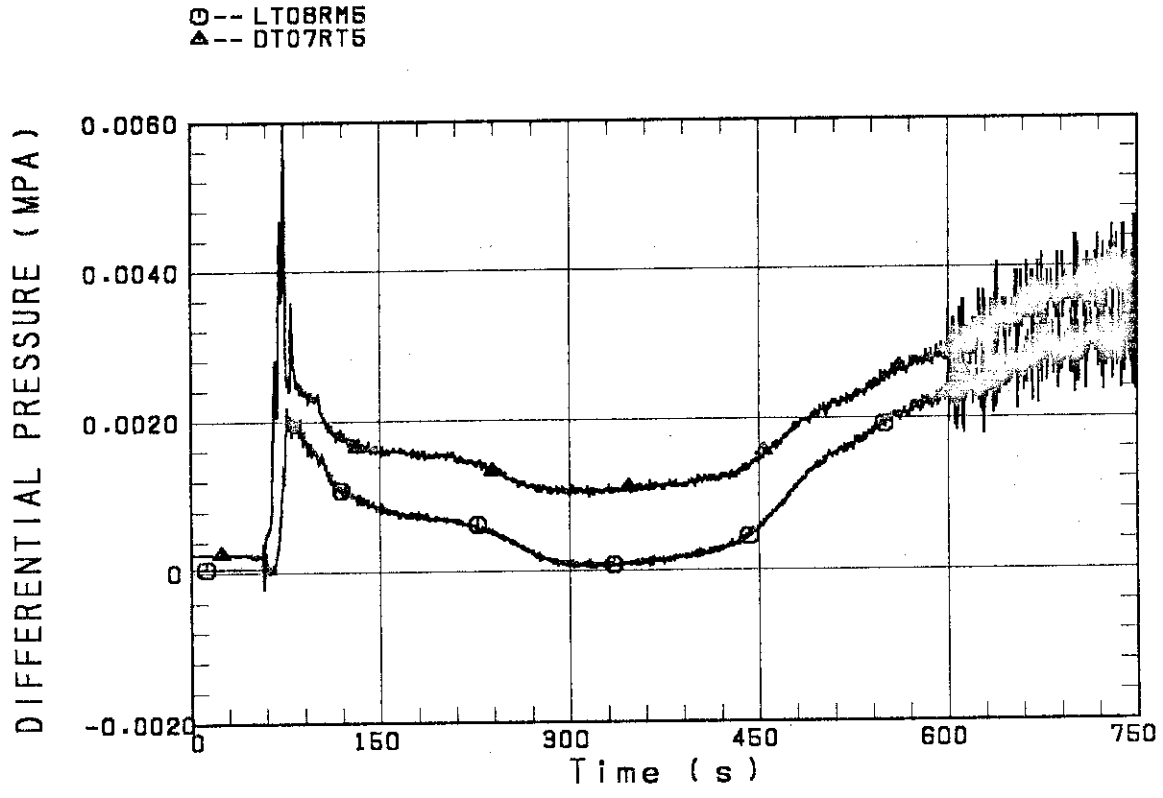

Fig. B.18 Differential pressure through upper plenum

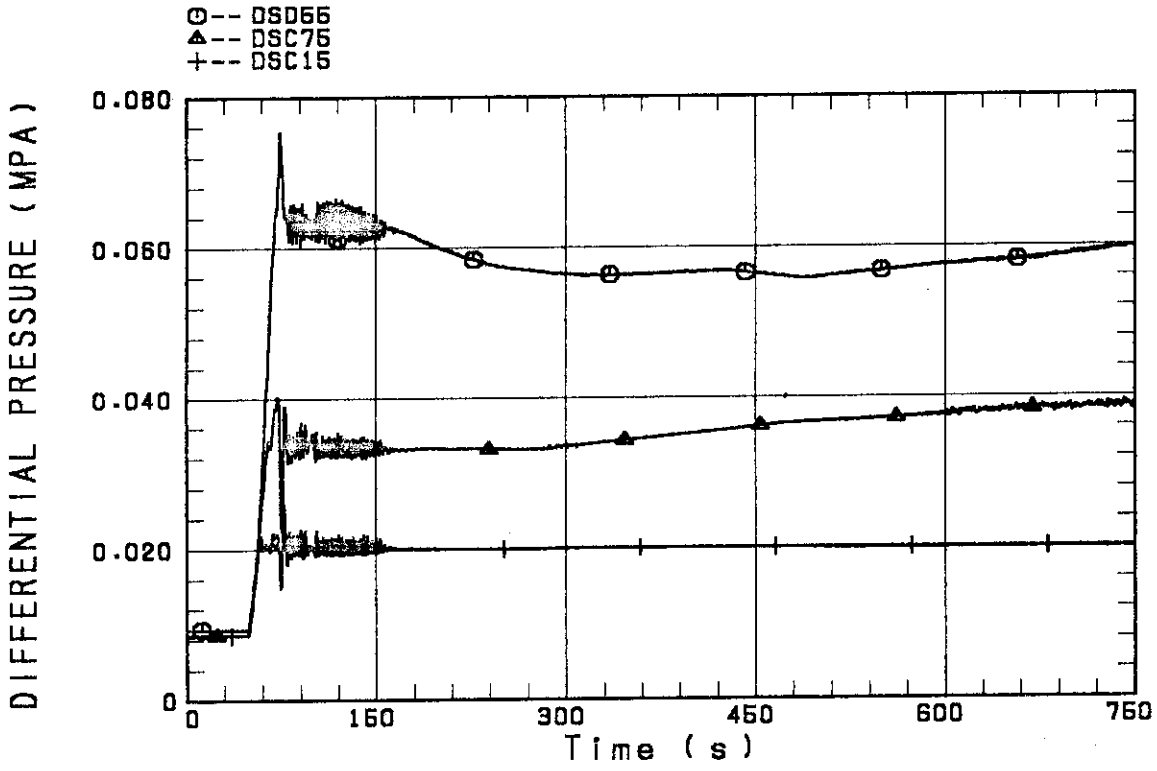

Fig. B.19 Differential pressure through downcomer, core, and lower plenum

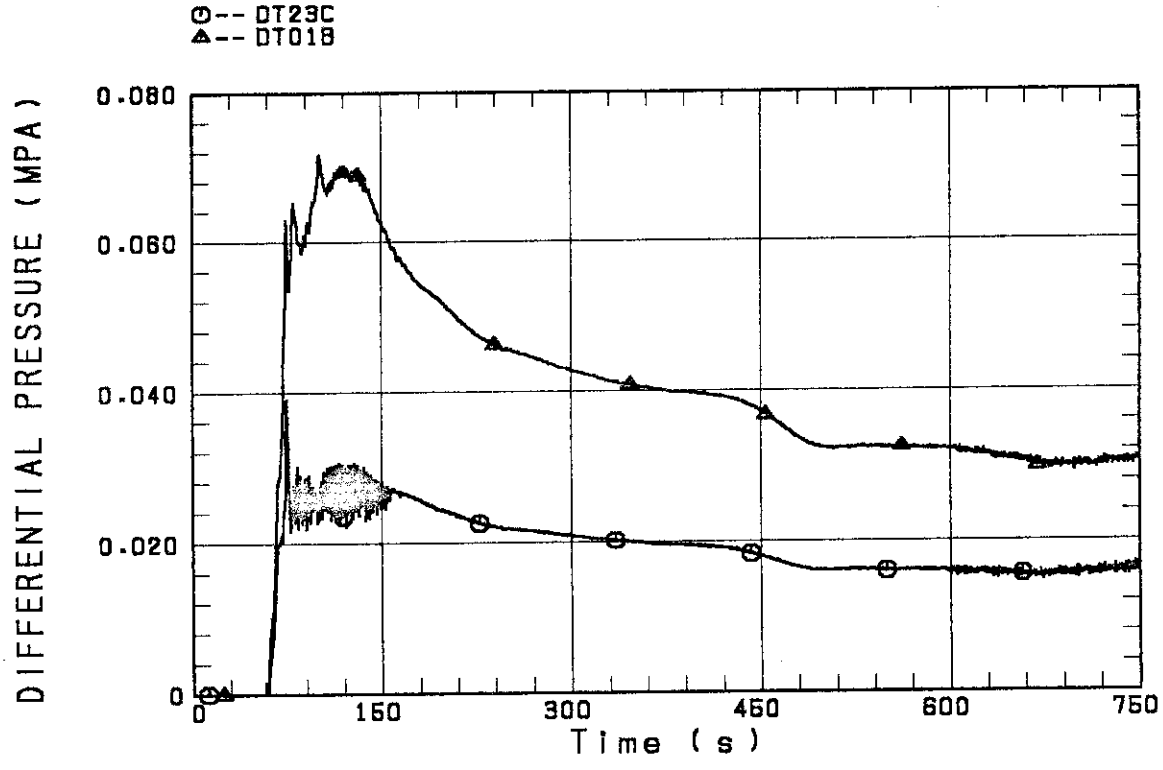

Fig. B.20 Differential pressure through intact and broken loops

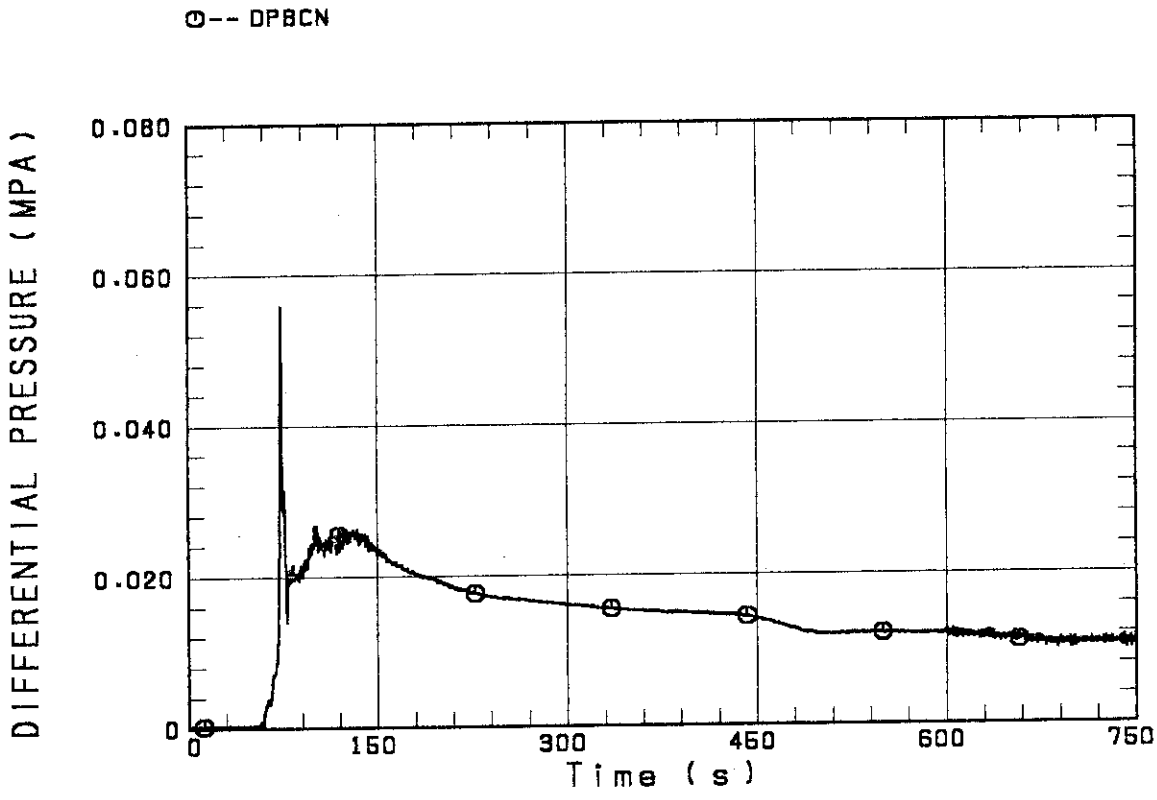

Fig. B.21 Differential pressure through broken cold leg nozzle

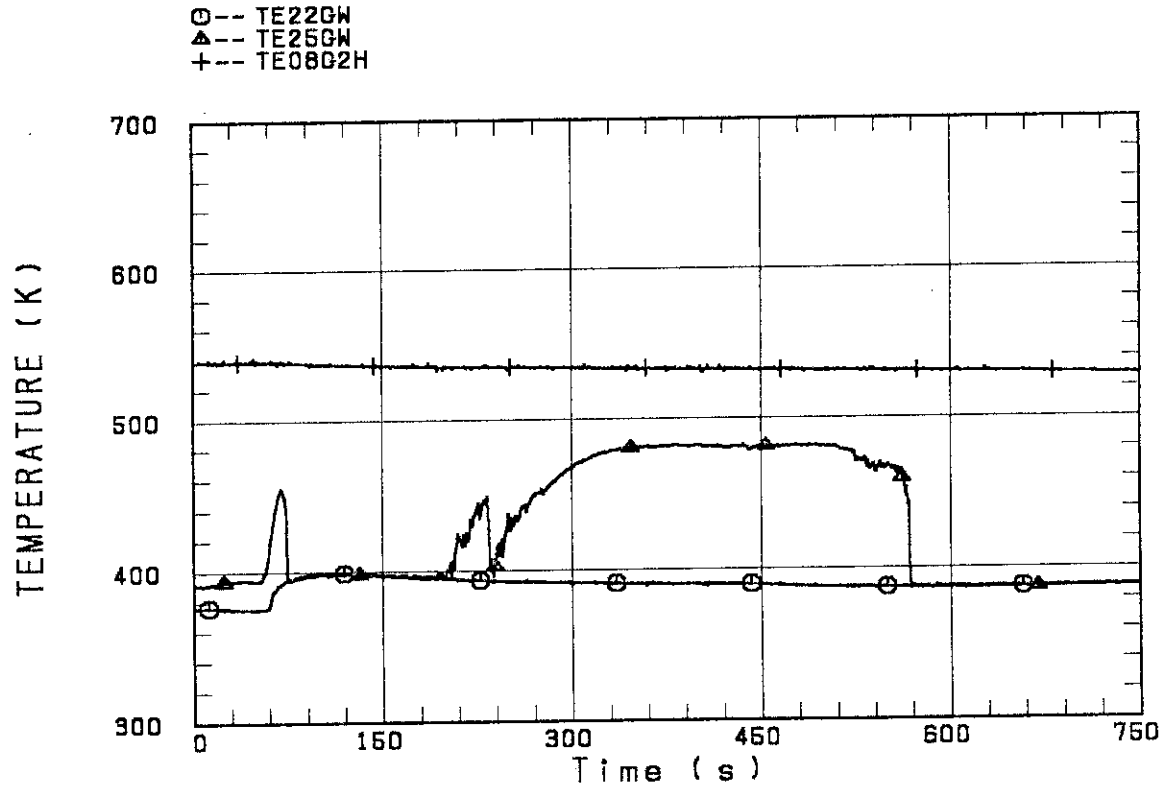

Fig. B.22 Fluid temperature in inlet plenum, outlet plenum, and secondary of steam generator 1

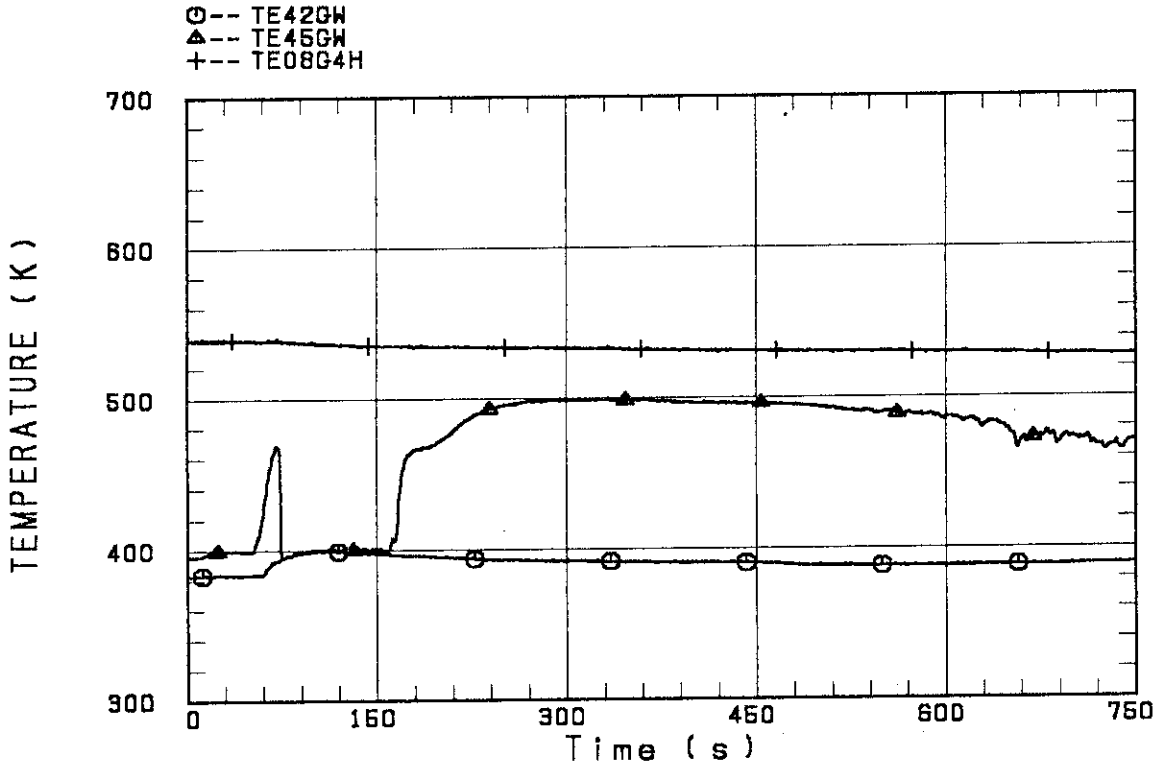

Fig. B.23 Fluid temperature in inlet plenum, outlet plenum, and secondary of steam generator 2

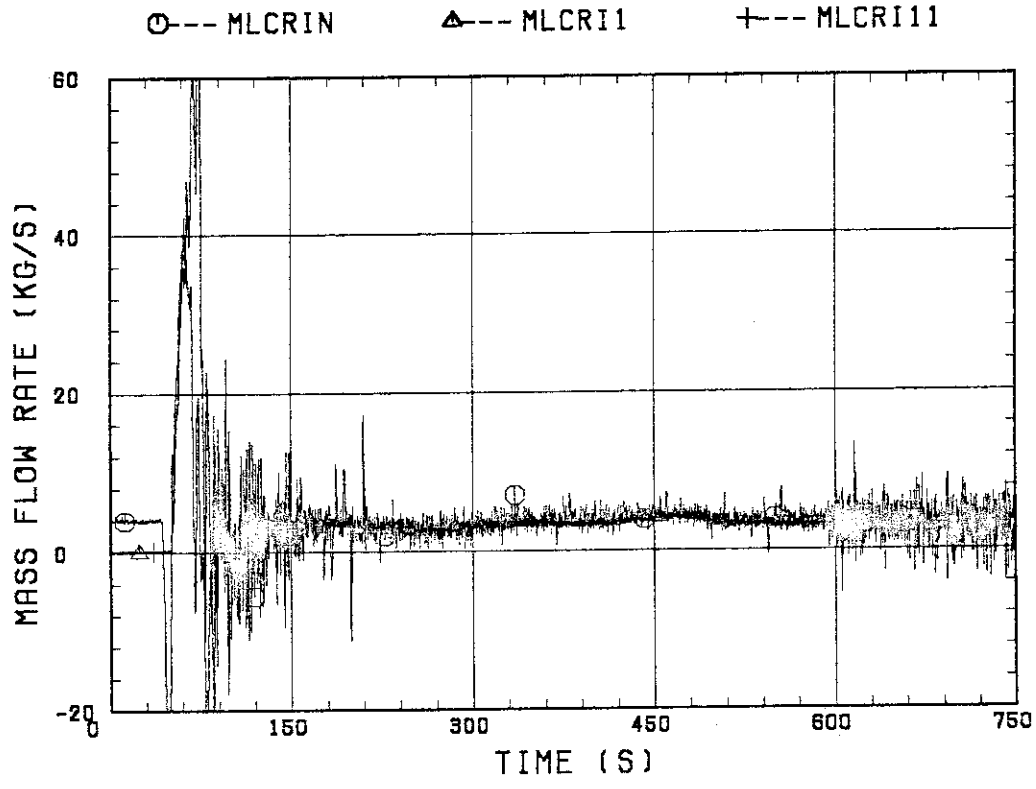

Fig. B.24 Core flooding mass flow rates evaluated with Eqs. (A.1) and (A.2)

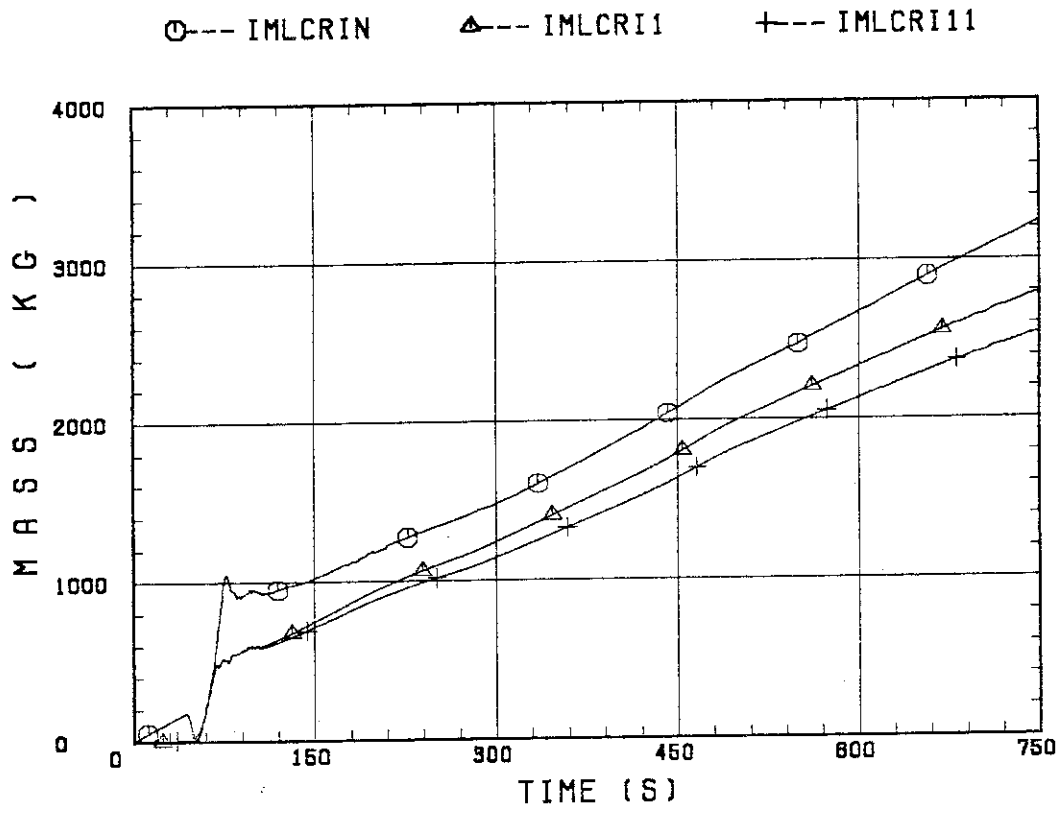

Fig. B.25 Time-integral mass flooded into core evaluated with Eqs. (A.1) and (A.2)

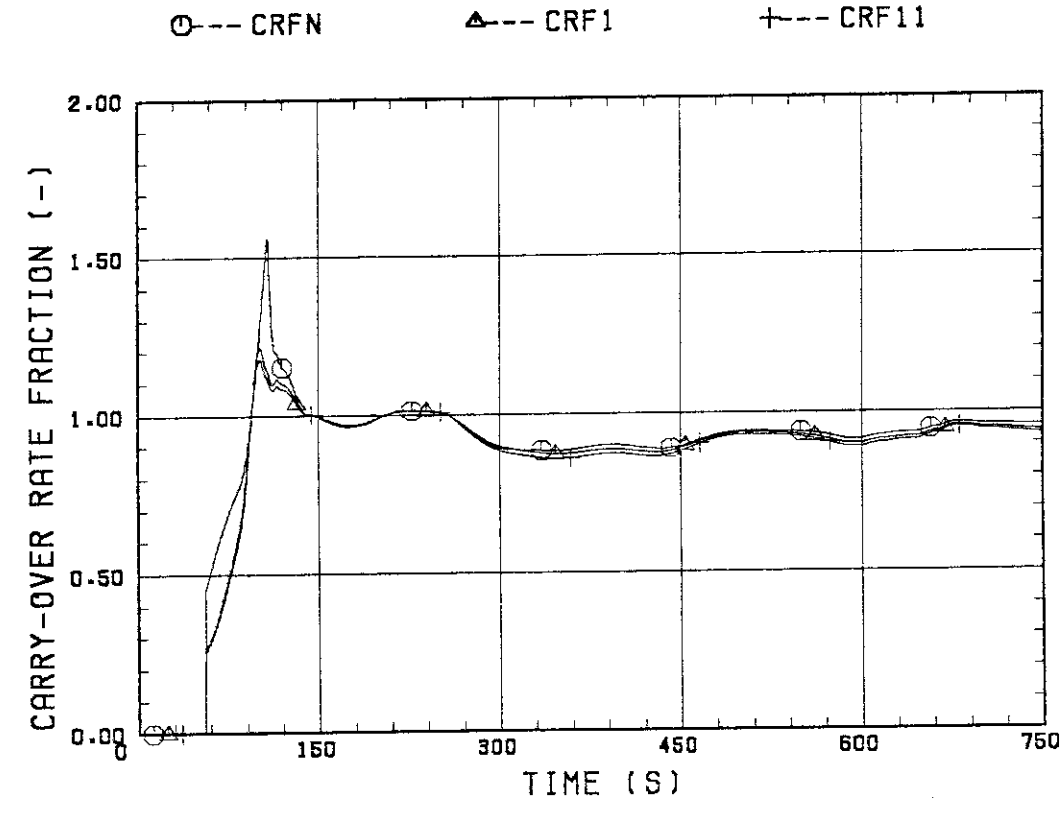

Fig. B.26 Carry-over rate fraction

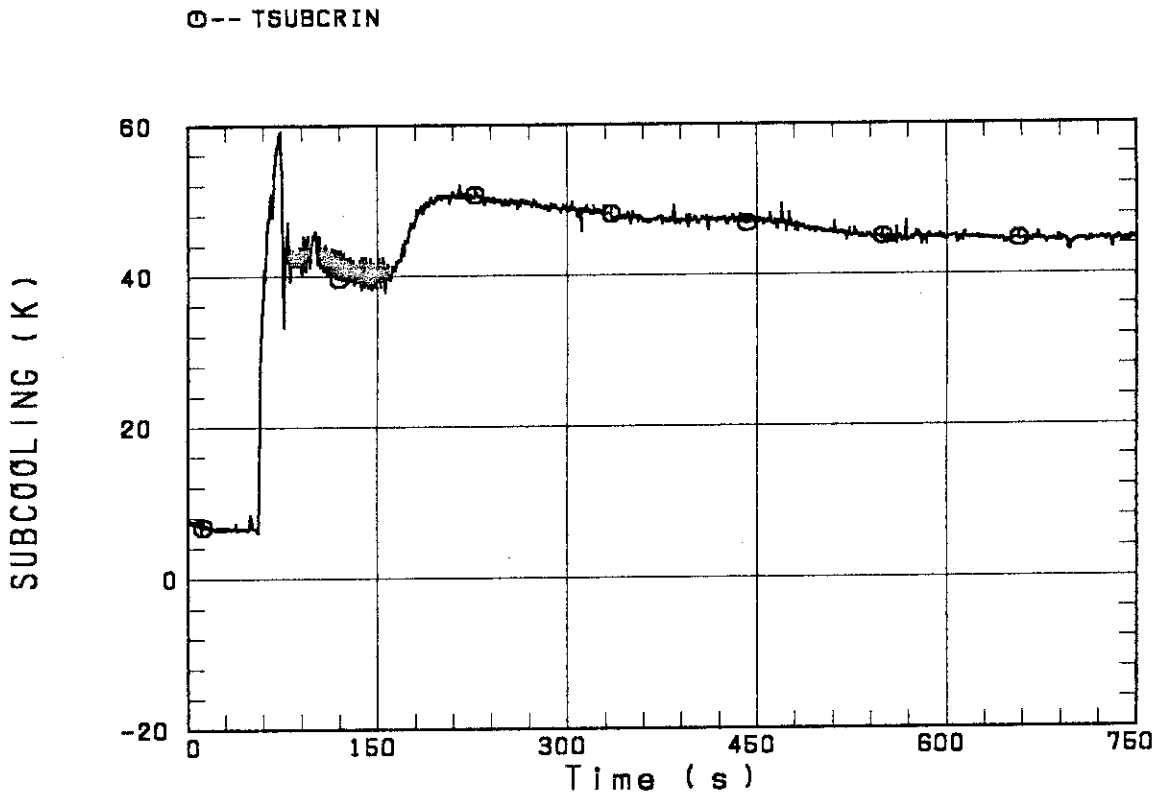

Fig. B.27 Core inlet subcooling

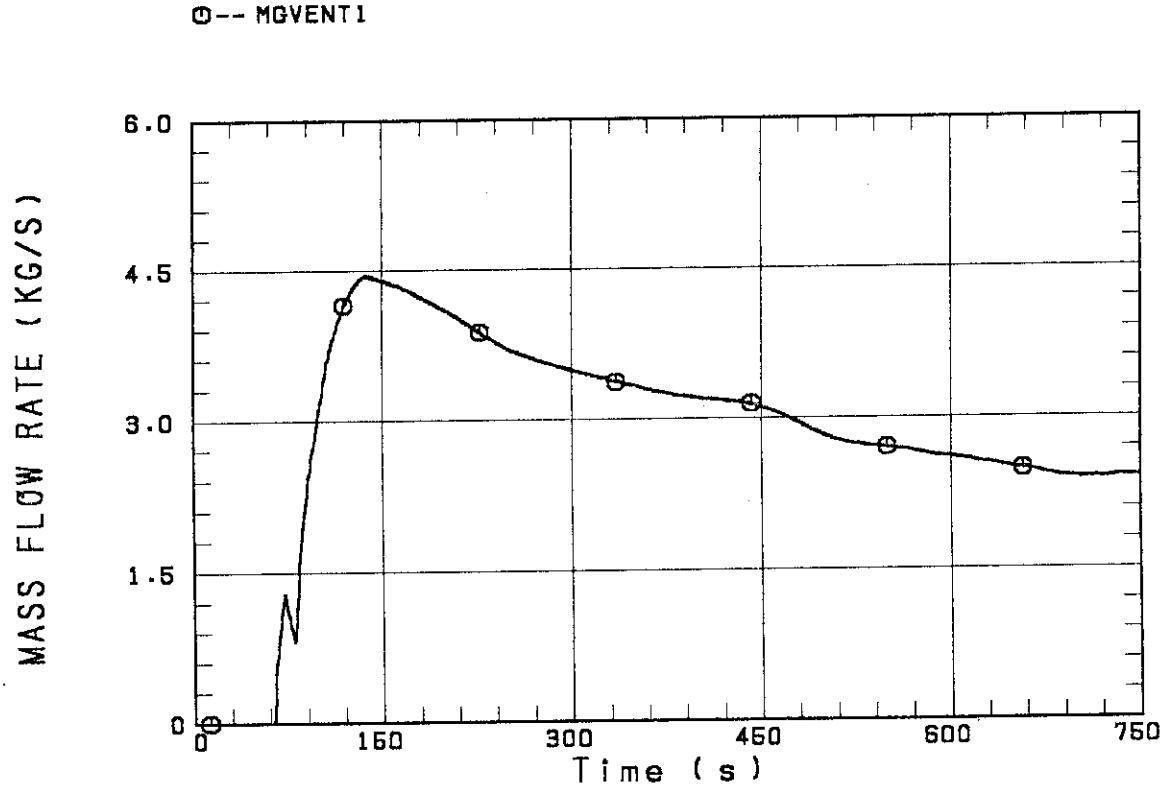

Fig. B.28 Exhausted mass flow rate from containment tank 2